QUASI-PERIODIC PATTERNS OF BRAIN INTRINSIC ACTIVITY COORDINATE THE FUNCTIONAL CONNECTIONS IN HUMANS

A Dissertation
Presented to
The Academic Faculty

By

Behnaz Yousefi

In Partial Fulfillment
Of the Requirements for the Degree
Doctor of Philosophy in Bioengineering
School of Biomedical Engineering

Georgia Institute of Technology

December 2019

QUASI-PERIODIC PATTERNS OF BRAIN INTRINSIC ACTIVITY COORDINATE THE FUNCTIONAL CONNECTIONS IN HUMANS

Approved by:

Dr Shella D. Keilholz, Advisor
School of Biomedical Engineering
Georgia Institute of Technology and Emory University

Dr Annabelle Singer
School of Biomedical Engineering
Georgia Institute of Technology and Emory University

Dr Bruce Crosson
School of Medicine
Emory University and Georgia State University

Dr Garth J. Thompson
iHuman Institute
ShanghaiTech University

Dr Eric H. Schumacher
School of Psychology
Georgia Institute of Technology

Date Approved: November 4 2019

ACKNOWLEDGEMENT

I thank all my committee members for their extremely constructive comments, previous and current lab members for the inspirational discussions, and several giants who I have cited here. I cannot thank my advisor enough for her comments, superhuman attitudes and support, just hope this thesis turns into a fair foundation for further research in the Keilholz Mind Lab.

TABLE OF CONTENTS

LIST OF TABLES

LIST OF FIGURES

LIST OF ABBREVIATIONS

aACC	anterior ACC
ADD	anterior cingulate cortex
Ag	angular gyrus
aI	anterior insula
AN	auditory network
ANS	autonomous nervous system
BG	basal ganglia
BNM	basal nucleus of Meynert
BOLD	Blood oxygenation Levels Dependent
CS	cortical signal
CSF	cerebroppinal fluid
dACC	dorsal ACC
DAN	dorsal attention network
DMN	default mode network
DR	dorsal raphe
ECoG	electrocorticography
EEG	electroencephalography
FC	functional connectivity
FCG	functional connectivity gradient
FD	frame-wise displacement
FEF	frontal eye field
fMRI	functional magnetic resonance imaging
FPC	frontopolar cortex
FPN	frontoparietal network
GM	gray matter

Gpe	globus pallidus external
Gpi	globus pallidus internal
GS	global signal
HCP	Human Connectome Project
hr	hour
HRF	hemodynamic response function
HTH	hypothalamus
HV	hear rate variation
Hz	hertz
ifg	inferior frontal gyrus
ifg	inferior frontal gyri
IFJ	inferior frontal junction
ifs	intermediate frontal sulcus
IPL	inferior parietal lobe
LC	locus coeruleus
LN	limbic network
LPCC	left posterior cingulate cortex
LPFC	lateral prefrontal cortex
MCC	mid cingulate cortex
MD	mediodorsal nucleus
MEG	magnetoencephalography
mfg	middle frontal gyri
mI	mid insula
min	minute
MR	median raphe
mTL	middle temporal lobe
NA	nucleus accumbens

OFC	orbitofrontal cortex
PAG	periaqueductal gray
PEF	premotor eye field
POS	parieto-occipital sulcus
PPN	pedunculopontine nucleus
preM	premotor area
QPPs	quasi-periodic patterns
RSC	retrosplenial cortex
rsfMRI	resting-state fMRI
RSN	resting-state network
RV	respiration variation
s	second
SC	superior colliculus
SE	spatial extent
sfg	superior frontal gyri
SFL	superior frontal language area
sma	supplementary motor area
smg	supramarginal gyrus
SMN	somatomotor network
SNc	substantia nigra pars compacta
SNr	substantia nigra pars reticulata
SPL	superior parietal lobe
sTL	superior temporal lobe
STS	superior temporal sulcus
STH	subthalamic nucleus
SWR	sharp-wave ripples
TOJ	temporo-occipital junction

TPN task positive network

TPOJ temporo-parieto-occipital junction

TR fMRI repetition time

V1 primary visual area

VAN ventral attention network

vmPFC ventromedial prefrontal cortex

VN visual network

VP ventral posterior nucleus

VTA ventral tegmental area

WM white matter

SUMMARY

The brain is a complex self-organizing biophysical system and intrinsically very active. How such intrinsic activity organizes the brain in humans is widely being studied during resting-state using functional magnetic resonance imaging (rsfMRI) and the functional connectivity (FC) metric. FC, calculated as the Pearson correlation between rsfMRI timeseries from different brain areas, indicates coherent activity on average over time, and can reflect some spatial aspects of the brain's intrinsic organization. For example, based on the FC profile of each area, the cerebral cortex can be parcellated into a few resting-state networks (RSNs) or exhibit a few functional connectivity gradients (FCGs). Brain is a complex system and exhibits varied dynamic spatiotemporal regimes of coherent activity, which are still poorly understood. A subset of such regimes should be giving rise to FC, yet they might entail significantly insightful aspects about the brain's self-organizing processes, which cannot be captured by FC. Among such dynamic regimes is the quasi-periodic pattern (QPP), obtained by identifying and averaging similar ~20s-long segments of rsfMRI timeseries. QPP involves a cycle of activation and deactivation of different areas with different timings, such that the overall activity within QPP resembles RSNs and FCGs, suggesting QPP might be contributing to FC.

To robustly detect multiple QPPs, method improvements were implemented and three primary QPPs were thoroughly characterized. Within these QPPs activity propagates along the functional gradients at the cerebral cortex and most subcortical regions, in a well-coordinated way, because of the consistencies and synchronies across all brain regions which reasonably accord with the consensus on the structural connections. Nuanced timing differences between regions and the closed flow of activity throughout the brain suggest drivers for these patterns. When three QPPs are removed from rsfMRI

timeseries, FC within and particularly between RSNs remarkably reduces, illustrating their dominant contribution. Together, our results suggest a few recurring spatiotemporal patterns of intrinsic activity might be dominantly coordinating the functional connections across the whole brain and serving self-organization. These intrinsic patterns possibly interact with the external tasks, affecting performance, or might provide more sensitive biomarkers in certain disorders and diseases.

CHAPTER 1: INTRODUCTION

The brain is a *complex self-organizing* biophysical system [1-7] and *intrinsically very active* [3-6]. In adult humans, it weighs 2% of body mass, but takes 20% of resting energy consumption, with any external task adding up to 5% [5-6]. *This extensive level of intrinsic activity might serve the purpose of self-organization*. One way to study this *hypothesis* is the *resting-state* paradigm, which is functionally imaging the brain while individuals are awake with no task for a few tens of minutes.

One of the widely used functional imaging modalities of our time is the functional magnetic resonance imaging (fMRI), which is non-invasive and covers the whole brain, but has its own limitations. Based on the most common image acquisition settings, fMRI timeseries are blood oxygenation levels dependent (BOLD) signals, indirect measures of the neuronal activity, with response function that is inherently slow and non-trivial to interpret due to the complexity of the involved physiology [3,5-6,8]. Despite limitations, BOLD timeseries reflects neuronal activity, as vastly supported by other more direct neuroimaging modalities [5-6,9-10] or the behavioral correlates which are attributed to the brain's functionality (historically) [6,10-11]. This fact can be utilized particularly if *infraslow (<0.1Hz)* processes across the *whole brain (macroscale)* are of interest and particularly if comparative approaches or metrics are adopted, e.g., difference between the resting-state and task paradigms or relative timings between areas.

The simplest metric of relative timing between brain areas is the *Pearson correlation between their timeseries*, called *functional connectivity (FC)*, which indicates coherent activity on average over time [6]. Intrinsic FC between different pairs of areas (FC for

brevity) is the most widely used metric to study the intrinsic organization of the human brain based on the resting-state BOLD-based fMRI (rsfMRI).

The most relevant application of FC is the parcellation of the cerebral cortex into *a small number of macroscale networks*, called *resting-state networks (RSN)* [12,5-7] – the term network refers to a set of areas or nodes that are not necessarily adjacent. *Each RSN is basically comprised of nodes that exhibit similar FC, and also domain-general functionality at the behavioral-level;* for example, in *a wide range of tasks* that require externally oriented attention, nodes of the task positive network (TPN) activate, while nodes of the default mode network (DMN) mostly deactivate [12,5-7]. In contrast, nodes of the DMN activate in a wide range of tasks that require internally oriented attention, e.g., thinking about self [12,5-7].

An equally relevant application of FC is the identification of the *macroscale gradients (FCGs)* across the span of the cerebral cortex [13]. *Each FCG is basically the spatial axes along which areas exhibit similar FC*. For example, in the primary FCG (FCG1) at the cerebral cortex, the areas that belong to the *unimodal networks of somatomotor (SMN) or visual (VN)* are located at one end, while the areas that belong to the *transmodal DMN* are located at the other end, showing the unimodal networks are similar to one another in terms of FC but maximally dissimilar to the DMN.

FC and its wide range of application are based on time-averaged coherence and can reflect some spatial aspects about the brain's intrinsic organization. Brain is complex and exhibits varied intrinsic *dynamic spatiotemporal regimes of coherent activity* [3,9-10,14-15]. A subset of such regimes *should be giving rise to the time-averaged coherence indicated by FC*, yet they might entail significantly insightful aspects about the brain's

self-organizing processes, which cannot be captured by FC, and it might be well impactful to characterize them independently.

Among such intrinsic dynamic spatiotemporal regimes of coherent activity is the *quasi-periodic pattern (QPP)* [16-18]. In the rsfMRI timeseries of the rat's brain, Majeed and colleagues [16] observed a lateral to medial propagation of activity in the somatomotor areas that seemed to occur quasi-periodically. Subsequently, a simple correlation-based method was implemented to *identify similar segments* of a functional scan and *simply average them for a representative spatiotemporal template, named quasi-periodic pattern or QPP*.

Applying such method in humans, using the rsfMRI timeseries of all brain areas, results in a QPP that is ~20-second long, and involves a cycle of activation and deactivation of different brain areas with different relative timings [16,18]. For example, the cerebral nodes of the TPN exhibit opposite phase relative to the nodes of the DMN, or the medial prefrontal cortex exhibit focal propagation of activity [16]. *Coherent activity within the QPP is overall reminiscent of macroscale RSNs and FCGs, which along its quasi-periodic recurrence suggests this pattern might be giving rise to FC*.

This thesis is an attempt to better understand QPPs in humans, as recurring spatiotemporal patterns of brain's intrinsic activity that might serve the purpose of self-organization. The first step towards such understanding, *in general*, is to detect QPPs robustly, and to characterize the activity within these patterns thoroughly. The next step can be to show the extent of the contribution of QPPs to FC, the most widely used metric reflective of the brain's intrinsic organization. If QPPs turn out to be the dominant contributors to FC, then perhaps they are serving self-organization, and thoroughly

characterizing them might be significantly insightful because of the novel aspects they might entail, such as nuanced timing differences between areas, which cannot be captured by FC. To address the abovementioned steps, this thesis is divided into the following parts: improving the detection of QPPs and showing their contribution to FC (chapter 2), characterizing the activity within the QPPs (chapter 3), and discussing the results (chapter 4).

Chapter 2. To better understand QPPs, the first step is to robustly detect these patterns. Therefore, the opening section of this chapter introduces a few improvements added to the method developed by Majeed and colleagues [16]. These improvements ensure the same QPP is repeatably detected, and such QPP is highly representative of its contributing segments and recur often. The next main section of chapter 2 introduces a new method to detect other QPPs, in addition to the primary QPP (QPP1). These improvements are applied to rsfMRI scans of ~800 individuals from the Human Connectome Project dataset [19] S900. To better understand QPPs, after robustly detecting them, the next step can be to show the extent of their contribution to FC, which appears in a main section. Given QPPs are macroscale and recurring patterns, they may be related to non-neuronal sources of BOLD signal fluctuations, such as slow variations in the respiration and heart rate [20-23]. Such non-neuronal sources have widespread effects and are inherently repetitive. This relation is essential to inspect for a better understanding of QPPs and is addressed in the closing sections of chapter 2.

Results. QPPs 1 to 3 all involve a ~20-second cycle of activation and deactivation of different brain areas such that the RSNs and their relative timing of activity are readily observable. However, within each QPP, the constellation of correlation between the RSNs is unique. These patterns are equally representative of their contributing

segments but progressively recur less often, and each QPP is more often followed by other QPPs than itself. QPPs 1 to 3 are dominant contributors to the functional connectivity particularly between RSNs, which suggests these intrinsic patterns might be serving self-organization. QPPs have a principled timing relation with the slow variation in the respiration and heart rate, which suggests a neurophysiological basis for these intrinsic patterns.

Chapter 3. To better understand QPPs, after robustly detecting them and showing their dominant contribution to FC, a thorough characterization of the activity they involve is necessary. QPPs might entail novel aspects about the brain's self-organizing processes (e.g., driving relation between regions), which cannot be captured by FC. This characterization is based on QPPs at the group-level (~800 individuals), in the grayordinate (~62K cortical vertices and ~30K subcortical voxels), obtained in chapter 2. To summarize the activity within these patterns, the timecourses of each QPP across cortical and subcortical areas are clustered and their time of peak activation is determined. Our description of activity is divided into seven regions which are the cerebral cortex, cerebellum, thalamus, hippocampus, amygdala, brain stem and deep brain nuclei, and striatum. For each region, to distinguish different areas and to compare the accordance of our results with the literature, an existing parcellation scheme is adopted, with priority given to the well-established parcellation schemes based on the FC and rsfMRI. For each region, any consensus on its tract-based connectivity and any already-reported FCG are considered as well.

Results. QPPs 1 to 3 involve well-coordinated propagating activity across the whole brain. Within each pattern, at the cerebral cortex, activity propagates along one of the cortical FCGs. Coarse summary of the cortical activity accords with the cortical RSNs.

Time-locked and consistent with the cortical propagation, all subcortical regions exhibit either propagation of activity or simple activity, such that the propagation axes are consistent with the cortex and consistent with any already-reported FCG in each region. Coarse summary of the subcortical activity mostly matches any consensus about tract-based connectivity, and to an extent, accords with the FC-based parcellations. Nuanced timing differences between brain regions suggest driving mechanism within QPPs. For example, the thalamus and brain stem lead the cortex as activity propagates to the nodes of DMN within QPP1, or to the nodes of TPN within QPP2. Closed flow of peak activity throughout the brain suggest origins for the cycles of QPPs.

Chapter 4. Our results in chapters 2 and 3 suggest a few recurring spatiotemporal patterns of intrinsic activity might be dominantly coordinating the functional connections across the whole brain and serving self-organization. QPPs reveal novel specific aspects about RSNs and FCGs, as well as the driving relations between regions and the origins of QPP cycles, which we discuss in chapter 4. Since our results are mainly based on contribution of QPPs to FC and propagation of activity, we also discuss how QPPs relate to the already known contributing factors to FC and existing reports of propagation.

CHAPTER 2: METHOD IMPROVEMENTS, OTHER QPPS, CONTRIBUTION TO FUNCTIONAL CONNECTIVITY, AND RELATIONSHIP WITH GLOBAL AND PHYSIOLOGICAL SIGNALS

2.1 Introduction

To better understand the quasi-periodic patterns (QPPs) of the brain's intrinsic activity that might serve self-organization, the first step is to robustly detect the QPPs. The next step can be to show their contribution to the functional connectivity (FC) between brain areas, since it is the most widely used metric reflective of the brain's intrinsic organization. Both steps are addressed in this chapter. While a thorough characterization of activity within QPPs is addressed in the next chapter, some basics aspects are included in this chapter. While a comprehensive discussion of the results appears in chapter 4, some method related topics are discussed in this chapter.

The current algorithm to detect a QPP [16,18] starts with an initial segment of a functional scan, with a present duration (~20s), identifies similar segments to that initial segment, based on a sliding correlation approach, replaces the initial segment with the average of similar segments and iteratively reidentifies the similar segments till convergence (Figure 1). The outputs are a spatiotemporal template, that is the average of a set of similar segments, and a sliding correlation timecourse with maxima indicating the start of the contributing segments to the output template, i.e., indicating the occurrence of the output template. The medians of correlation values at maxima and times between successive maxima respectively are referred to as the *strength* and *periodicity* of the output template.

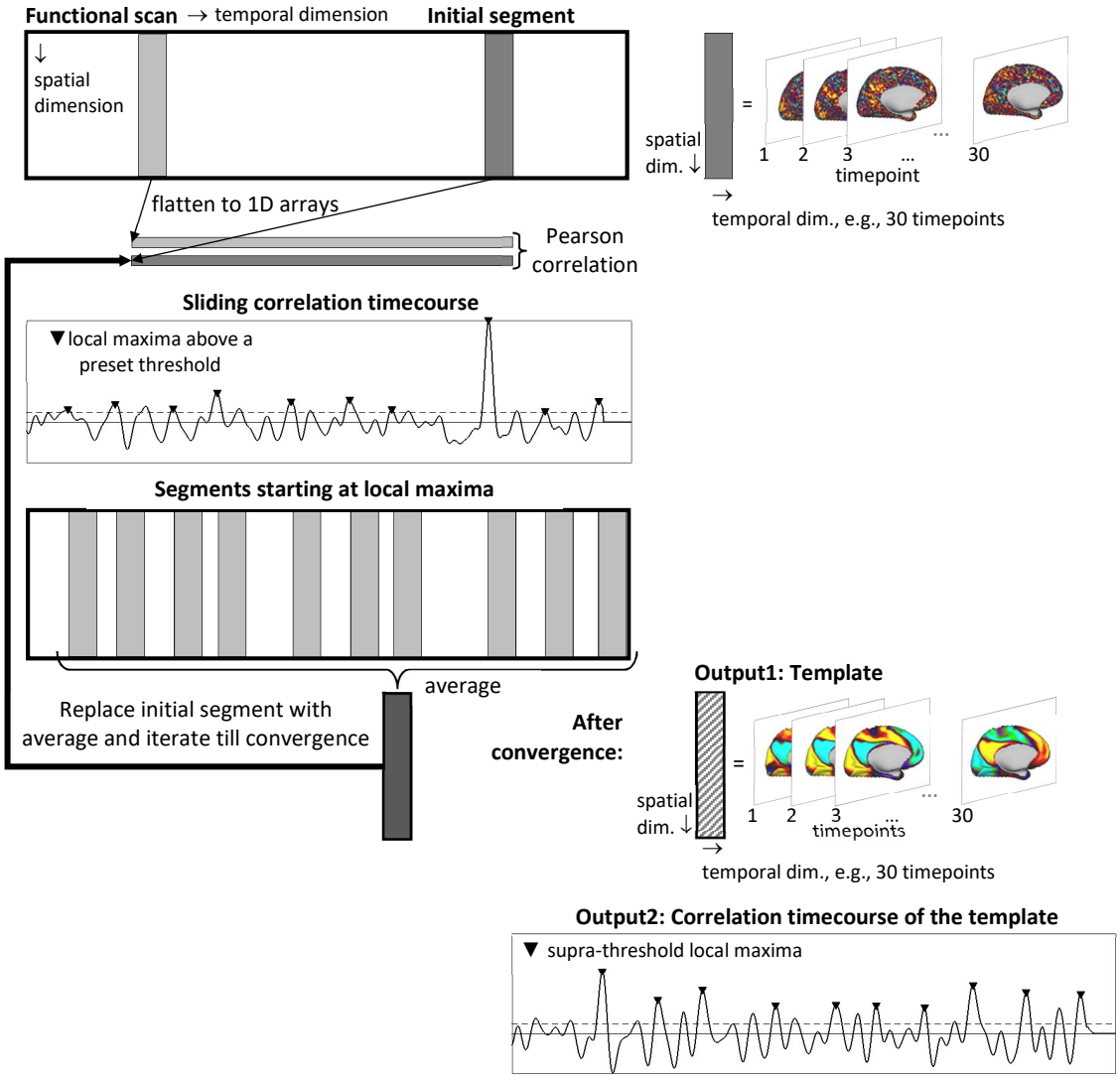

Figure 1 The main algorithm to detect a QPP is correlation-based, iterative, identifies similar segments of a functional scan and averages them for a representative spatiotemporal template.

The original method to detect a QPP [16] inspects a limited number of randomly selected initial segments and performs a hierarchical clustering of the resulted templates to select the QPP. However, inspecting some initial segments *may* result in a template that has low strength or periodicity [18]. Inspecting some other initial segments *may* result in the same template but at different phases [18]. *Taken together,* the original method might not repeatably detect the best pattern which has high strength and periodicity.

To ensure robust detection of the QPP, a few improvements are implemented. Starting from the individual-level analysis, all possible initial segments are inspected and the QPP is selected with a customized criterion to have high strength and periodicity [18]. To obtain the group-level QPP, first the QPP of each individual is phase-adjusted, such that a seed area exhibits activation at the first half of the ~20s cycle. Then the average of the phase-adjusted QPPs is correlated with all scans of all individuals for a fine-tuned identification of similar segments whose average constitute the group-level QPP. These improvements are applied to resting-state functional MRI (rsfMRI) scans of ~800 individuals from the Human Connectome Project (HCP) dataset [24], ~1hr/individual.

Thus far, only one QPP has been reported, hereon called QPP1. To examine the existence of other QPPs, QPP1 is regressed at the individual-level, residual scans (after QPP1 regression) are reanalyzed using the improved method, and QPP2 is detected at the individual and group levels. Further, QPPs 1 and 2 are regressed and QPP3 is detected in a similar fashion. While QPP4 and above can also be detected, we decided to limit the scope of this thesis to the three primary QPPs, as will be discussed. For QPP regression, two methods are implemented and the resulting QPPs 2 and 3 are compared between methods. Crucially, to examine the existence of QPPs 2 and 3 in the original

scans, the average of their contributing segments based on the original scans and the residual scans are compared.

Activity within QPPs 1-3 reminds of the macroscale resting state networks (RSNs) [12]. To coarsely characterize, correlation between the RSNs within the ~20s duration of each QPP are calculated and differences are compared. As basic metrics of QPPs, their strength and periodicity are quantified. Occurrence of QPPs relative to one another throughout the rsfMRI timeseries is also characterized. Reproducibility of QPPs across different populations is examined by randomly dividing individuals into equal subgroups, multiple times, and comparing subgroup QPPs.

That the activity within QPPs 1-3 is reminiscent of macroscale RSNs, that RSNs are obtained based on FC, and that QPPs 1-3 are recurring patterns, together suggest these patterns might be giving rise to FC. If QPPs turn to be dominant contributors to FC, first, these patterns perhaps serve the brain' self-organization, and second, a better understanding of them is insightful because of the novel aspects they might entail. The contribution of QPPs 1-3 to FC is examined by comparing the FC matrices of the original scans and the residual scans after regressing these patterns.

Because QPPs are macroscale and recurring patterns, they might have relationships with non-neuronal sources of BOLD signal fluctuations, such as head motion or slow variations in the respiration and heart rate, which can influence the whole brain [20] and are inherently repetitive. To better understand QPPs, it is essential to inspect such relationships. The simplest and most common summary metric of signal fluctuations across the whole brain is the global signal (GS), a 1D timeseries obtained by averaging all timeseries inside the brain [20]. Since among the contributors to the GS are non-

neuronal sources of BOLD signal fluctuations (motion and physiological variation), and since the GS is a simple and common summary metric, *first*, the relation between QPPs and the GS are inspected. *Later,* head motion levels are considered. *Finally,* the relation between QPPs and slow variations in the respiration and heart rate are examined.

To inspect the relationship between QPPs and the GS, as the primary approach, the contributing segments of QPPs 1-3, identified based on the scans with GS regression (GSR), are averaged over the scans without GSR and the resulted templates are compared with QPPs 1-3. As a complementary approach, the scans without GSR are reanalyzed to detect QPPG and the relative occurrence of QPPG with other QPPs are examined. Suggested by a noticeable individual variability within QPPG, the spatial extents (SEs) of strong negative and positive correlation between the DMN and other areas within QPPG are quantified. Two subgroups of individuals with the highest negative and positive SEs are formed and subgroup QPPGs are obtained. Moreover, the contributing timeslots of each subgroup QPPG are averaged over the 1D timeseries of GS to obtain a ~20s timecourse for the GS, based on which a novel point about the spatiotemporal dynamics of the global activity is specified. As a support for this point, relative occurrence of QPPG and the GS fluctuations is examined and the basic metrics of QPPG are quantified. To examine the effect of head motion [20], QPPG of two subgroups of individuals with the lowest and the highest motion levels are compared.

To inspect the relationship between QPPs and slow variations in the respiration (RV) and heart rate (HV), first, two timeseries for RV and HV are constructed [21-22]. As a common approach, estimates of induced fMRI signal fluctuations due to RV and HV are regressed from the scans without GSR, QPPG is redetected and SEs are recalculated. As a customized approach, the contributing timeslots of all QPPs are averaged over RV

and HV timeseries to build ~20s timecourses for the RV and HV, and their timings are compared to those of the GS and DMN.

2.2 Method

The main algorithm to detect a QPP is correlation-based and iterative, identifies similar segments of a functional scan and averages them for a representative spatiotemporal template. Its steps are as follows (Figure 1). A segment with a preset duration is initially selected. Sliding correlation of this initial segment with the scan is calculated. Local maxima above a preset threshold, or maxima for brevity, in the sliding correlation timecourse are identified. Segments of the scan starting at these maxima are averaged together to create a template. The abovementioned process is then repeated with the template in place of the initial segment and the process repeats until negligible change between iterations is reached. Output of the algorithm after it converges are (i) a template, that is the average of a set of similar segments, and (ii) a sliding correlation timecourse with its maxima indicating the start of the contributing segments to the output template, in other words, the occurrence of the output template. The median of correlation values at maxima and the median of times between successive maxima respectively are referred to as the strength and periodicity of the output template.

2.2.1 Robust detection of QPP

The *original method* [16] to detect the QPP involved running the main algorithm for a limited number of randomly selected initial segments, using hierarchical clustering on the resulted templates, and selecting the template that has the maximum average correlation with the rest of the templates in the biggest cluster as the most representative template or the QPP. However, inspecting some initial segments may results in a template that has a low strength or periodicity [18]. Inspecting some other initial

segments may result in the same template but at different phases [18]. Taken together, the original method might not reproducibly detect the best pattern.

To ensure robust detection of QPP, all possible initial segments were inspected [18], starting from the individual-level analysis, using a computationally efficient Matlab script, in terms of analysis time and memory usage. For each resulted template corresponding to each initial segment, the values of its correlation timecourse at supra-threshold local maxima were summed and the template with the highest sum was designated as the most representative template or the QPP [18] (Figure 2). Selected in this way, the QPP is guaranteed to have both high strength and high periodicity relative to other templates.

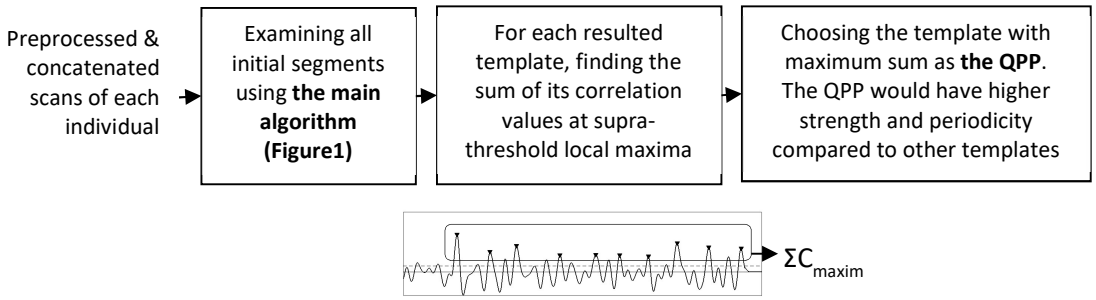

Figure 2 Robust detection of the QPP for an individual.

In order to obtain the group-level QPP by averaging the individual QPPs, the first step is to phase-adjust each individual QPP, in other words, to have a spatiotemporal template whose timecourse at a certain node starts around zero at timepoint 1 and reaches maximum during the first half of the cycle.

To phase-adjust a QPP, the following steps were implemented (Figure 3). The QPP was compared with all other templates, corresponding to all the inspected initial segments.

Templates with comparison values greater than 0.88 were kept since they were similar to the QPP though they could have different phases. These templates were sorted, in descending order, based on their sum of correlation at maxima, the same metric previously used to select the QPP. The first template whose left early visual area (left V2 or parcel 184, the seed for phase-adjustment, which I chose arbitrary, at an early stage of my work) had the following conditions was designated as the phase-adjusted QPP: timepoint 1 being near-zero, average of the first three timepoints being positive, maximum occurring during the first half of the cycle and before minimum. These conditions were set based on the abovementioned definition of the phase-adjust. If no such template was found, only the last condition was enforced. When comparing the QPP with other templates, a fine phase-matching procedure was performed (Figure 3d), by time-shifting other templates, a few timepoints forward and backward, and taking the maximum Pearson correlation across different time-shifts. When the QPP and other templates were compared for all individuals, a bimodal distribution was obtained, and the threshold 0.88 used above is the peak of the smaller mode (Figure 3c).

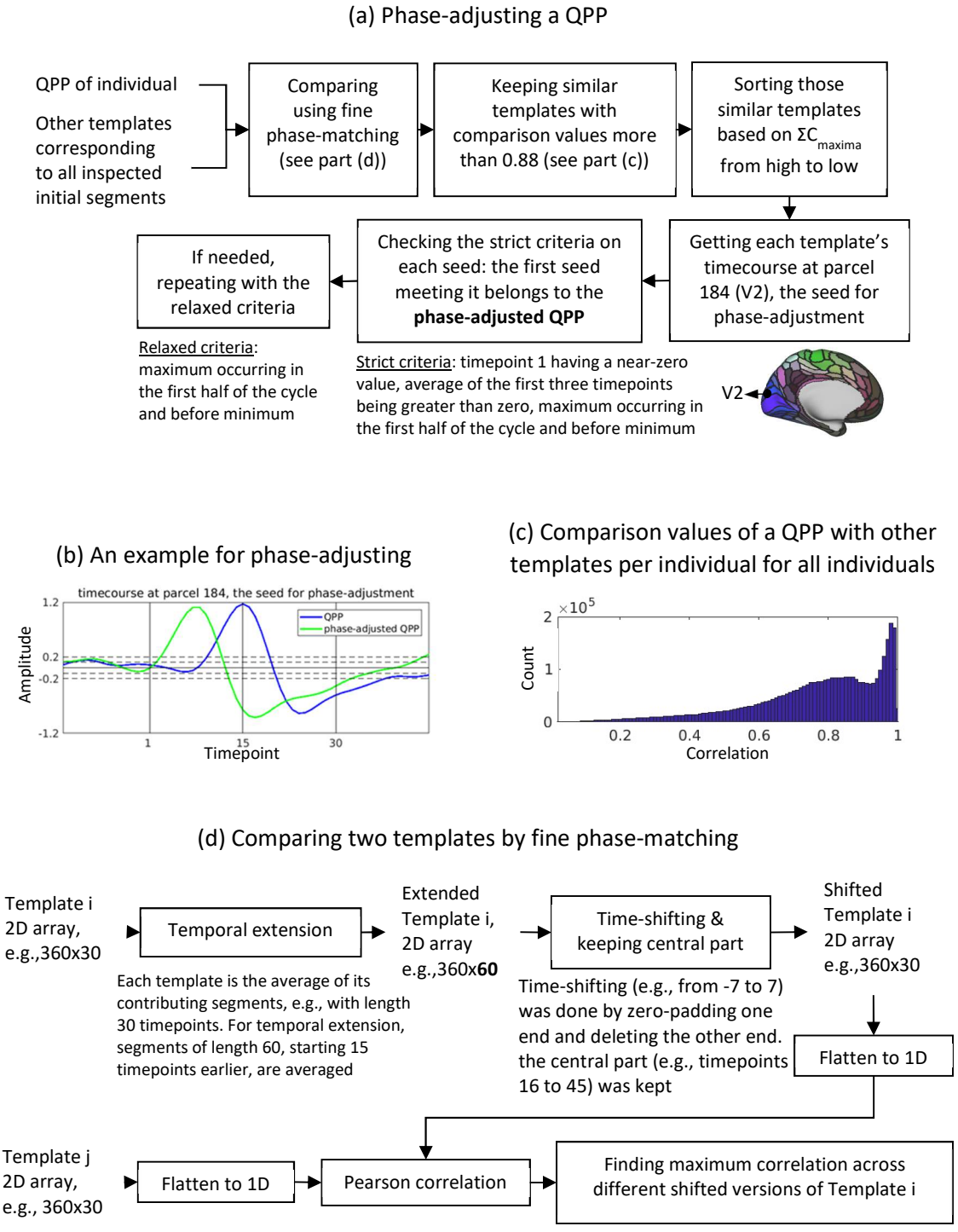

Figure 3 Phase-adjusting a QPP and comparing templates by fine phase-matching. (a) Phase-adjusting the QPP of an individual. (b) An example for phase-adjusting. (c) Comparing QPP of an individual with other templates corresponding to other inspected initial segments results in a bimodal distribution, with lower mode (0.88) taken as the threshold in part (a). (d) Comparing templates by fine phase-adjusting.

To obtain group QPP, the following steps were implemented (Figure 4). The phase-adjusted QPP of all pairs of individuals were compared, using the fine phase-matching procedure (Figure 3d), and the matrix of inter-individual comparison was constructed. The sum of each row of this matrix was calculated, and the individual with the maximum sum was designated as the reference individual since he/she was the most similar to others. The phase-adjusted QPP of all the individuals were fine phase-matched to that of the reference individual and averaged to obtain *a prior template*. This prior template was further correlated with the scans of all the individuals, the supra-threshold maxima in the correlation timecourse were identified, and the fine-tuned contributing segments starting at maxima were averaged to obtain the group QPP. The last stage was implemented to mitigate the imperfections in phase-adjusting the individuals' QPPs, and to ensure that any group QPP is just a simple average of similar segments across the individuals.

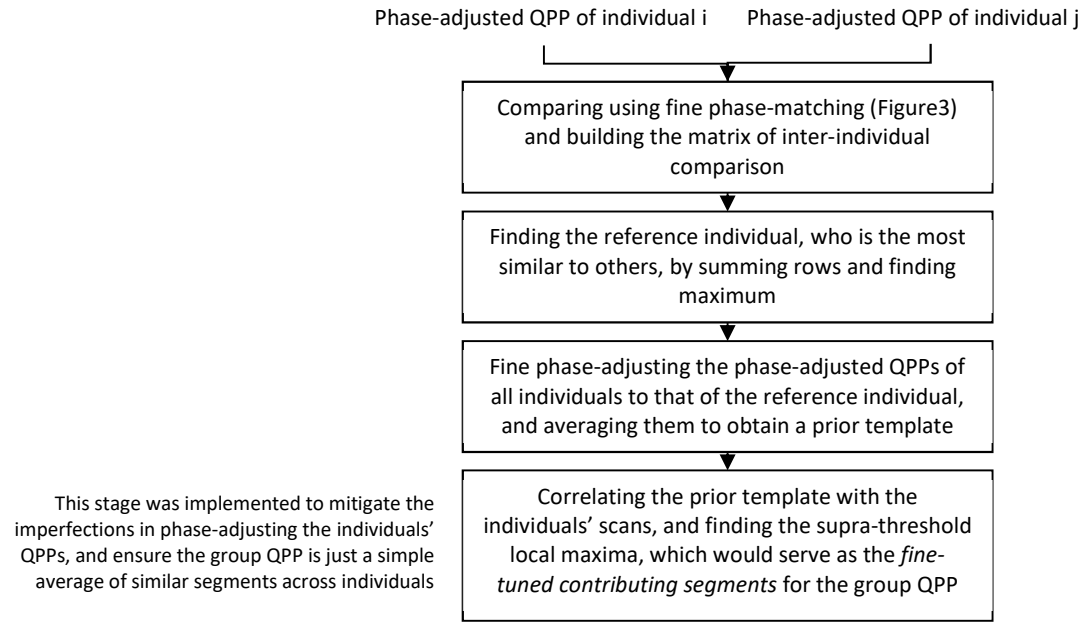

Figure 4 Obtaining the group QPP by fine-tuned averaging.

2.2.2 Data, preprocessing and free parameters

Data. Minimally preprocessed grayordinate and FIX de-noised resting-state scans were adopted from HCP S900 dataset [24]. Grayordinate includes ~31K surface-based cortical vertices per hemisphere and ~30K subcortical voxels and excludes the white-matter and CSF voxels. All 817 individuals with complete four resting-state fMRI (rsfMRI) scans were considered for further analysis, regardless of the head motion levels, since head motion does not majorly influence the infraslow (<0.1Hz) quasi-periodic patterns [18] (will be shown here as well). Each HCP rsfMRI scan has 1200 timpoints and is ~15min, fMRI repetition time (TR) or time resolution is 0.72s, and four scans were taken in two successive days, with two back-to-back scans around the same time in each day.

Preprocessing. The timeseries of each cortical vertex and subcortical voxel per scan underwent the following additional steps (Figure 5a): demeaning and filtering, nuisance regression, and parcellation.

Preprocessing: demeaning and band pass filtering. After demeaning, a fourth order Butterworth filter with 1dB cutoff frequencies of 0.01 and 0.1Hz was applied using Matlab fdesign and filtfilt functions. To minimize transient effects, zero pads were inserted at both ends, before filtering and removed afterwards.

Preprocessing: nuisance regression. White matter (WM) and cerebrospinal fluid (CSF) signals, which were obtained by demeaning and filtering (0.01-0.1Hz) the timeseries that HCP provides, were regressed. Unless noted otherwise, the gray matter (GM) signal was also included among the regressors. The GM signal was obtained by averaging all the timeseries resulted from the previous step.

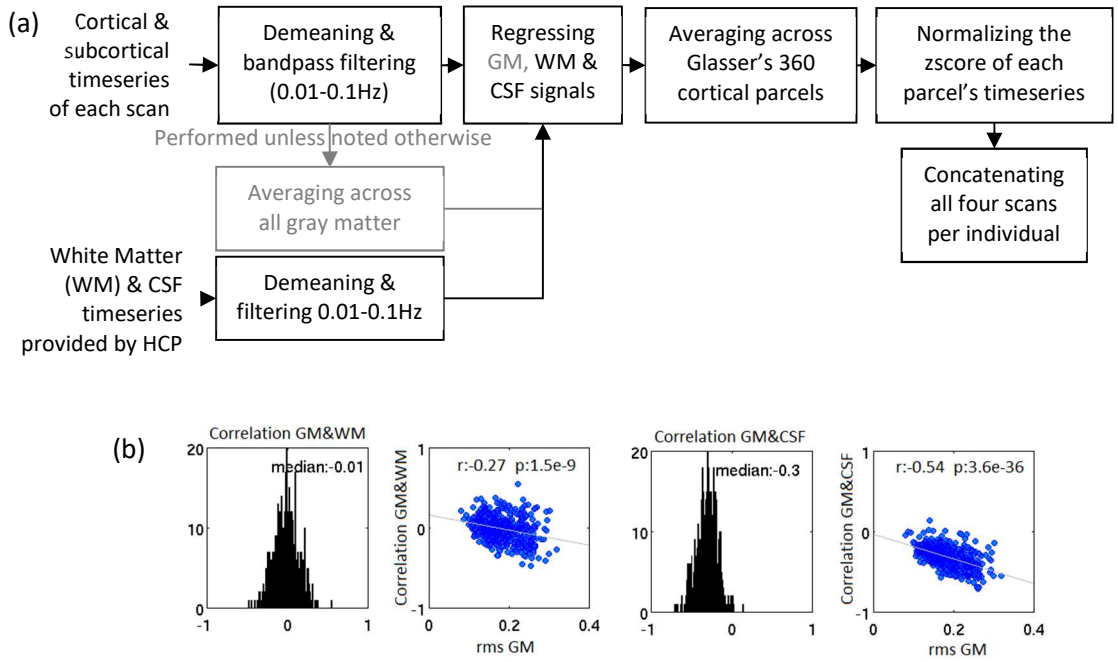

Figure 5 Further preprocessing performed on the FIX denoised grayordinate rsfMRI timeseries of HCP S900 dataset (a). GM and CSF are negatively correlated (b), particularly in individuals with stronger GM or higher root mean square (rms) of GM.

When the GM signal is also regressed, the nuisance regression is referred to as the global signal regression or GSR, the rational is as follows. In the volumetric format, the global signal (GS) is the average of all the voxels' timeseiries that are inside the brain mask. Therefore, the GS entails signals from mainly three tissue types, GM, WM, and CSF. In the grayordinate format, three separate signals for the GM, WM and CSF are available, therefore, we considered three separate nuisance regressors at the same time and refer to them as the global signal.

Note, the GS is strongly correlated with the GM [25] (based on which the GS is viewed as a neuronal signal). The GS and GM are weakly and negatively correlated with the CSF (Figure 5b) [25] (which is linked to the overall cerebral blood circulation).

Considering the GM, WM, CSF as separate regressors does not cause error in our codes, despite the slight correlation between each pair.

In the literature, WM and CSF signals are commonly regressed [23], however, including the GS (precisely, sum of all voxels inside the brain, which is strongly correlated with the GM) along those nuisance regressors is a controversial practice [20-23]. The relationship between QPPs and the GS are elaborately examined in a later section. As will be shown, GSR has negligible effect on the QPPs 1-3 obtained post GSR, which shows these QPPs are not artifacts of GSR. This also implies the contributing segments of these QPPs, on average, have negligible global fluctuations at the first place.

Preprocessing: parcellation. To decrease the analysis time and memory usage, the spatial dimension of rsfMRI timeseries was reduced from ~92K cortical vertices and subcortical voxels to 360 cortical parcels of Glasser's parcellation scheme [26] by averaging the timeseries of cortical vertices across each parcel. Each parcel's timeseries was then norm zscored - note, Glasser's scheme is based on the multimodal HCP data including rsfMRI.

Crucially, in detecting a QPP, reducing the spatial dimension by parcellation can be considered as a very effective expediting step to identify the contributing segments of that QPP. To have a QPP with original spatial resolution in grayordinate (~92K cortical vertices and subcortical voxels), or generally in volumetric voxel-space, its contributing segments can be averaged in grayordinate or voxel-space (Figure 6). A supporting analysis, performed on 35 randomly selected individuals, showed very similar template is obtained when using the grayordinate timeseries to identify the contributing segments, particularly in the group-level, compared to only using cortical parcels' timeseries. Note,

for this supporting analysis, the two resulting templates, each with a spatial dimension of ~92K, were compared using the fine phase-matching procedure (Figure 3d).

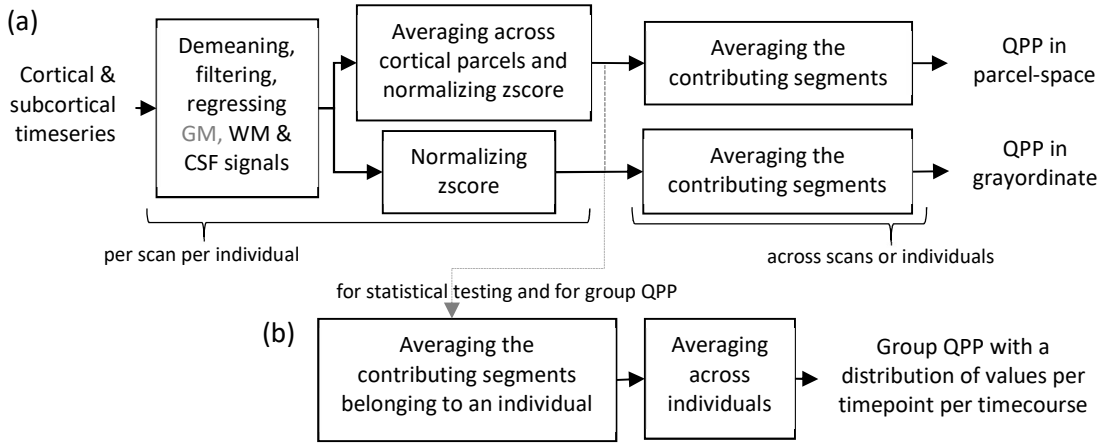

Figure 6 Obtaining a QPP in grayordinate in addition to parcel-space, either for each individual or for group. The contributing segments of the QPP are identified based on a parcel-space analysi (only cortical parcels in the current work), while grayordinate includes ~92K cortical vertices and subcortical voxels.

Preprocessing: concatenating. To detect QPP per individual, four scans of each individual were concatenated (4800 timepoints, ~1hr).

Free parameters. QPPs in healthy adult humans is approximately ~20s long [16,18]. Therefore, the duration of QPP was set to 30 timepoints (21.6s) and 4×(1200-30+1)=4684 initial segments were inspected per individual (Figure 2). Correlation threshold for the first iteration of the main algorithm (Figure 1) was set to 0.2 and for the rest of iterations was set to 0.3.

2.2.3 Detecting other QPPs

Thus far, only one QPP has been reported [16,18], hereon called QPP1, which we robustly detected based on the described improvements and the free parameters, at the individual and group levels. To examine the existence of other QPPs, *QPP1 was regressed and residual scans (after QPP1 regression) were reanalyzed* (Figure 7).

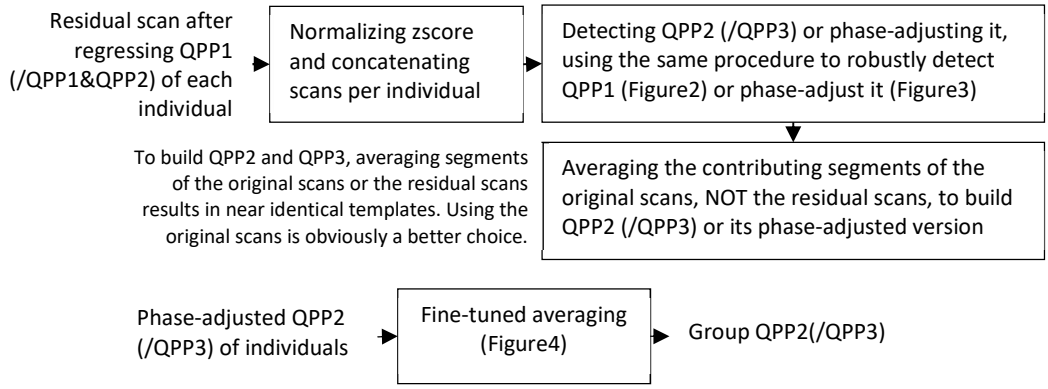

Figure 7 Detecting QPP2 or QPP3.

Two methods for regression was implemented both using GLM.

First, scan-wise regression (Figure 8a), where QPP1 of each individual was convolved with its correlation timecourse to build a regressor for each rsfMRI scan. Since QPP is a spatiotemporal pattern and its timecourses are different for each parcel (i.e., spatial dimension), convolving each QPP with its correlation timecourse and regressing from each scan was done per parcel (i.e., to regress each QPP, each of its 360 timecourses was convolved with the correlation timecourse, and was regressed from the corresponding parcel's timeseries).

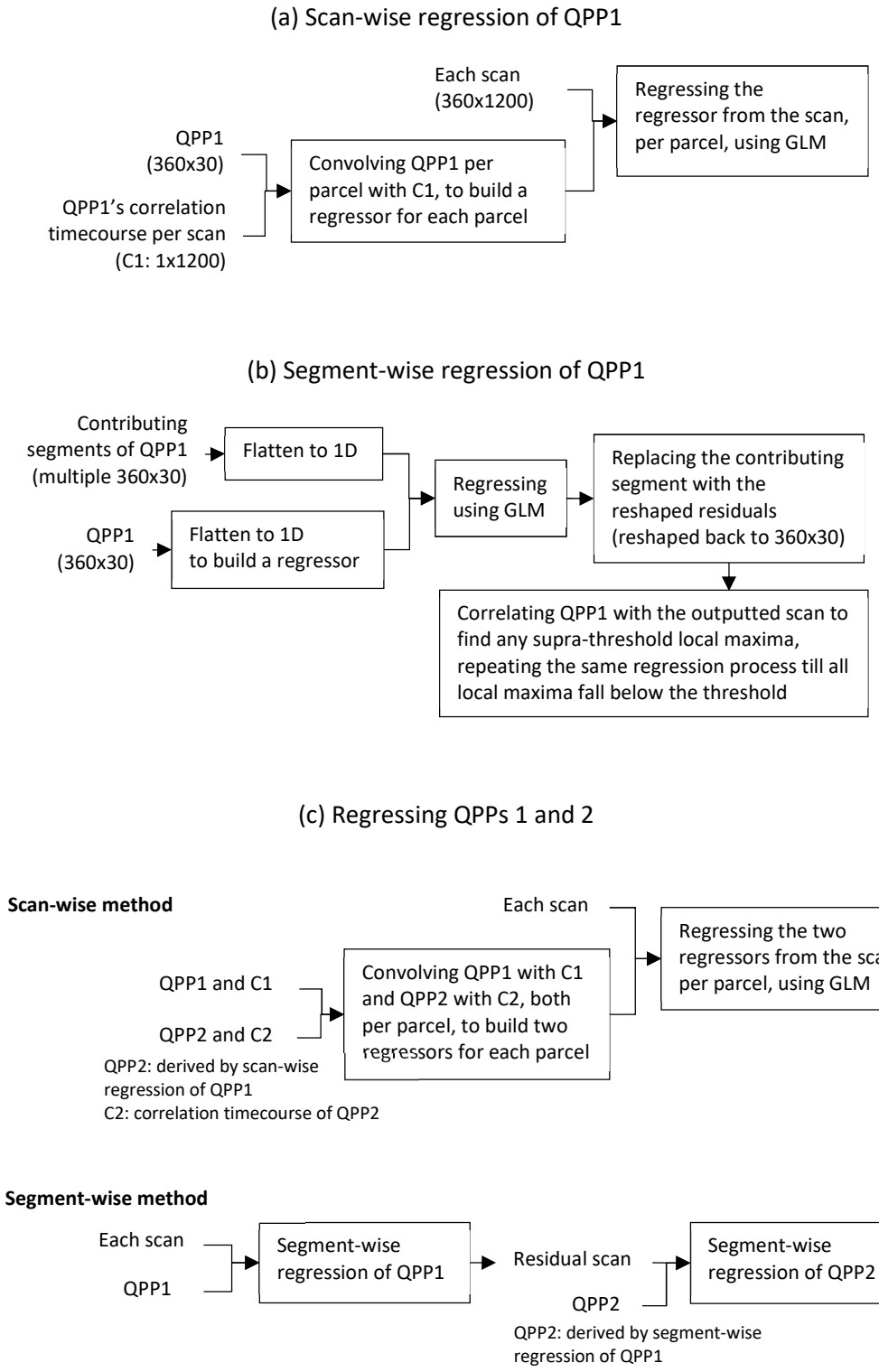

Figure 8 Scan-wise (a) and segment-wise (b) regression of QPP1. Regressing QPPs 1 and 2 (c).

Second, segment-wise regression (Figure 8b), where QPP1 of each individual, a 2D array of 360x30, was flattened to a 1D array of 1x10800 and was regressed from each of its contributing segments, which were flattened to 1D arrays as well. Each contributing segment was then replaced by the reshaped residuals (reshaped back to 2D array of 360x30). To ensure no supra-threshold maxima exists in the residual scan, QPP1 was correlated with the residual scan and was regressed from the segments corresponding to any detected supra-threshold maxima.

After regressing QPP1 of each individual per scan, the residual scans per individual were norm zscored and concatenated, QPP2 was robustly detected based on the same improved method and free parameters described earlier, first at the individual-level then at the group-level (Figure 7).

QPP1 and QPP2 of individuals were further regressed and the residuals were reanalyzed to robustly detect QPP3, using similar method and parameters, for individuals and group (Figure 7). In regressing QPP1 and QPP2, the same regression method to derive QPP2 was used (Figure 8c). In that, when using the scan-wise method, we made two regressors, per parcel, by convolving the QPP1 with its correlation timecourse and convolving the QPP2 with its correlation timecourse, and regressed them, per parcel, in a single step from the scan. When using the segment-wise regression, we regressed QPP1 and QPP2 in two sequential steps. As will be discussed, we decided to limit the scope of this thesis to QPPs 1 to 3.

Crucially, as will be shown, to build QPP2 and QPP3, averaging their contributing segments based on the original scans or the residual scans (using either of the regression methods) results in near identical templates. *In other words, QPP2 and QPP3*

exist in the original scans, just as QPP1 exists. Using the original scans is a better choice, because there would be no concerns about possible distortions due to regression. Therefore, we built QPP2 and QPP3 based on the original scans. *Moreover,* as will be shown, QPPs 1-3 are indeed three different templates, and QPPs 2-3 derived based on the two regression methods are identical. *Note,* comparison of any pairs of templates, to support the abovementioned statements, was based on the phase-adjusted version of templates and the fine phase-matching procedure (Figure 3d). Such comparisons were performed at the individual-level to obtain a distribution, and particularly to have minimum or maximum values, whichever shows the worst case.

2.2.4 QPPs coarse characteristic, basic metrics, relative occurrence, and reproducibility

Coarse characteristic. All three QPPs involve a 30-timepoint (~20s) cycle of activation and deactivation of different brain areas with different timings, such that the overall activity within these patterns resembles the macroscale resting state networks (RSNs), as will be shown and discussed. Coarse characteristic of a QPP, as we defined, is the constellation of correlation between the RSNs within the duration of a QPP. To quantify, Yeo's seven RSNs [12] were adopted. The 30-timepoint timecourses of each group QPP were averaged across the parcels belonging to each RSN. This resulted in a 2D array of 7x30 for each group QPP, for which the 7×7 Pearson correlation matrix was calculated.

Basic metrics. To obtain a metric to reflect how well a QPP represents its contributing segments, the median of the correlation values at the supra-threshold maxima in the sliding correlation timecourse of that QPP was calculated, named *QPP strength*. Furthermore, to obtain a metric that shows how often the contributing segments to the

QPP occur, the median of the time between successive supra-threshold maxima was calculated, named *QPP periodicity*.

Relative occurrence. To examine how the QPPs occur relative to one another, in other words, how their contributing segments are located in time versus one another, the following was implemented. For the contributing segments of QPPi, i=1,2,3, the number of the immediately following contributing segments of QPPj, j=1,2,3, were counted. A 3×3 transition count matrix, showing the counts from QPPi to QPPj, was calculated per individual, and averaged across the individuals. The average time between QPPi to QPPj was also calculated.

Reproducibility. To examine whether QPPs are reproducible across different population of individuals, for each pattern, the 817 individuals were randomly divided into two subgroups of 408 and 409, 100 times, and the subgroup QPPs were compared with one another as well as with the main group QPP.

2.2.5 Contribution of QPPs to functional connectivity

To better understand QPPs, as intrinsic patterns of brain activity that might serve self-organization, after robust detection and coarse characterization, the next step can be to show the extent of their contribution to functional connectivity (FC), the most widely used metric reflective of the brain's intrinsic organization. To show the contribution of QPPs to FC, we compared two FC matrices built based on the original timeseries and the residual timeseries after regressing QPPs 1-3.

To build each FC matrix, the Pearson correlation between all pairs of cortical parcels' timeseries were calculated per individual, and the FC matrices of individuals were averaged using Fisher transform. Null distribution for the FC values were built, by phase-

randomizing [16,18] the original and the residual timeseries and again averaging across individuals. Before building each FC matrix, 360 Glasser's cortical parcels were re-arranged according to Yeo's Seven RSNs, e.g., first the parcels that belong to the visual network (VN) in the right and left hemispheres were located, then the parcels that belong to the somatomotor network (SMN) in the right and left hemispheres, etc.

2.2.6 QPPs versus global signal and head motion

Because QPPs are macroscale and recurring patterns, they might have relationships with non-neuronal sources of BOLD signal fluctuations, such as head motion or slow variations in the respiration and heart rate, which can influence the whole brain [20] and are inherently repetitive. To better understand QPPs, it is essential to inspect such relationships. The simplest and most common summary metric of signal fluctuations across the whole brain (global activity) is the global signal (GS), a 1D timeseries obtained by averaging all timeseries inside the brain [20], described in the preprocessing section as well. Since non-neuronal sources of signal fluctuations (motion and physiological variation) contribute to the GS [20], and since the GS is a simple and common metric, we first inspected the relation between QPPs and the GS.

As the first step, the gray matter (GM) signal was NOT included as a nuisance regressor in the preprocessing stage – as noted before, the GS is strongly correlated with the GM. The *primary approach* was to re-average the contributing segments of QPPs 1-3 (identified earlier based on the GM-Regressed timeseries) using the new timeseries and compare the results with QPPs 1-3.

Additionally, a *complementary path* was pursued. The new timeseries was reanalyzed to detect QPPG of individuals, using the same improved method and free parameters.

Occurrence of QPPG relative to other QPPs was examined by simply including it in the transition count matrix described earlier, which resulted in a 4x4 matrix showing the counts from QPPi to QPPj, i,j=G,1,2,3.

A *very noticeable characteristic within QPPG* was the individual variability in the *spatial extents (SEs)* of strong negative and positive correlation between the nodes of the DMN and other brain areas. To quantify, the following was implemented (Figure 9). As a prominent neuroanatomical region in the Glasser's scheme that very likely contains the nodes of the functional default mode network (DMN), we considered the left posterior cingulate cortex (LPCC). Each of 14 parcels of LPCC were taken as a seed, one at a time. For each seed, the Pearson correlation between the QPPG's timecourse at that seed with the QPPG's timecourses at all 360 parcels was calculated. These correlation values were summarized in a histogram with bin centers -0.9:0.2:0.9, i.e., 14 histograms in total, with bins showing number of parcels or the spatial extent. The histogram with the maximum number of parcels in the first bin was selected. For each individual, the two SEs were reported according to the first and the last bin of the selected histogram, respectively. In case of zero count for the first bin in all 14 histograms, the QPPG's timeseries at all 14 seeds were averaged. One histogram of correlation values with all 360 parcels was calculated, based on which the two SEs were reported.

Both SEs are wide-range continuums across individuals. For further understanding, the following steps were taken. *First*, the SEs were correlated with the root mean square (rms) of GS, indicative of GS fluctuation level. Note, we use the term rms of GS but in fact we included the rms of the cortical signal (CS) here, because this part of the analysis is only based on the cortical parcels, and also CS, GM signal, and GS are all strongly correlated.

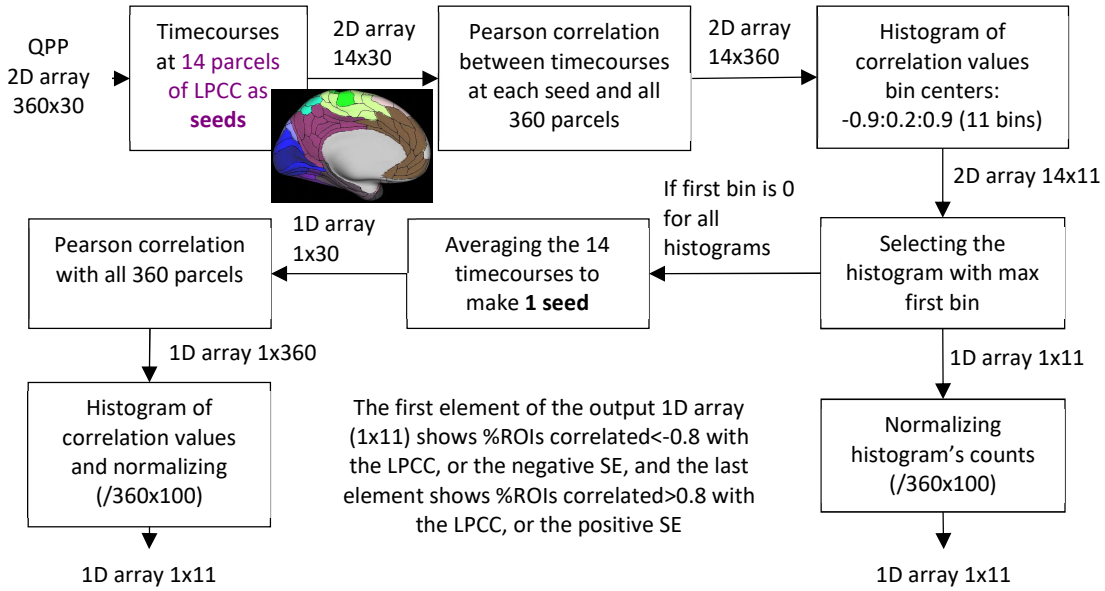

Figure 9 Calculating the spatial extents (SEs) of strong negative and positive correlation within a QPP

Second, the SEs were calculated for QPP1 for comparison, using similar approach. *Third,* two subgroups were formed by including 200 individuals with the highest negative and positive SEs (see Figure 17c), named, *high anti-correlators and high correlators*. Subgroup QPPGs were obtained by fine-tuned averaging the individual QPPGs.

As suggested by the subgroup QPPGs, nodes of the DMN have systematic timing difference with other brain areas, which could explain the wide-range continuums of the spatial extents. To quantify, timeslots of the GS, a 1D timeseries, were averaged according to the contributing timeslots of the QPPG, to obtain a 30-timepoint timecourse for the GS. Precisely, the fine-tuned contributing timeslots of each subgroup QPPG were considered. Averaging the timeslots of the GS was performed first per individual and later across individuals per subgroup, to obtain error bars for each timepoint for the GS timecourse. Here again, we used the term GS but in fact we included the cortical signal,

specifically the average of all 360 parcels' timeseries, each of which were norm zscored. Similarly, a 30-timepoint timecourse for the DMN was made with error bars per subgroup. The difference between peak times of the GS and DMN timecourses were compared using dependent t-test. In order to include all 817 individuals, the procedure above was repeated per individual QPPG and the difference between peak times of the GS and DMN timecourses were calculated. The resulted distribution was compared to a zero-mean null distribution using dependent t-test.

Together, our complementary path in characterizing QPPG resulted in a novel suggestion about the spatiotemporal course of the global activity, thus far always summarized into a 1D timeseries, or the global signal. As will be shown, *QPPG also enriches our interpretations regarding* the fluctuations of the physiological signals and arousal, appearing in the next section and the next chapter, respectively. *However,* these implications depend on a reasonable coincidence of QPPG, i.e., its contributing segments, with the fluctuations of GS. To examine such coincidence, the sliding correlation timecourse of QPPG was first convolved with the average of QPPG across all parcels. The Pearson correlation of the outcome with the GS was then calculated. Moreover, basic metrics of QPPG were quantified.

Finally, since high positive SE within QPPG might have a relationship with the high head motion level [20,23], the following approach was taken. Two subgroups of 60 individuals with the lowest and the highest head motion levels were formed and the continuums of positive and negative SEs within QPPG were qualitatively compared. We further selected 12 individuals with the highest positive SE from each subgroup, averaged their QPPGs by fine-tuning and qualitatively compared the results with the previously obtained subgroup template of 200 high correlators. The most common metric for head

motion is based on frame-wise displacement (FD), a timeseries that reflects timepoint-by-timepoint shifts and rotations. Temporal percentage of FD larger than a threshold and average FD were taken as the criteria for subgrouping.

2.2.7 QPPs versus physiological signals

QPPs, as macroscale and recurring patterns, might have a relationship with the slow physiological sources of BOLD signal fluctuations, the most common being the slow variations of the respiration rate and depth and heart rate, which can affect the whole brain [20-23] and are repetitive. Although these physiological variations contribute to the GS, examined in the previous section, it is essential to directly inspect their relationship with QPPs, since *physiological and neuronal variations can influence one another*.

To inspect, first, the raw physiological traces were preprocessed and two timeseries for the *respiratory variation (RV)* and *heart rate variation (HV)* were calculated according to the procedure described in appendix A and Figure 10. Briefly, RV at each timepoint was calculated as the standard deviation of the respiratory trace within a sliding window of ~ two respiratory cycles, taken as 7.2s or 10 timepoints, centered around that timepoint [21]. Similarly, HV was calculated as the average of time between successive peaks of the cardiac trace within a sliding window of 7.2s [21].

Note, RV and HV timeseries turn negatively correlated (~-0.4), see Figure 10d for an example of timeseries during scan. *Increase in RV indicates deeper and more spaced breaths and decrease in HV indicates faster heart beats.*

Out of 817 individuals, 487 have acceptable physiological data to be included for further analysis.

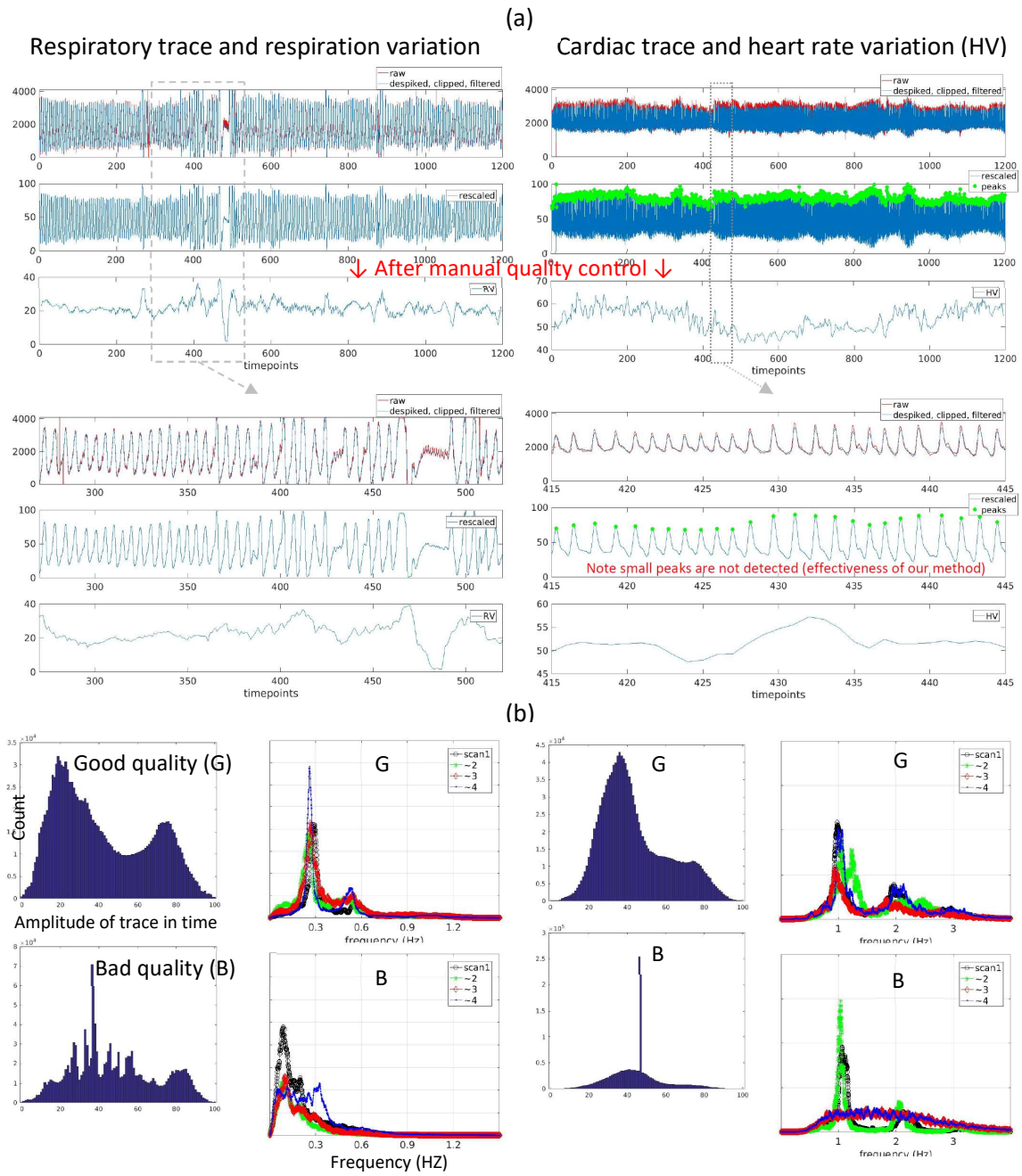

Figure 10 Calculating timeseries of the respiration variation (RV) and heart rate variation (HV). (a) Preprocessing of the respiratory and cardiac traces. (b) Histograms of amplitudes in time domain and spectra in frequency domain of the preprocessed respiratory (left) and cardiac (right) traces for manual quality control. (c) Histograms of standard deviations of RV and HV per scan to identify the outlier scans, for additional quality control. (d) Example of RV and HV timeseries which are negatively correlated. (e) Respiratory and cardiac response functions (RRF and CRF) that are respectively convolved with RV and HV for estimates of fMRI signal fluctuations induced by slow physiological variations. $RRF=0.6\ t^{2.1}\ exp(-t/1.6)-0.0023\ t^{3.54}\ exp(-t/4.25)$. $CRF=0.6\ t^{2.7}\ exp(-t/1.6)-16/\sqrt{(18\pi)}exp(-(t-12)^2/18)$.

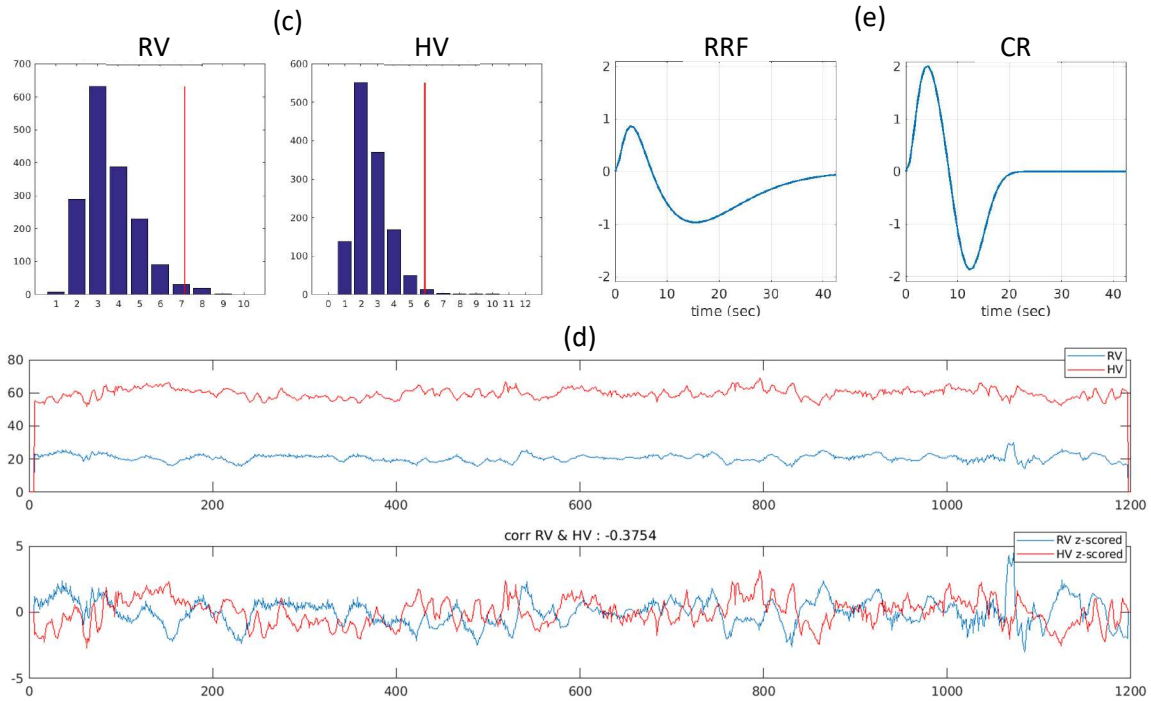

Figure 10 continued

A *common approach* to inspect the influence of RV and HV is to convolve these timeseries by the respiratory and cardiac response functions (Figure 10e) to obtain estimates of induced fMRI signal fluctuations [20-23]. These estimates are further regressed from the fMRI timeseries and the metrics of interest are compared before and after physio-regression. An optimal lag for each of the two regressors for each brain area can be calculated and included as well. This common approach was taken, only QPPG was redetected, and the SEs within QPPG were compared. As will appear, *such approach is not effective enough, particularly when studying the dynamic regimes of coherent activity*, hence, we did not redetected QPPs 1-3.

A *customized approach* was taken to inspect the relationship between all QPPs and slow physiological variations. Similar to the previous section on QPPs versus the GS,

30-timepoint timecourses for the RV and HV were obtained, with error bars for each timepoint, by averaging the fine-tuned contributing timeslots of (sub)group QPPi (i=G,1,2,3), first per individual then across individuals, using WM-CSF-Regressed rsfMRI timeseries, without and with physio-regression. The difference between timings of the timecourses of the RV, HV, GS, DMN, even SMN and VN were qualitatively compared. Before averaging the timeslots, RV and HV timeseries were norm zscored, similar to each parcel's timeseries, to have comparable amplitudes between all the timecourses.

2.3 Results

QPPs 1-3 all involve a ~20-second cycle of activation and deactivation of different brain areas (Figure 11), such that the RSNs and their relative timing of activity are readily observable. However, within each QPP, the constellation of correlation between the RSNs is unique (Figure 12). In QPP1, the unimodal networks of SMN and VN are correlated with the attention networks of DAN and VAN and together are anticorrelated with the networks of DMN, FPN and LN. In QPP2, the unimodal networks are correlated with the DMN and together are anticorrelated with the task positive networks of FPN, VAN, and DAN, with the DAN exhibiting relatively weaker correlation values with other networks (the reason will be evident in the next chapter). In QPP3, the unimodal networks are anticorrelated with one another, the VAN and DMN are correlated with the SMN, and the DAN and FPN are correlated with the VN.

Comparing QPPs 1-3 at the individual-level quantitatively verifies that they are indeed different patterns, with the median of correlation between pairs of QPPs being less than 0.2 (Figure 12).

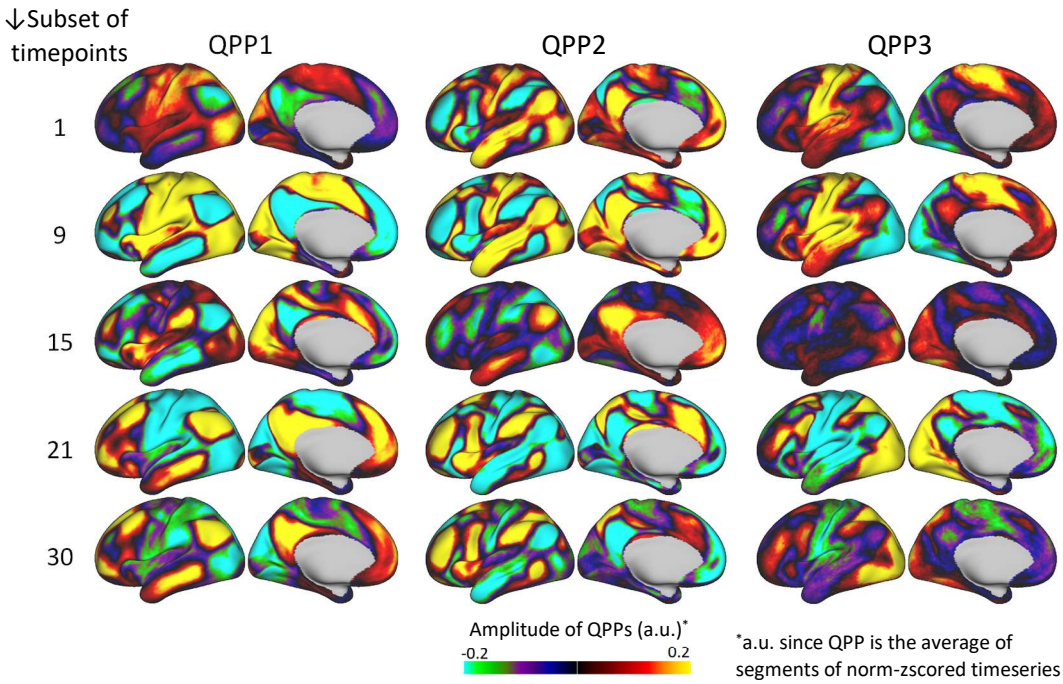

Figure 11 QPPs 1-3, each a spatiotemporal pattern, 30-timepoint or ~20s long, obtained by averaging a set of similar segments across individuals, shown at a subset of timepoints (TR=0.72s). Each pattern involves a cycle of activation and deactivation of different areas, such that resting-state networks (RSNs) and their relative timing are readily observable.

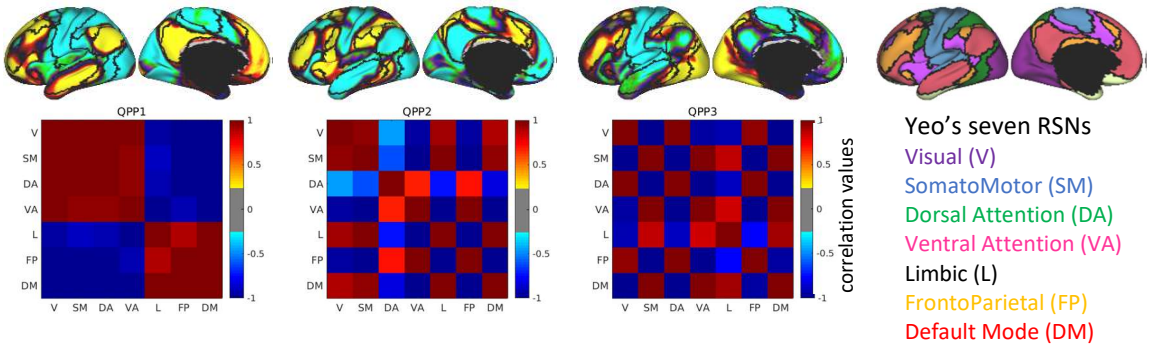

Correlation between QPPs median, max (817 individuals)

	QPP2	QPP3
QPP1	0.18,0.59	0.19,0.63
QPP2		0.12,0.39

Figure 12 Constellation of correlation between RSNs is unique for each QPP. Quantitative comparison at the individual-level confirms that QPPs 1-3 are indeed different patterns.

To build QPPs 2 and 3, averaging their contributing segments based on the original scan or the residual scan results in near identical templates, regardless of the regression method (Figure 13a). This demonstrates that QPP2 and QPP3 exist in the original scans, just as QPP1 exists. QPPs 2 and 3 are reasonably robust to the regression method (Figure 13b). Further inspection revealed individuals for whom the regression method matters, more likely exhibit weaker and less often patterns (average r~0.2, p~0).

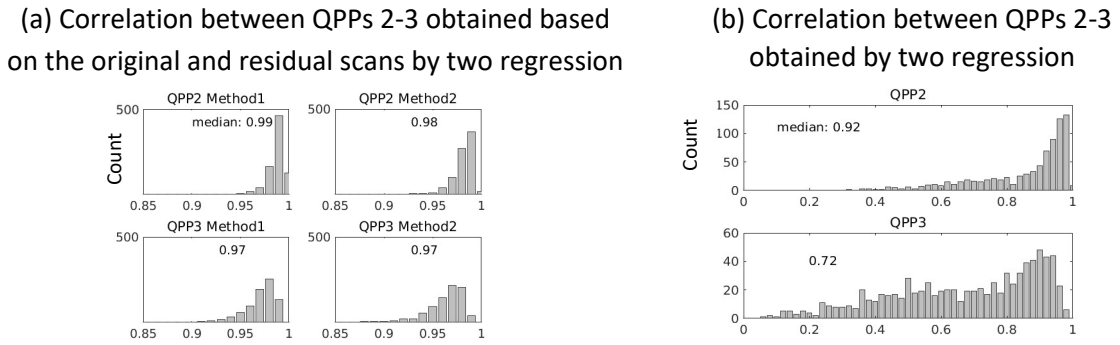

Figure 13 Existence of QPPs 2 and 3. (a) To build QPPs 2 and 3, averaging their contributing segments based on the original scan or the residual scan results in near identical templates, regardless of the regression method. These patterns exist just like QPP1. (b) QPPs 2-3 are reasonably robust to the regression method.

QPPs 1-3 are reasonably strong or representative of their contributing segments, with the median of correlation being 0.4, 0.38, and 0.37, respectively (Figure 14a). Quasi-periodic patterns 1-3 are progressively less periodic, with the median of time between their successive occurrences being 50, 70, and 90 seconds. Each QPP is more often followed by other QPPs than itself (Figure 14b), and expectedly, the more periodic QPP more often follows other QPPs. The average time between occurrences of any two different QPPs is ~18s (Figure 14c), which is close to but less than the duration of QPPs.

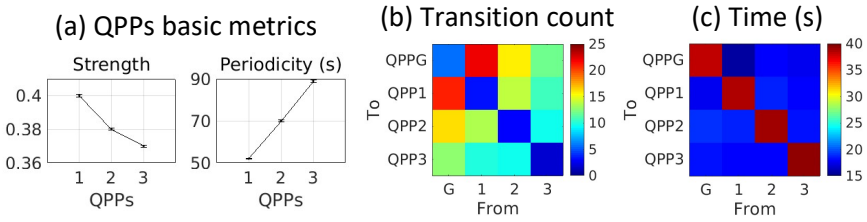

Figure 14 Basic metrics and relative occurrence of QPPs. (a) QPPs 1-3 are reasonably strong but progressively less periodic. (b) Each QPP is more often followed by other QPPs than itself, and expectedly, the more periodic QPP more often follows other QPPs. (c) Average time between any two different QPPs is ~18s.

QPPs are reproducible across different population of individuals. Any two subgroup QPPs, based on a random division of individuals, were near identical to one another and with the group QPP that included all, with medians being 0.99, 0.96 and 0.90.

QPPs are dominant contributors to functional connectivity particularly between RSNs (Figure 15). Regressing each QPP, progressively reduces the variance in FC,

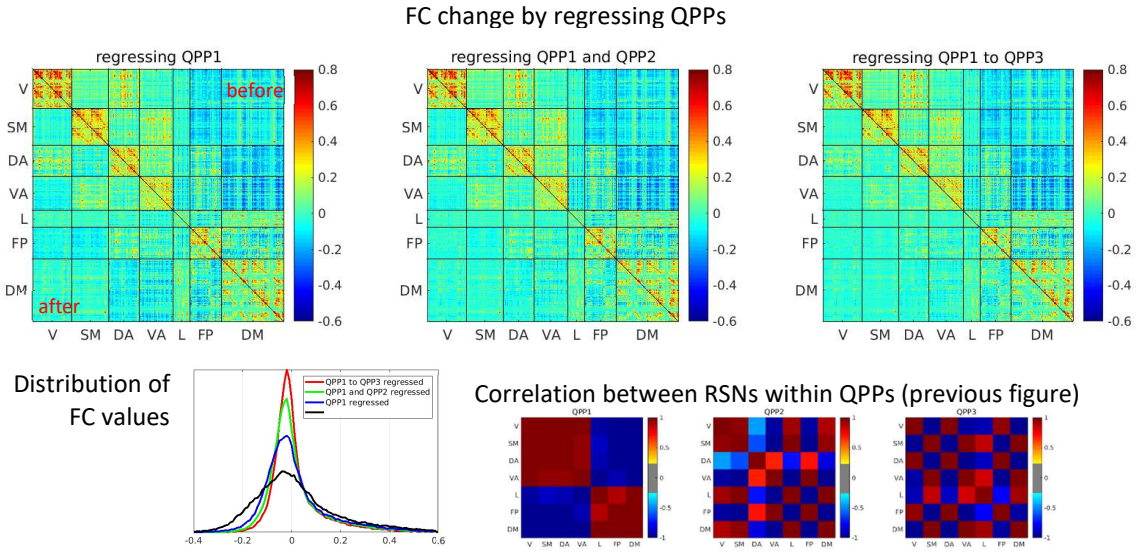

Figure 15 QPPs 1-3 are dominant contributors to FC, particularly between RSNs. Regressing each QPP, progressively reduces the variance in FC.

particularly between RSNs which are anticorrelated within that QPP. Within each RSN, particularly in the VN, SMN and DAN, FC between the homologous parcels of two hemispheres are the least affected by regressing QPPs, which are macroscale patterns (note the parallel bands to the diagonal).The FC distribution after regressing the QPPs is still wider from the null distribution made from the phase-randomized timeseries.

QPPs 1-3 are not artifacts of the global signal (GS) regression (Figure 16), since excluding the gray matter signal as a nuisance regressor does not affect these patterns. This implies the contributing segments of QPPs 1-3, on average, contain negligible levels of GS fluctuations or negligible root mean square (rms) of GS.

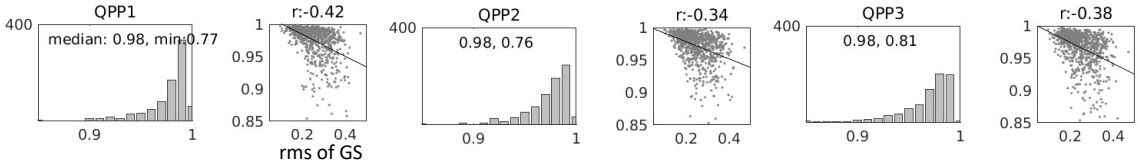

Figure 16 GSR does not affect QPPs 1-3. Histograms and vertical axes show correlation between each QPP and the average of its contributing segments over the timeseries from which the gray matter (GM) signal is NOT regressed. Contributing segments of each QPP were identified based on the GM-regressed timeseries.

Similar to QPPs 1-3, QPPG also involves a ~20s cycle of activation and deactivation of different brain areas (Figure 17a,f), however, its contributing segments are interleaved with those of other QPPs (Figure 14b-c). Within QPPG, the spatial extents (SEs) of strong negative and positive correlation between the DMN and other areas both form wide-range continuums across individuals (Figure 17a-c).The SEs are related to the rms of GS (Figure 17d), e.g., QPPG of an individual who has higher rms of GS likely entails higher positive SE. In contrast, within QPP1, SEs are more homogenous across individuals (Figure 17e).

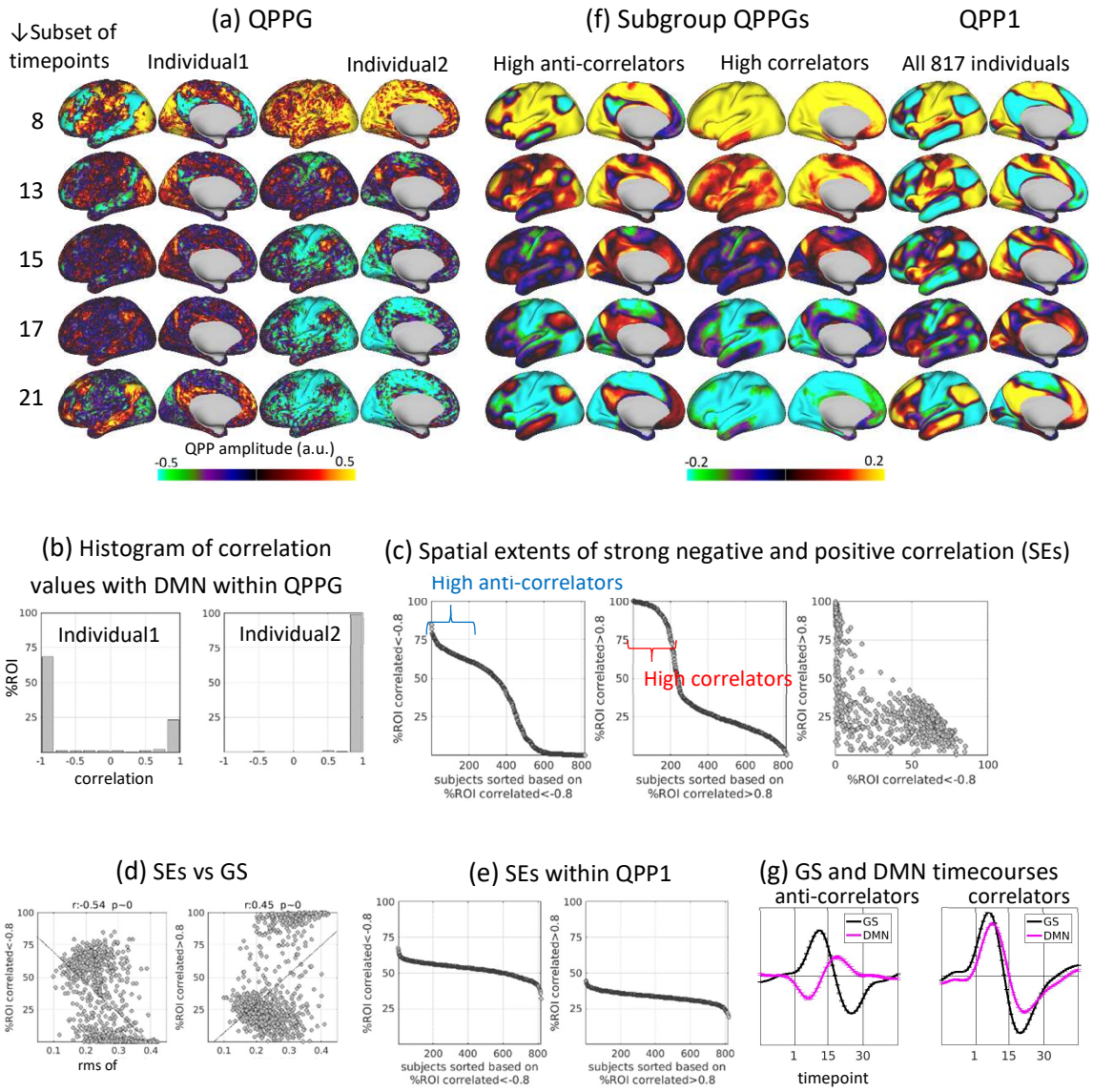

Figure 17 QPPG and the noticeable individual variability in the spatial extents (SEs) of strong negative and positive correlation between the DMN and other areas (a-c). The SEs are related to the root mean square (rms) of GS (d). In contrast, within QPP1, SEs are more homogenous across individuals (e-f). Two subgroup QPPGs, each including the individuals with the highest SEs, reveal the DMN lags the GS (f-g). This lag ranges from near half a cycle for the high anti-correlators to a few timepoint for the high correlators.

Two subgroup QPPGs, each including those individuals with the highest negative or positive SE, revealed the DMN lags the GS within a QPPG (Figure 17f-g). This lag ranges from near half a cycle for the high anti-correlators to a few timepoints for the high correlators, with intermediate values for the rest of the individuals. This lag give rise to the wide-range continuums of SEs and relates to the rms of GS (r=-0.46, p~0). Moreover, for the high correlators, this lag explains a few timepoints that the DMN remains active, contrary to the other areas, as the activity levels switch (Figure 17f). QPPG with a reversed phase exhibit similar relative timing (not shown).

QPPG reasonably coincides with the GS fluctuations (Figure 18a) and is even stronger and more periodic than QPP1 (Figure 18b-c), particularly when the rms of GS is higher. *Taken together,* the complementary characterization of QPPG, that involves a principled timing difference across brain areas and across individuals, offered a novel suggestion about the spatiotemporal course of the global activity, thus far only summarized by a 1D timeseries, i.e., the global signal.

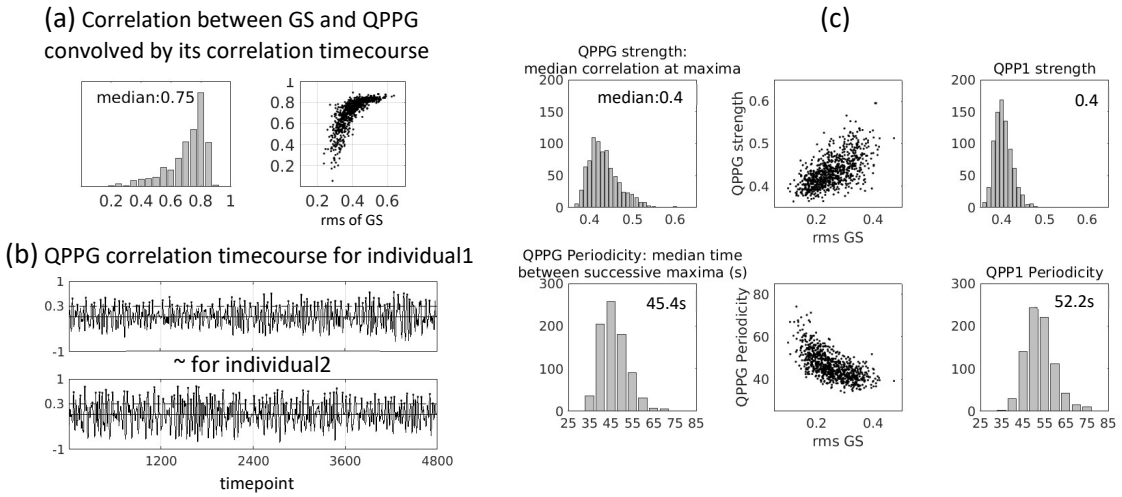

Figure 18 QPPG occurrence and basic metrics. (a) QPPG reasonably coincides with the fluctuations of the GS. (b-c) QPPG is even stronger and more periodic than QPP1. (a-c) Particularly when rms of GS is higher.

Across the two subgroups of individuals with the lowest and the highest head motion levels, both negative and positive SEs within QPPG are still wide-range continuums (Figure 19). Particularly note, QPPGs of the highest movers can exhibit high negative SE or wide-spread anticorrelation. Moreover, regardless of head motion levels, QPPGs with high positive SE exhibit dynamics very similar to the high correlators described previously (not shown). Therefore, such QPPGs are not artifacts of head motion.

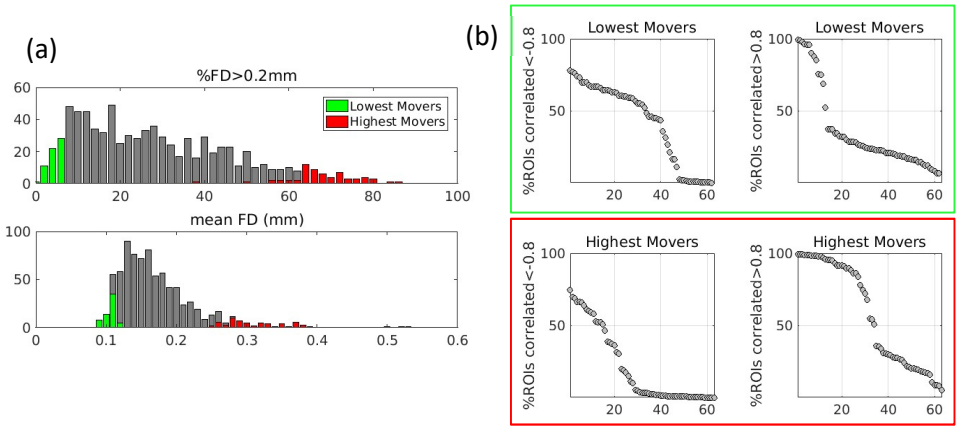

Figure 19 QPPG versus head motion levels. (a) Temporal percentage of the frame-wise displacement (FD) larger than 0.2mm and average FD were taken as the criteria to identify individuals with the extreme head motion levels. (b) Even across individuals with extreme motion, both negative and positive SEs within QPPG are still wide-range continuums.

Regressing the estimates of fMRI signal fluctuations induced by physiological variations, based on the common approach, slightly decreases high values of positive SE and increases low values of negative SE, within QPPG (Figure 20a). Overall, this is in line with the consensus that the physiological variation, particularly respiration, increases the average of correlated activity across macroscale as reflected in the GS or the FC matrix [20-21], and the regression of the corresponding effects increases the average of anticorrelated activity as reflected in the FC matrix [20-21].

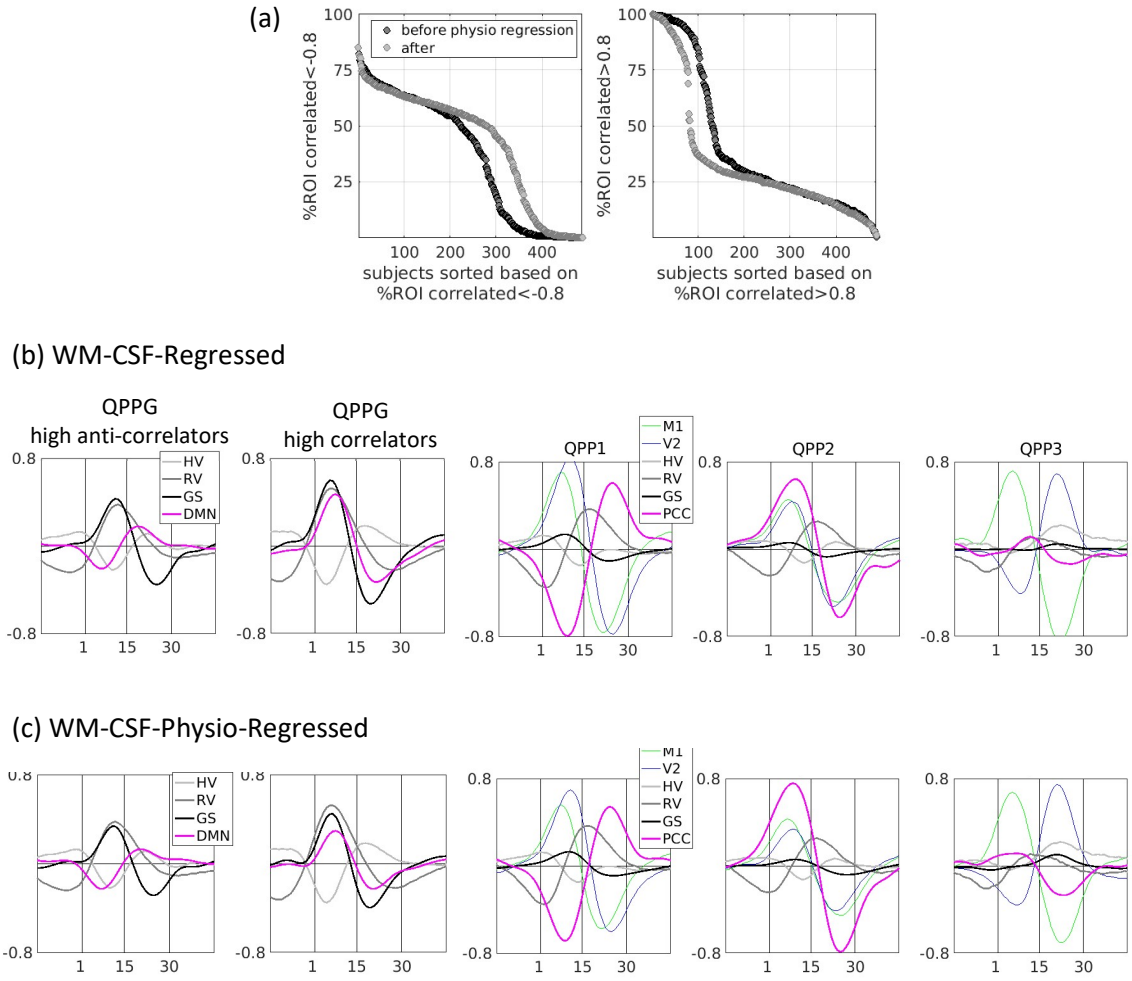

Figure 20 QPPs versus variations in respiration and heart rate. (a) Within QPPG, regressing the physiological variations slightly decreases high values of positive SE and increases low values of negative SE. (b) Within QPPG, respiratory variation (RV) and global signal (GS) peak at the same time. RV peak around the switching time in QPPs 1-3 and dip at the start of the cycle in all QPPs. HV is biphasic and coarsely anti-correlated with RV. (c) Described timings remain unchanged by regressing the physiological variations. Error bars were all small and not shown. Number of included subjects with acceptable physiological data: 478/817, 134/200 high anti-correlators and 105/200 high correlators.

Based on our customized approach, the respiration variation (RV) and the GS peak at the same time, within the QPPGs of both subgroups of high anti-correlators and high correlators (Figure 20b), which is in line with the aforementioned consensus. RV peak around the switching time in QPPs 1-3 and dip at the beginning of the cycle in all QPPs. HV timecourse has a biphasic behavior but roughly negatively correlated with the RV timecourse within all QPPs. Note that the relation between HV and RV timecourses are similar to the relation between their timeseries. Recall, RV peak indicates deeper and more spaced breaths and HV dip indicates faster heart beats.

Described timings remain unchanged by regressing the effects of RV and HV based on the common approach – only the amplitude of a few timecourses are slightly changed (Figure 20c).

Taken together, our results reveal QPPs have a principled relation with the respiration and heart rate variations, which suggest a neurophysiological basis for these intrinsic patterns that dominantly give rise to functional connectivity.

2.4 Discussion

Summary. Several improvements were implemented to ensure robust detection of a QPP at the individual and group levels. In addition to the primary QPP, reported thus far [16,18], two new QPPs were robustly detected. These three QPPs were characterized in terms of correlation between the RSNs within a QPP, basic metrics, relative occurrence and reproducibility. Dominant contribution of QPPs 1-3 to the functional connectivity was demonstrated. Examination of QPPs 1-3 versus global signal primarily revealed these patterns are not artifacts of GSR. QPPG, obtained without GSR, suggested the spatiotemporal dynamics of the global activity involves timing difference across areas

and across individuals. Examination of all QPPs versus respiration and heart rate variations suggested a principled relationship.

Significance of QPPs 1-3. QPPs 1-3, as simple averages of similar timeslots during the resting-state, are dynamic spatiotemporal regimes of coherent activity that dominantly give rise to functional connectivity (FC), a metric indicative of time-average coherence and reflective of some spatial aspects of the brain's intrinsic organization. The contribution of QPPs 1-3 to FC tells that these intrinsic patterns perhaps serve the brain's self-organization and are worth understanding because of the novel aspects they might entail. The contribution of QPPs to FC is a main part of this thesis and will be referred to in chapter 4, yet it is worth hinting on one of its significances here.

QPPs give rise to FC, which is the basis to obtain the cortical RSNs. RSNs and their relative timing of activity are observable within QPPs. *These statements together imply QPPs 1-3 very likely give rise to the RSNs. Borders of the major RSNs*, e.g., between FPN and DMN or between SMN and DAN, *are attainable based on the summary of activity of at least two QPPs*, e.g., QPPs 1 and 2 or 1 and 3. This point alone significantly enriches our insight about RSNs, suggesting they are overlaid snapshots of a few patterns, each entailing a handful of nuanced information about relative timings. This point can implicate in the parcellations of the subcortical regions with regards to the cortical RSNs, as will be discussed in chapter 4. It can also inform the hypotheses about task interactions or behavioral correlates given the specific functionality of each RSN and it unique timing relative to other RSNs within each QPP.

QPP4 and above. While only three primary QPPs are addressed in this thesis, QPPs 1-3 can be regressed and the residuals can be reanalyzed to detect QPP4. The same

process can be continued to detect more patterns. A supporting analysis performed on 35 randomly selected individuals showed QPPs 1-3 on average explain ~25% of the variance of the cortical parcels' timeseries, with a wide range of 5-50% across parcels. QPP4 and above progressively explain less variance without a clear cutoff. We decided to only focus on QPPs 1-3 because they readily match the first three cortical gradients, as will be shown, and their characterization along with QPPG turned extensive enough for this thesis.

Detection method of QPPs. The current method to detect QPPs requires selecting an initial segment with a preset duration and choosing a correlation threshold. This method was developed near a decade ago as the first attempt to identify similar segments, still, as viewed by peers [14,27-28], its main novelty is in place. Taking similar spatiotemporal units, averaging them and obtaining a spatiotemporal course, as opposed to, for instance, clustering similar spatial units, which are per timepoint, and obtaining spatial cluster centroids. Another nuanced novelty of the current method, in our view, is taking the sliding window correlation and its local maxima which finds the spatiotemporal units with the same phase. To this date, we know of two recent and very different methods (unpublished), with minimal requisites, that can detect patterns which are qualitatively very similar to QPPs 1-3 and QPPG. As recommended for further research, an optimal method to detect QPPs is worth investigating.

Method improvements and impacts. All parts of the method improvements to obtain a group QPP, i.e., inspecting all initial segments per individual, selecting the QPP based on a customized criterion, phase adjusting individual QPPs, averaging them and fine-tuning, might not be necessary if the computation time is crucial. A supporting analysis performed on 35 random individuals showed the original method (i.e., concatenating

scans of individuals and inspecting a random subset of initial segments) results in a similar group QPP compared to our improved method. However, this conclusion is based on the exemplary HCP dataset and healthy adults and requires replication in other datasets, for instance, clinical conditions with higher heterogeneity across individuals. *If it is crucial to have a robust and thorough characterization in a large dataset using the current QPP detection method, the implemented improvements are necessary and sufficient, in our view.*

Duration of QPPs. As simple averages of similar ~20s-long timeslots, all QPPs introduced here involve a cycle of activation and deactivation of different brain areas. ~20s is equivalent to ~0.05Hz, the mid frequency in the BOLD-fMRI-based band of 0.01-0.1Hz. Neuronal activity in the infraslow band (<1Hz, liberally defined), as recorded by more direct neuroimaging modalities than BOLD-fMRI, is widely known to be arrhythmic, with 1/f distribution, arising from the collective interactions of the neuronal activity in the higher frequency bands [14]. As will be shown and discussed, the closed flow of *peak activation* between brain areas and the involvement of cardinal infraslow oscillators such as the thalamocortical unit, offer a novel suggestion that ~0.05Hz rhythms comprised of back-to-back ~20s-long cycles might also exist. As recommended for further research, this is well worth investigating in a more solid setting, e.g., in an invasive and controlled way in non-humans. *In sum, in our view, the explanation for the duration of QPPs is an open question and very fundamental to address.*

Basic metrics and relative occurrence of QPPs. That all QPPs are reasonably strong, with correlation of 0.43 to 0.37 for QPPG to QPP3, is due to the correlation threshold of 0.3, set when identifying their contributing segments. That QPPs are progressively less periodic, with spacing of 45s to 90s for QPPG to QPP3, questions the usage of term

"quasi-periodic". Still, we have chosen to keep this term throughout this thesis, as opposed to using a general term, such as "recurring spatiotemporal pattern". The relative occurrence of QPPs was examined in the most elementary way. As will be discussed and recommended for further research, it is worth further examining *how cycles of QPPs might be initiated relative to one another throughout time*.

Significance of QPPG. As a complementary approach, characterization of QPPG offered a novel suggestion about the spatiotemporal dynamics of the global activity and enriched our interpretations regarding the fluctuations of the physiological signals. As appears in the next chapter, characterization of QPPG complements those of other QPPs. Similar to other QPPs, QPPG can also be included when forming the hypotheses about task interactions or behavioral correlates.

QPPs and physiology. Principled relation between QPPs and the respiration and heart rate variations, suggestive of a neurophysiological basis, is definitely worth investigating. *Respiratory and cardiac variations reflect systemic physiological status, which can be modulated by the autonomous nervous system, one of the links between brain and body*. Our attempt to better understand QPPs, as the brain's intrinsic patterns that dominantly give rise to rsfMRI-based functional connectivity, particularly between networks, is now pointing us to the next level of depth and complexity.

CHAPTER 3: COORDINATED ACTIVITY WITHIN QPPS AT CORTICAL AND SUBCORTICAL REGIONS

3.1 Introduction

To better understand QPPs, as intrinsic recurring spatiotemporal patterns, that dominate functional connectivity (FC), it is necessary to thoroughly characterize the activity they entail and identify novel aspects they might reveal about the brain's self-organizing processes. Such characterization is addressed in this chapter and is based on QPPs robustly detected in the previous chapter at the group-level, 817 individuals, in grayordinate, ~92K cortical vertices and subcortical voxels.

Simple averaging a set of similar ~20s-long segments of the resting-state fMRI (rsfMRI) scans across individuals to build each QPP, as will appear, results in a *well-coordinated* cycle of activation and deactivation across the whole brain; each area in each region exhibits a specific timing such the overall activity seems consistent and synchronous, resembling the resting-state networks (RSNs), functional connectivity gradients (FCGs), even, the consensus on the tract-based connections.

To summarize such well-coordinated activity, the timecourses of each QPP at all the cortical vertices and subcortical voxels are clustered and their time of peak activation are determined. *Our description* of activity is divided into seven regions which are the cerebral cortex, cerebellum, thalamus, hippocampus, amygdala, brain stem and deep brain nuclei, and striatum. For each region, *to distinguish different areas and to compare the accordance of the results with the literature*, an existing parcellation scheme is adopted, with priority given to a well-established scheme based on the FC and rsfMRI.

Any already-reported FCG for each region or any consensus on its tract-based connectivity are considered as well.

Preprocessing steps, such as band pass filtering or nuisance regression, particularly when including the gray matter signal, might distort the relative timing between areas. To examine, the average of each QPP's contributing segments over timeseries that had only been demeaned, but not filtered or nuisance regressed, was qualitatively compared with that QPP. Particular phase of a QPP cycle might influence the relative timings or even our description of the activity. To examine, QPPs with a reversed phase were detected and qualitatively compared.

While a comprehensive discussion of the results appears in the next chapter, some method related topics are discussed at the end this chapter.

3.2 Method

QPPs 1-3 obtained in the previous chapter at the group-level, 817 individuals and 1hr/individual, in the grayordinate, ~31K cortical vertices per hemisphere and ~30K subcortical voxels, are the basis for characterization in this chapter. As a complementary part, QPPG of the two subgroups of 200 individuals is also considered.

As pointed in the previous chapter, to build QPPs in grayordinate, the contributing segments of QPPs were identified by analyzing the cortical parcels' timeseries but were averaged over grayordinate timeseries. This approach dramatically expedites the detection process and is based on our supporting analysis that showed analyzing the grayordinate timeseries or cortical parcels' timeseries results in very similar QPPs, particularly at the group-level. This supporting analysis also implies *cortical events dictate the outcome*, possibly due to higher signal-to-noise ratio (SNR), and *crucially, all*

the subcortical activities are co-activities locked with the cortical events, as reflected in our wordings when describing the results.

Clustering timecourses for a coarse summary of activity within QPP. To have a coarse summary of the activity within each QPP, the timecourses of the cortical vertices and subcortical voxels were clustered using the following procedure. Each timecourse was compared with all other timecourses, using fine phase-matching, introduced in the previous chapter, with ±2 time-shifts, and a comparison matrix between pairs of timecourses was built. The upper triangle of the comparison matrix was flattened row-wise and used as the distance vector for the hierarchical clustering, with the type of distance set to "correlation". For QPPs 1-3, the cut-off was respectively set to 1-0.9=0.1, 1-0.89=0.11, and 1-0.85=0.15. The clusters with more than four hundred members were kept. *These choices, although qualitative, resulted in robust clusters with regards to the changes described in the supporting analyses at the end of this chapter* (clustering is to have a coarse summary of the activity and does not influence the core of our results). Only the timecourses with reasonable SNR were included, which were those with a peak-to-dip amplitude higher than 0.1 for the cortical and 0.05 for subcortical regions.

Peak times of for a fine summary. To have a fine summary of the activity within each QPP, the time of peak activation, or peak time, was determined for the timecourses with strong peak-to-dip, as defined in the clustering section.

Testing significance of timing differences. For each QPP, significance of difference in the following timings were tested: peak times of all areas versus the left posterior cingulate cortex (LPCC), peak time of each cluster of a QPP versus other clusters, peak time and switching time (time of sign switching between activation and deactivation) of

each RSN within a QPP versus other RSNs. For these statistical testing, similar to a part in the previous chapter, the fine-tuned contributing segments of the group QPP were averaged per individual (*QPPi, only here and for brevity*).

First, for the QPPi of each individual, the following timecourses were obtained. A timecourse for the LPCC, by averaging the QPPi's timecourses across the cortical vertices belonging to the five most central parcels of the Glasser's neuroanatomical posterior cingulate region (shown in the previous chapter). A timecourse for each cluster of the group QPP, by averaging the QPPi's timecourses across all vertices belonging to the spatial map of that cluster. A timecourse for each of Yeo's RSNs [12], by averaging the QPPi's timecourses across the cortical vertices belonging to that RSN. *Next,* based on the QPPi of all individuals, the distribution of peak time of each area was compared with the distribution of peak time of the LPCC, using dependent t-test. Similarly, the peak times of pairs of the group QPP clusters, and the peak times and sign changing times of pairs of RSNs were compared.

Parcellations, gradients, and tract connections for comparison. Activity within each QPP, as a simple average of a set of similar segments of rsfMRI timeseries, can be described *independent of dividing the brain into regions, parcels, networks or gradients*. However, to frame our report, we parsed our description into seven regions which are the cerebral cortex, cerebellum, thalamus, hippocampus, amygdala, brain stem and deep brain nuclei, and striatum. For each region, to distinguish different areas and to compare the accordance of the results with the literature, an existing parcellation scheme is adopted, with priority given to a well-established scheme based on FC and rsfMRI. Any already-reported FCG for each region or any consensus on its tract-based connectivity, particularly with the cerebral cortex, are considered as well.

Note, FCGs, which qualitatively arise from the activity within QPPs (as introduced and will appear), are principle components of the similarity matrix of areas, in terms of their FC [13]. As already described, each FCG is an axis along which areas have similar FC. FCGs mostly match FC-based parcellation, particularly at the cortex, however, rather than parcels and boundaries, they entail gradual and sharp changing values of gradient.

As an important note, almost all credited reports on subcortical parcellation or FCG, which are based on non-invasive fMRI or diffusion tensor imaging in humans, have compared their results with the established atlases, which are based on invasive techniques such as tract-tracing, mostly in primates. As my personal conclusion, the *commonality* between a few of such reports involves areas for which there is a consensus about their cortico-subcortical tract-based connectivity. *As a simple tip learned in a long and hard way,* I decided to directly compare our results with any such consensus (as will be described next and repeated in the discussion of this chapter).

The adopted parcellation schemes, gradient axes, and consensus on the tract-based connections are listed below along with brief description (in appendix C, a summary of general functionality of each (sub)region is provided).

Cerebral cortex. Seven RSNs by Yeo and colleagues [12] which are the unimodal networks of somatomotor (SMN) and visual (VN), task positive networks (TPN) of dorsal attention (DAN), ventral attention (VAN), and executive control or frontoparietal (FPN), task-negative or default mode network (DMN), and limbic network (LN).

First three FCGs by Margulies and colleagues [13] which are as follows. In FCG1, the unimodal networks are on one end and the transmodal DMN is on the other end, with the TPN situated in between. In FCG2, each of the unimodal networks are on the

opposite ends. In FCG3, the unimodal networks and DMN are on one end, and the TPN is on the other end.

Cerebellum. FC-based parcellation scheme by Buckner and colleagues [29], where each cerebellar voxel is assigned to one of the Yeo's seven RSNs, based on its maximal FC or coactivity with one of the RSNs. The cerebellar lobules I-VI and crus I, in an orderly way, are parcellated as SMN, TPN and DMN, and together are called the primary map of RSNs. Crus II and lobules VII-VIII are parcellated as DMN, TPN, and SMN and called the secondary map of RSNs. Lobules IX-X are parcellated as SMN, TPN, DMN and LN and called tertiary map of RSNs. The VN is minimally represented in the cerebrum.

Two FCGs by Guell and colleagues [30] which are similar to the cortical FCGs 1 and 3. In the cerebellar FCG1, SMN and DMN are at opposite ends, and in the cerebellar FCG2, SMN and DMN are on one end, and TPN is on the other end. *Note,* there are contralateral polysynaptic tract connections, from the cortex to the pontine nucleus to the cerebellum, and from the cerebellum to the thalamus and to the cortex [29].

Thalamus. Tractography-based parcellation scheme by Behrens and colleagues [31], and Morel's atlas [32] (only the mediodorsal nucleus (MD) mask is used here). *Unimodal parcels and nuclei* are located the most postero-laterally*. The rest of the thalamus* includes parcels and nuclei that are *mainly* connected to and interact with the non-unimodal cortical areas. *FCG* has not yet been reported for the thalamus.

Hippocampus. Multi-modal parcellation by Robinson and colleagues [33], cytoarchitectonical subfields in the Anatomy Toolbox by Eickhoff and colleagues [34]. *Two FCGs* by Vos de Wael and colleagues [35], with FCG1 being along the long-axis of hippocampus and FCG2 along the short-axis. Many aspects are differentiated along

hippocampal long-axis from the microanatomy to function [33-34]. Our examination of the hippocampal short-axis is based on the difference between hippocampal subfields.

Amygdala. Parcellation by Tyszka and Pauli [36] based on a specific registration of T1- and T2-weighted structural images using the HCP dataset (see appendix B for the name of parcels, some of which we have grouped together to simplify a qualitative comparison). *FCG* has not yet been reported for the amygdala.

Brain stem and deep brain nuclei. Probabilistic maps of locus coeruleus (LC) by Keren and colleagues [37], ventral tegmental area (VTA), substantia nigra pars compacta and pars reticulata (SNc and SNr), subthalamic nucleus (STH), globus pallidus external and internal (GPe and GPi), hypothalamus (HTH) by Pauli and colleagues [38] using the HCP dataset, basal nucleus of Meynert (BNM) by Li and colleagues [39], pedunculopontine nucleus (PPN), dorsal raphe (DR), median raphe (MR), periaqueductal gray (PAG) by Edlow and colleagues [40] , and nucleus accumbens (NA) mask by HCP. *For plotting,* we sorted theses nuclei based on their neuromodulatory neurotrasmitters based on the following order: norepinephrinergic LC, dopaminergic VTA, SNc, SNr, acetylcholinergic BNM and PPN, and serotonergic DR and MR.

Striatum. FC-based parcellation scheme by Choi and colleagues [41], where similar to the Buckner's scheme, each striatal voxel is assigned to one of Yeo's seven RSNs, based on its maximal FC. *Two FCGs* by Marquand and colleagues [42], where FCG1 is along the rostro-caudal axis of the striatum and FCG2 along its medial-lateral axis. *Note,* there are topographical tract connections, along rostro-caudal and medial-lateral axes, from the cortex to the striatum. The striatal projections are to other basal ganglia regions (GPe/STH, GPi/SNr) then to the thalamus and to the cortex [41-42].

Correlation map as another summary for QPPG. For each of the two subgroup QPPGs, as another summary of activity and particularly to ease the comparison with a recent related report, a correlation map was also calculated. The seed timecourse was built by averaging all the timecourses of cortical and subcortical regions, which is basically equivalent to a timecourse for the global signal (GS). Correlation map was based on the Pearson correlation between the seed timecourse and all the timecourses.

Supporting analyses. To examine the effect of filtering and nuisance regression including gray matter signal on various aspects of the activity within QPPs, the average of each QPP's contributing segments over timeseries that had only been demeaned, but not filtered or nuisance regressed, was qualitatively compared with that QPP.

To examine the effect of a certain phase of QPPs on various aspects of the activity within these patters, QPPs with a reversed phase were detected and qualitatively compared. For such detection, instead of considering the left early visual area (left V2) as the seed for phase-adjustment, another area was considered. For QPPs 1 and 3 and QPPG, the central LPCC, and for QPP2, a node of the frontoparietal network (FPN) at the left supramarginal gyrus (smg).

3.3 Results

QPPs involve well-coordinated propagating activity across the whole brain. Within QPPs 1, 2 and 3, at the cerebral cortex, activity propagates respectively along the cortical FCGs 1, 3 and 2. Coarse summary of the cortical activity accords with the cortical RSNs. Time-locked and consistent with the cortical propagation, all subcortical regions exhibit either propagation of activity or simple activity, such that the propagation axes are consistent with the cortex and consistent with any already-reported FCG in each region.

Coarse summary of the subcortical activity mostly matches any consensus about tract-based connectivity, and to an extent, accords with the FC-based parcellations. Nuanced timing differences between brain regions and the closed flow of activity throughout the brain suggest drivers and origins for QPPs.

Figure 21 shows QPPs 1-3 at a subset of timepoints, and in another page, with the borders of Yeo's RSNs and Glasser's multi-modal parcels overlaid. Table 1 lists the propagation axes and involved networks and areas in each region. *Consistent and synchronous flow of peak activity between such areas forms the propagation axes.*

Figures 22, 23 and 24, respectively correspond to QPPs 1, 2 and 3, and show clusters of timecourses and map of peak times as summaries of activity along with the existing parcellations for comparison.

Detailed descriptions for each QPP and each region are as follow, *with the coarse summary of activity appearing first*. *Note the abovementioned figures and the table along the descriptions in general*. In the maps of peak times, the non-significant values from the LPCC are masked. Described timing difference between QPP clusters and RSNs are all significant.

3.3.1 QPP1

Cerebral cortex. Within QPP1, the cortical areas that belong to the unimodal RSNs, networks of SMN and VN, are correlated with the cortical nodes that belong to the attention RSNs, networks of DAN and ventral attention VAN. Together, these cortical areas or nodes are anticorrelated with the cortical nodes belong to the networks of DMN, FPN and LN.

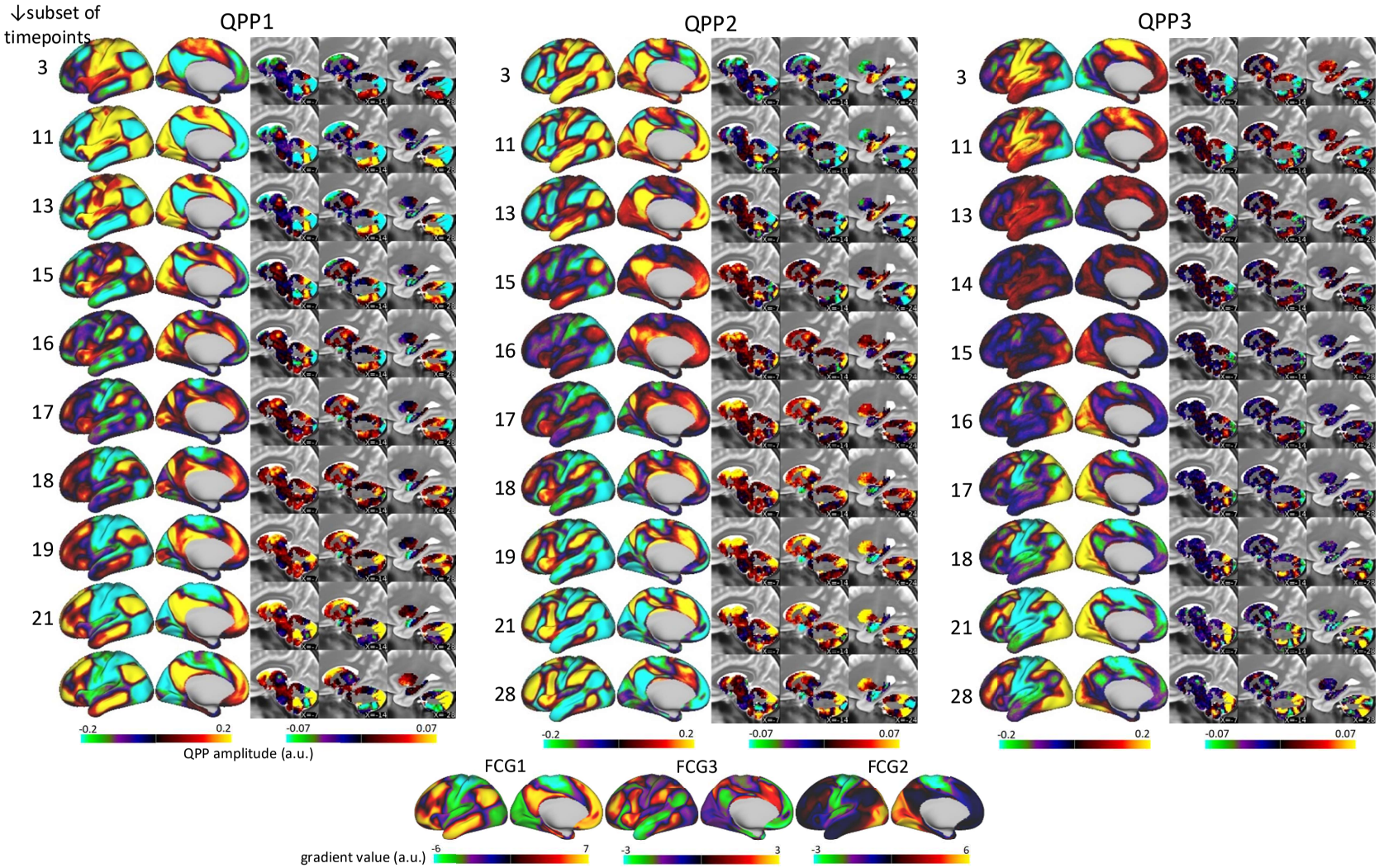

Figure 21 QPPs 1-3 involve coordinated propagation of activity along functional connectivity gradients (FCG)

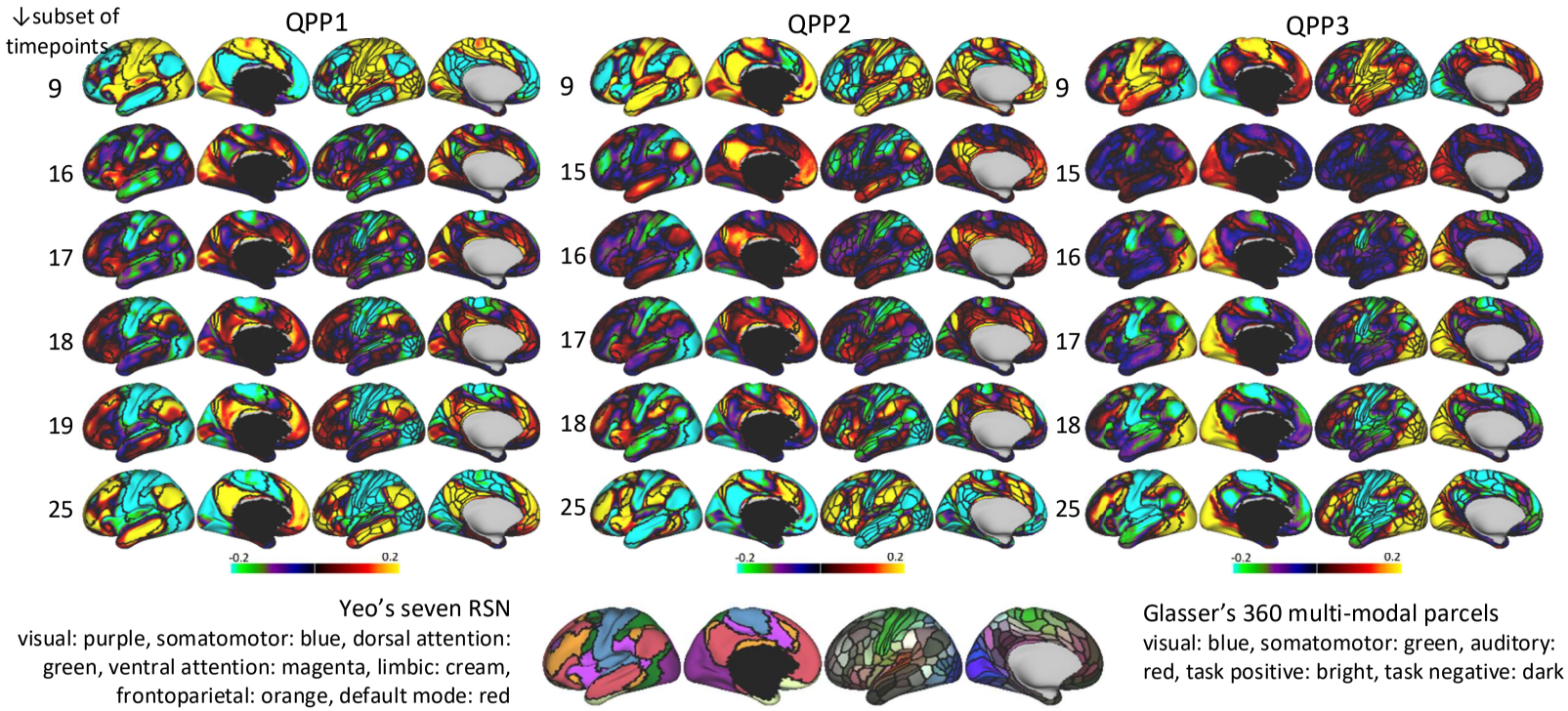

Figure 21 continued

Table 1 (a) Axis of propagation of activity or simple coactivity

	Brain region	Coarse axis	Fine axis
QPP1	Cortex	**Cortical FCG1** SM→TP→DM	SM→DA & VA→FP/DM & V~FP/DM
	Cerebellum	**Cerebellar FCG1** TP→DM	DA/VA→FP/DM
	Thalamus	**Novel,** SM→TP→DM	SM/DA→VA→FP/DM
	Hippocampus	**Hippocampal FCG1,** Posterior → Anterior	
	Amygdala	**Novel,** Center → Edges on medial/lateral	
	Brain stem	**Novel,** Coactive with DM	Coactive with FP/DM
	Striatum	**Striatal FCGs** TP→DM	Orbital/Caudal → Rostral, Latera l→ Medial FP→FP/DM & L→DM
QPP2	Cortex	**Cortical FCG3** TP→SM/V&DM→TP	DA→SM/V & DM→FP→VA→DA
	Cerebellum	**Cerebellar FCG2** DM→TP	DM→FP→DA/VA
	Thalamus	**Novel,** DM→TP	DM→FP→VA
	Hippocampus	**Hippocampal FCG1,** Anterior → Posterior	
	Amygdala	Coactive with DM	
	Brain stem	**Novel,** Coactive with TP	Coactive with FP/VA
	Striatum	**Striatal FCGs** DM→TP	L→FP/VA Rostral → Caudal, Medial → Lateral
QPP3	Cortex	**Cortical FCG2** SM↕V (↕ anticorrelation)	SM/DM/VA↕V/DA/FP & SM/DM→VA→DA→FP→DM
	Cerebellum	SM↕V	SM/DM↕FP & FP→DM
	Thalamus	SM↕V	
	Hippocampus	Coactive with SM	Coactive with SM/DM/VA
	Amygdala	Coactive with SM	Coactive with SM/DM/VA
	Brain stem	-	-
	Striatum	Coactive with SM	Coactive with SM/DM/VA

(b) Cerebral nodes of networks in the fine axis

QPP1	SM→DA	foot/genitalia→sma lower/upper limb→preM/SPL
	VA→FP/DM	ACC→vmPFC aI→ifg ifs→sfg/mfg/ifg mTL: posterior→anterior Ag/PCC: surround→center
	DM→Language	TL: medial→superior left 55b/IFJ/SFL: anterior→posterior
QPP2	DA→SM/V	DA-bordering-SM/V→SM/V
	DM→FP→VA→DA	vmPFC→aACC→dACC ifg→aI→mI→inferior-preM sfg/mfg/FPC→ifs TL: mid-anterior→infero-posterior→posterior Ag→smg→PF/SPL PCC→RSC/POS→postero-medial VA/DA
QPP3	SM/DM→VA→DA→FP→DM	SM-eye→55b→PEF→DLPFC→ifg SM-eye→55b→FEF→superior-preM FPC→ifs→DLPFC→ifg FPC→lOFC→ifg mI→aI TPOJ→MT→TOJ→ mTL PF→IPL→Smg→Ag SM-foot→MCC→dACC PCC→RSC/POS/VN-band

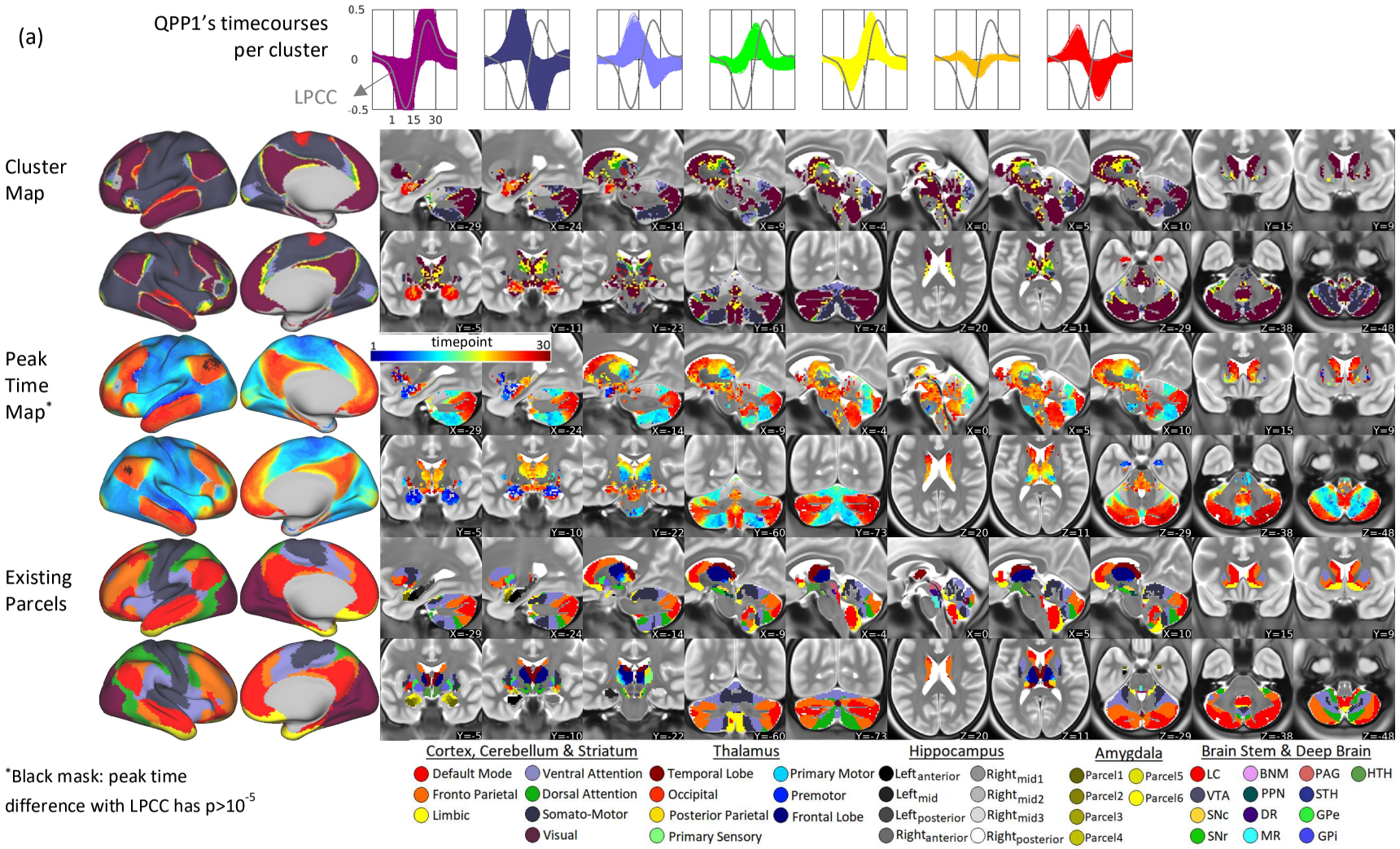

Figure 22 (a) QPP1's summary of activity. (b) Examples of timecourses per existing parcels. (c) Number of voxels per peak time and per cluster. (d) Dip time map, (e) Closed flow of peak activation.

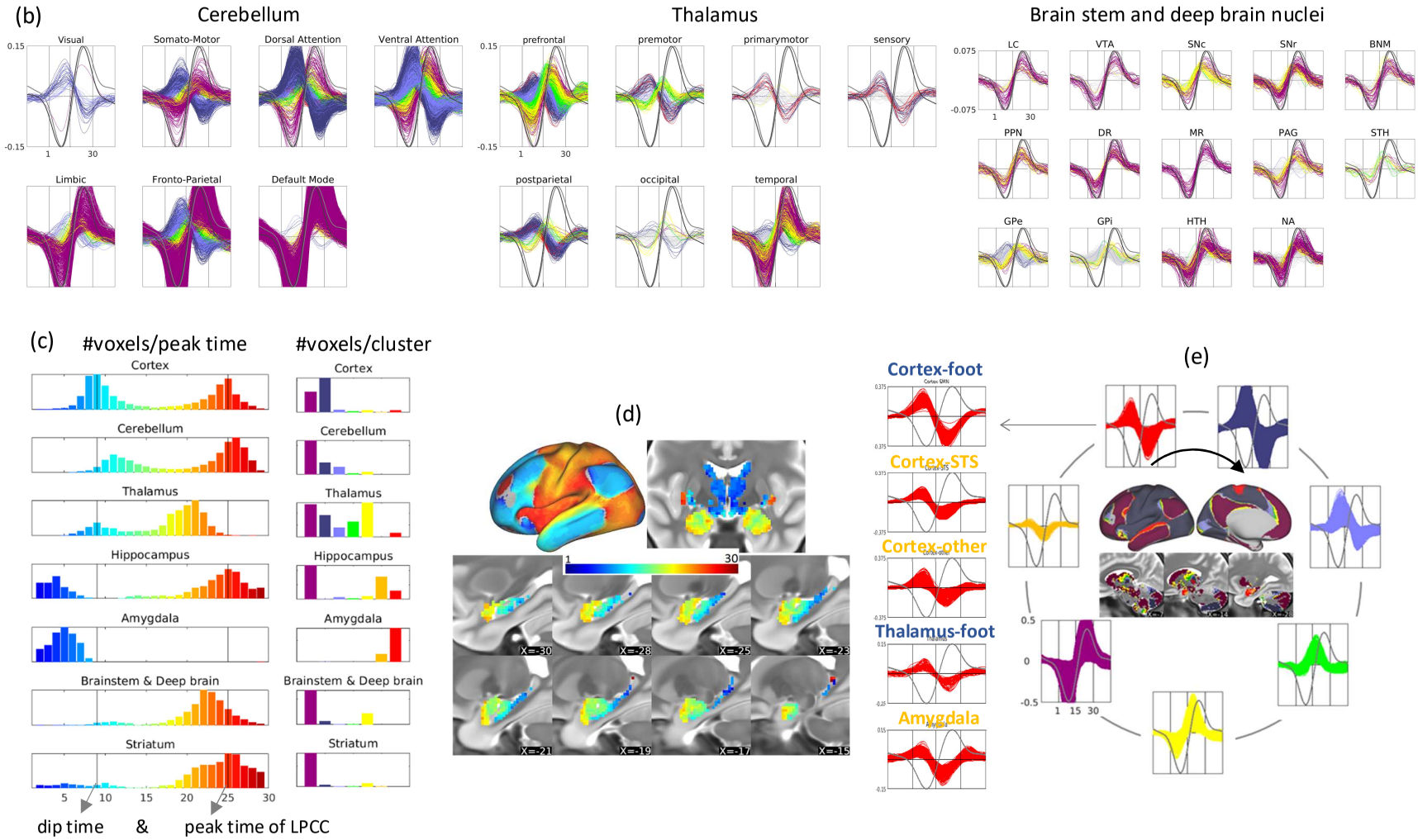

Figure 22 continued

Within QPP1, activity propagates along the cortical FCG1, from the areas of SMN to all the nodes of the DMN, with intermediate activity in nodes of the DAN, then the VAN, and later the FPN. Based on timepoints 11-18, deactivation initially starts in the lower and upper limb areas of SMN, and from there, deactivation spatially expands to the surrounding nodes of the DAN, namely, the premotor area (preM), superior parietal lobe (SPL) and supplementary motor area (sma). Furthermore, based on timepoints 15-19, or the *sign-switching timepoints* of the central LPCC, activation expands across the following nodes from the VAN to FPN to DMN. From the anterior cingulate cortex (ACC) to the ventromedial prefrontal cortex (vmPFC), from the anterior insula (aI) to the inferior frontal gyrus (ifg), in the lateral prefrontal cortex (LPFC) from the centrally located intermediate frontal sulcus (ifs) to the surrounding areas of superior, middle and inferior frontal gyri (sfg, mfg and ifg), in the middle temporal lobe (mTL) from posterior to anterior, and finally, around the angular gyrus (Ag) and PCC from the surrounding areas to the center.

Clusters of timecourses, with the intermediate location and timing of the transitory areas, the map of peak times, with pronounced gradients, and the list of the involved cortical networks and areas summarize the described dynamics.

It is worth highlighting, QPP1 additionally exhibits the following noteworthy features.

First, although VN (V2, V3, MT, etc) along with the frontal/premotor eye field (FEF/PEF) are anticorrelated with nodes of DMN, the primary visual area (V1) exhibits clear propagation of activity from anterior to posterior, from the periphery to the center of the visual field, or along the already-reported FCG in V1 [43]. Note, the center of the visual field in V1 is positively correlated with nodes of DMN, which is in line with [13,43].

Second, nodes of the DAN and VAN, as two components of the task positive network (TPN) [12,44], are anticorrelated with nodes of the DMN. However, nodes of the FPN, as another component of the TPN [12,44], are positively correlated with nodes of the DMN, which is only the case in QPP1.

Third, the last two clusters of timecourses are fully described in sections related to the thalamus and amygdala, with the following two subpoints introducing the cortical share of these two clusters. The most noticeable early deactivation in SMN starts medially, in the foot and genitalia areas (timepoint 11 and the medial red area in Figure 22a).

Furthermore, deactivation expands from the mTL towards the superior temporal sulcus (STS), with well-known involvement in language [26,45] and also social inferences [45-46] (timepoints 13-16). This focal propagation is summarized by the progressive time of deactivation dip in the first and the last two clusters in Figure 22a (also the map of the maximum dip time in Figure 22d). Similar focal trends from a node of DMN towards an area mostly recognized as language-related [26] occur in other areas such as area 55b, inferior frontal junction (IFJ) posterior to Broca area 44, and superior frontal language area (SFL), all on the left hemisphere.

Finally, about laterality as a neurocognitive feature, the first cluster, which maximally overlaps with the DMN, is narrower at the right ifg and mTL, while the second cluster, which maximally overlaps with the TPN, together with the transitory clusters are wider at the right LPFC and aI, all accord with the consensus [12-13,44-4847] (see appendix C).

Cerebellum. Cerebellar activity matches the FC-based parcellation by Buckner and colleagues [29], such that the cerebellar areas parcellated as the DMN are strongly correlated with the cortical nodes of the DMN (also note Figure 22b), etc. As in the

cortex, areas that coactivate with the cortical nodes of the DMN and FPN, here on called DMN- and FPN-coactive areas, are positively correlated with each other and are anticorrelated with DAN-/VAN-coactive areas. *Note,* DMN-coactive areas are wider at the right cerebellar hemisphere (Y=-61,-74), similar to the trend in the left cortical hemisphere, matching their tract-based polysynaptic connectivity [48].

Time-locked and consistent with the cortex, at the sign-switching timepoints, and around crus I/II, activation expands from DAN-/VAN-coactive to FPN-/DMN-coactive areas (Figure 21bo, 22a). This axis of activity propagation follows the already-reported cerebellar FCG1 [30]. Activity of other cerebellar areas are discussed in the next chapter. Interestingly, as indicated by the distribution of peak times in Figure 22c, the *cerebellum slightly lags the cortex*, and such lag is in line with [49].

Thalamus. Thalamic areas that are coactive with the cortical SMN and nearby nodes of the DAN are mainly located postero-laterally, in line with the consensus about their tract-based connections [31-32, 50-51]. In the ventral posterior nucleus (VP), the foot area is the most lateral [50], perhaps around the red voxels in X=-9,-14 in Figure 22a, since it is clustered along the cortical areas of foot and genitalia, together exhibiting the earliest deactivation. *This is interesting given* the reported evidence that thalamic relay neurons can initiate an infraslow rhythm (<0.1Hz), i.e., spike bursts which are a-few-tens-of-seconds apart [52-53], and the consensus that thalamus and cortex closely interact to generate the low arousal rhythms (~1-10Hz) [54-55]. Other than the *postero-lateral part*, hereafter broadly referred to as *SMN-coactive areas, or for a helpful brevity, the unimodal thalamus*, a large portion of the thalamus is coactive with the narrow cortical transitory clusters located between nodes of the VAN and FPN/DMN, while a small portion, medially located, is coactive with the cortical nodes of the FPN/DMN (X=-

14,Z=11, Figure 22c right histogram). *These portions, which are the thalamic areas other than the postero-lateral (or unimodal thalamus, from hereon), will be broadly referred to as transmodal-coactive areas, or for a helpful brevity, the transmodal thalamus.*

Time-locked and consistent with the cortex, in the thalamus, activity expands from the SMN-coactive to the transmodal-coactive areas (Figure 22a). This is *novel evidence for the existence of a macroscale FCG across the thalamus, in accord with the cortical FCG1*. *As activity expands to the cortical nodes of the FPN/DMN, the transmodal thalamus takes a lead by a median of 6 timepoints (4.3s) specifically compared to the LPCC* (Figure 22c). This can be inferred given that a large portion of the thalamus is clustered as transitory, however, a small portion of the thalamus that belongs to the first cluster also has slightly earlier peak times compared to the cortical nodes of FPN/DMN (Figure 22b).

Hippocampus. The posterior part of the hippocampus is coactive with the cortical nodes of the DMN and its anterior part is coactive with the amygdala. This is in accord with the consensus that the hippocampus is a node of DMN and exhibits functional specialization along its long axis, with its anterior part closely interacting with the amygdala [33-34].

Activity propagates along the hippocampus from posterior to anterior (note progressive dip times of the first and the last two clusters in Figure 22a, dip time map in Figure 22d), which is also along the already-reported hippocampal FCG1 [35]. The cortical parahippocampal area also has a gradient in peak time, such that the part neighboring the retrosplenial cortex (RSC) belongs to the transitory clusters. Hippocampal subfields exhibit slight differences (not shown), e.g., different shares of clusters with different amplitudes, which might be due to the hippocampal FCG2 across the short axis [35].

Amygdala. Propagation of activity towards the amygdala via the posterior part of the hippocampus (a DMN node) occurs at the same time that activity propagates from the mTL (a DMN node) towards the STS (Figure 22a, first and last two clusters), or along area 55b, IFJ and SFL. Deactivation propagates across the amygdala from the center to the edges, sequentially sweeping the main parcels [36] (Y=-5 and the gradient of dip times in Figure 22d), suggesting *FCG across the amygdala* that matches a focal cortical gradient from mTL towards STS.

A fundamental point should be made here which requires separation of the timecourses in the red cluster in Figure 22a that belong to the *amygdala (Am)* from those that belong to the *unimodal thalamus (T1)*, note the inset related to the red cluster in Figure 22e. Using Am and T1 for the moment and ignoring their cortical coactive areas, based on our description so far, *activity initiates in T1, propagates along FCG1 in different brain regions including hippocampus, and terminates in Am, with Am and T1 belonging to the same cluster and Am being slightly earlier than T1*. Flow of activity cannot be tracked between Am and T1, but between their cortical coactive areas which are STS, IFJ, 55b, and SFL. Therefore, *timings of peak activation in different regions form a closed flow within ~20s-long cycle of QPP1* (Figure 22e), suggesting *cycles of QPP1 can occur back-to-back*. This indicates the *origin of an infraslow rhythm (~0.05Hz) comprised of back-to-back cycles*. We will discuss this point in more details and depth in the next chapter but close with questions, e.g., *is the synchrony between the unimodal thalamus and Amygdala or their corresponding cortical areas or any other area critical within a cycle and for its continuous occurrence?*

Brainstem and deep brain nuclei. These arousal promoting nuclei primarily coactivate with the cortical nodes of the FPN/DMN, noteworthy, their *median peak time is 4*

timepoints (2.9s) before the LPCC (Figure 22c). This suggests a *driving influence, but the thalamic lead is more pronounced*. While difficult to resolve, the probable locations of dopaminergic substantial nigra (SN), acetylcholinergic pedunculopontine nucleus (PPN), globus pallidus (GP), and hypothalamus (HTH) contain the most voxels with the earliest peak times (Figure 22b). The earliest voxels are slightly more on the right side (X=10 vs X=-9), in line with their ipsilateral projections to the right cortical hemisphere with a stronger role in the tonic alertness [44]. Voxels which are anticorrelated with the FPN/DMN are pronouncedly located in the pons, possibly the pontine nucleus, that relays the cortical input to the cerebellum.

Striatum. Striatal areas are mostly coactive with the cortical nodes of the FPN/DMN, however, the tail of the caudate and the ventro-lateral striatum are coactive with the cortical transitory clusters (transitory-coactive areas). Negligible amplitude in the posterior and mid putamen, parcellated as VAN and SMN by Choi and colleagues [41] is observed only in QPP1.

As in the cortex and most other subcortical regions, at the sign-switching timepoints, activation expands from the transitory-coactive areas to FPN/DMN-coactive areas, both along the caudate and across the coronal planes, or along rostro-caudal and medial-lateral axes. The axis of propagation is also along the already-reported striatal FCG [42]. Voxels with the latest peak times are located in the anterior caudate, Choi's DMN parcel, and more precisely, propagation is from the most rostral/caudal to the rostral areas.

3.3.2 QPP2

Cerebral cortex. Within QPP2, the cortical areas belonging to the unimodal RSNs, SMN and VN, are correlated with the cortical nodes of the DMN. Together, these cortical

areas are anticorrelated with the cortical nodes of the task positive RSNs, FPN, VAN and DAN. Within QPP2, activity propagates along the cortical FCG3, from the nodes of DAN to the areas of SMN and VN, and from the nodes of DMN to the nodes of FPN, then to the nodes of VAN, and finally back to the nodes of DAN.

Based on timepoints 11-16, deactivation initially starts in the areas of DAN that lie in the border with the SMN and VN, and from there deactivation spatially expands to the areas of SMN and VN (also note the first and last clusters in Figure 23a). Furthermore, based on timepoints 15-19 or the sign-switching timepoints of the central LPCC, the intermediate location of the transitory clusters and the obvious gradients in the peak time, activity expands across the following nodes, from DMN to FPN then VAN and finally to DAN. From vmPFC to anterior ACC (aACC) then to dorsal ACC (dACC), from ifg to aI then to mid insula (mI) and finally to inferior preM, in LPFC from the surrounding sfg, mfg and frontopolar cortex (FPC) to the centrally located ifs (Figure 23d), from mid-anterior TL to infero-posterior then posterior TL, from Ag to supramarginal gyrus (smg) then area PF and finally to SPL, and lastly, from central PCC to RSC and parieto-occipital sulcus (POS) then to postero-medial nodes of VAN and DAN.

It is worth highlighting, QPP2 additionally exhibits the following noteworthy features.

First, based on our description, *activity initiates in areas of the DAN that border the SMN and VN* (red cluster), *propagates along FCG3, and terminates in areas of DAN that lie side-by-side with the initiation areas* (yellow and orange clusters). Therefore, not only the timings of peak activation in different regions again form a closed flow (Figure 23f), indicating the origin for an infraslow rhythm, but also, the *flow can be clearly tracked or is spatially closed*.

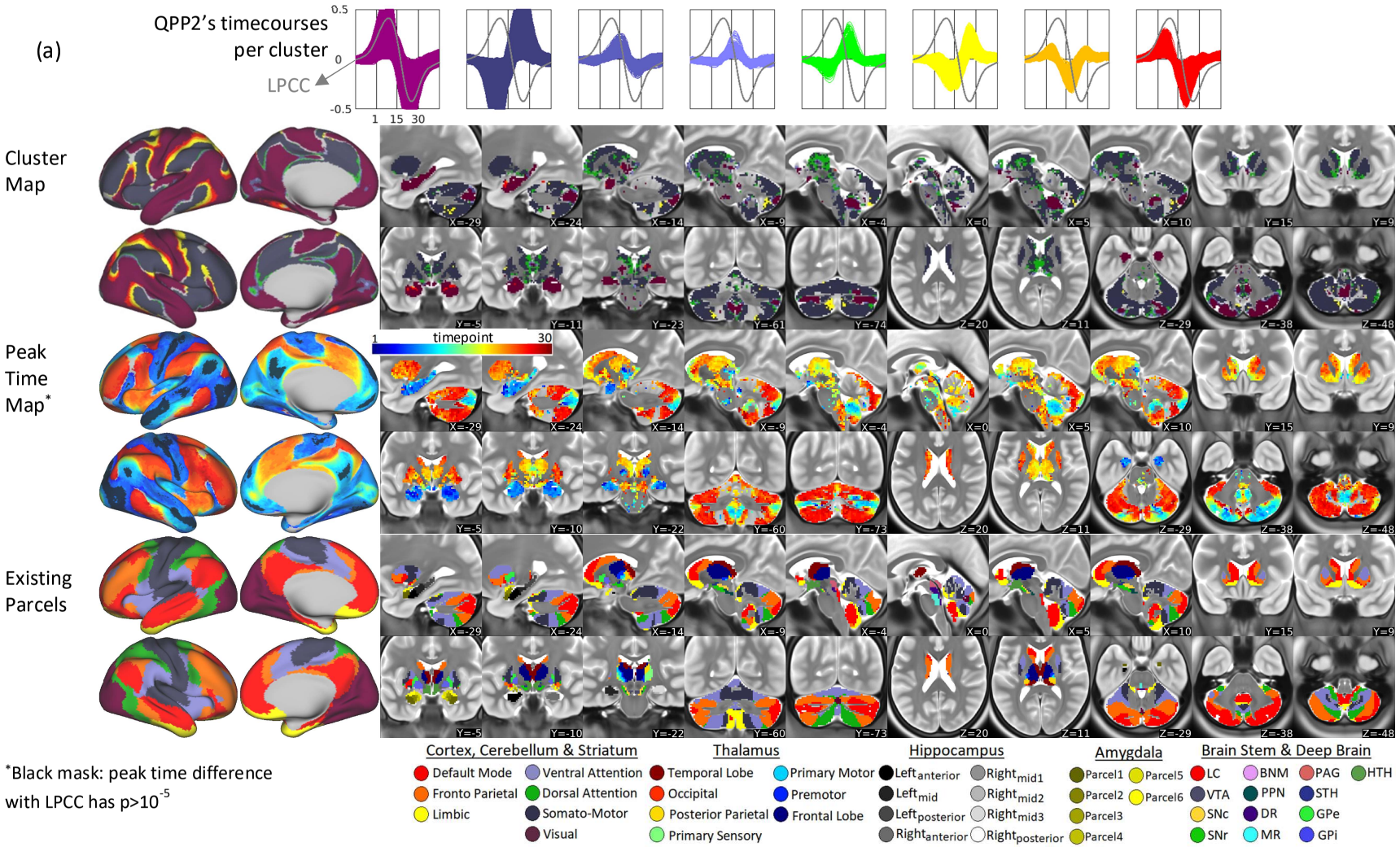

Figure 23 (a) QPP2's summary of activity. (b) Examples of timecourses per existing parcels. (c) Number of voxels per peak time and per cluster. (d) Peak time map frontal view. (e) Cluster map dorsal view. (f) Closed flow of peak activation. (g) Dip time map.

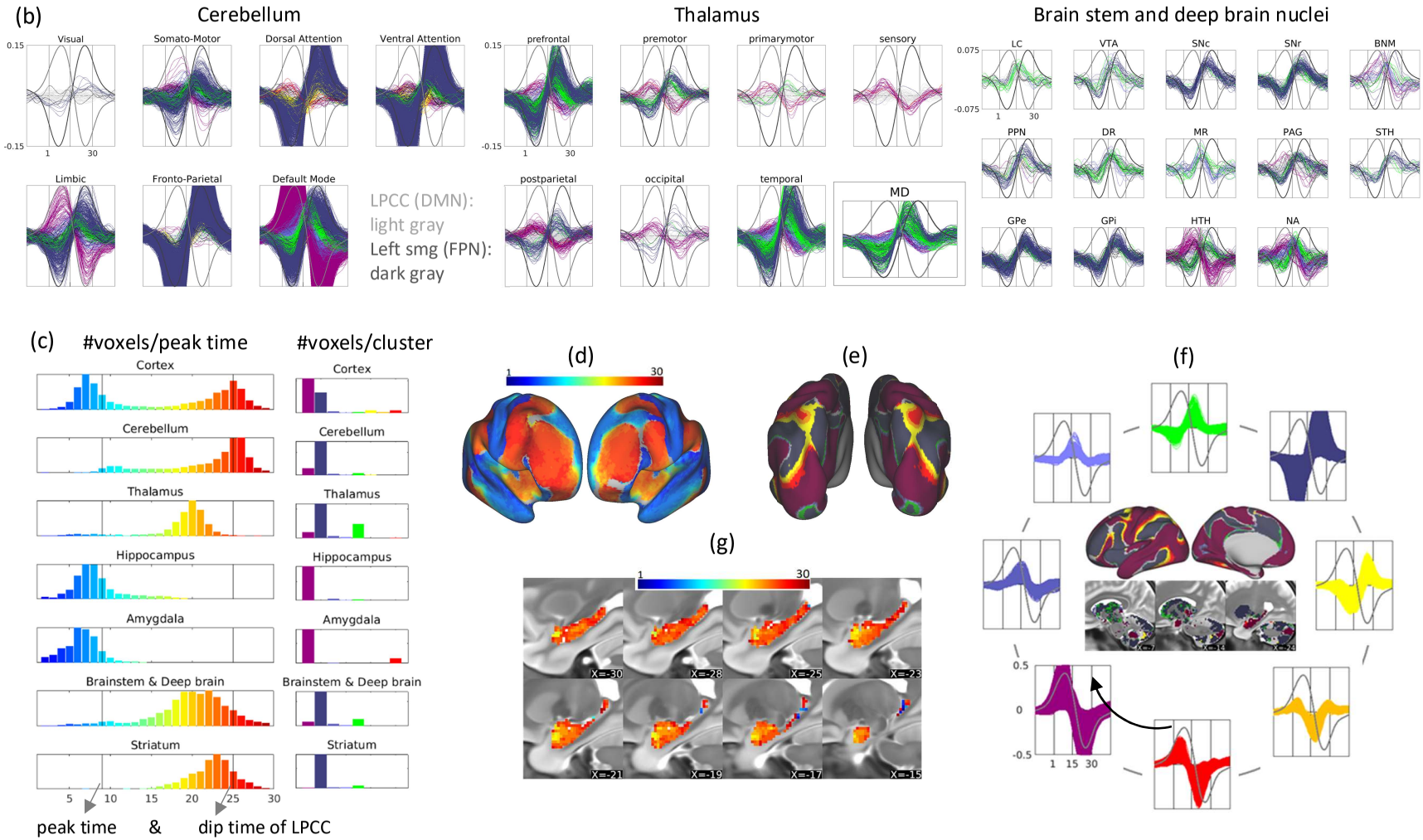

Figure 23 continued

Second and equally important, a few areas outside Yeo's DAN exhibit the earliest peak time (red cluster), i.e., participate in the initiation of the cycle, notably left areas of 55b, IFJ, even SFL, and also mid ventral visual stream.

Third, in the parieto-occipital part of the DAN, there is a rostro-caudal band between SMN and VN, maximally distant from PCC and Ag, with a late peak time (Figure 23e, yellow band). In the superior parietal lobe (SPL) of the DAN, the initiator areas are protruded along this band, wider on the right side.

Fourth, V1 exhibits a distinct activity compared to other areas of VN, although not homogenously as in QPP1. The center of the visual field is positively correlated with nodes of FPN.

Fifth, reflected in the peak time map, medial nodes of FPN or VAN peak sooner than lateral nodes. Also, areas of SMN, ventral VN, and auditory network (AN) including superior temporal lobe (sTL) peak sooner than medial nodes of DMN.

Finally, about laterality as a neurocognitive feature, the first cluster, which includes nodes of DMN, is narrower in the right ifg and Ag.

Cerebellum. Cerebellar activity matches Buckner's parcellation, such that cerebellar areas parcellated as the DMN, in addition to a strong correlation with the cortical nodes of the DMN, are anticorrelated with the cerebellar areas parcellated as TPN (FPN, VAN and DAN) and cortical nodes of TPN. Note, the DMN-coactive areas are wider at the right cerebellar hemisphere (Y=-61,-74, Z=-29,-38). At the sign-switching timepoints, and around crus I/II, activation expands from DMN-coactive to TPN-coactive areas, or along the cerebellar FCG2 [30]. The *cerebellum slightly lags the cortex* (Figure 23c).

Thalamus. Thalamic areas that are coactive with the cortical SMN and VN are mainly located postero-laterally, in line with the consensus about their tract-based connections. The majority of the remaining thalamus is coactive with nodes of the FPN/VAN, while a smaller medial portion is coactive with the narrow transitory areas between the nodes of the FPN/VAN and DMN. A very small portion located in the medial part of the mediodorsal nucleus (MD), is coactive with nodes of DMN (Y=-11, X=-14 to 10, Z=11, right histogram in Figure 23c). Note, the medial part of MD has tract connections with the medial PFC and the lateral parts of MD with the lateral PFC [51].

Consistent with the cortex, at the sign-switching timepoints, activity expands from the medial-MD (coactive with the DMN) to the lateral-MD (coactive with the FPN) and further to the antero-lateral areas of the thalamus (note the gradient of peak times in Y=-11, and the thalamus-MD timecourses in Figure 23b). This is *evidence for existence of another macroscale FCG across the thalamus*. As in QPP1, and *as activity propagates to the cortical nodes of the FPN/VAN, the thalamus takes a lead with a median of 6 timepoints (4.3s)*, specifically before the FPN node in the left smg (Figure 23c).

Hippocampus and amygdala. These regions are coactive with the DMN, yet *like the SMN, ventral VN and AN, they peak slightly earlier than the DMN* (Figure 23c), with parts of the amygdala belonging to the initiator cluster (Y=-5). Furthermore, the posterior part of the hippocampus slightly lags the anterior (Figure 23g), although not as pbvious as in QPP1. This reveals propagation along the long axis, or the hippocampal FCG1, but now from anterior to posterior. The cortical parahippocampal area also exhibits a similar anterior-posterior lead, such that its border with the RSC belongs to a transitory cluster. Different from other subfields, the subiculum, located the most medially, contains a range of clusters (not shown), perhaps due to the hippocampal FCG2.

Brainstem and deep brain nuclei. These arousal promoting nuclei are now mostly coactive with the cortical nodes of the FPN/VAN, and interestingly, during the activation regimen, they *take a lead with a median of 5 timepoints (3.6s) which is now comparable to the lead time of the thalamus* (Figure 23c). The *earliest voxels are located more medially*, at the probable space of neuroadrenergic locus coeruleus (LC), seretonergic dorsal and medial raphe (DR/MR), dopaminergic ventral tegmental area (VTA), and hypothalamus. There are more voxels with strong amplitude on the right side (X=-9 to 10). Voxels which are anticorrelated with the FPN/VAN are located in the pons (possibly pontine nucleus), hypothalamus and nucleus accumbens (NA).

Striatum. Striatal areas are now mostly coactive with the cortical nodes of the FPN/VAN. However, the ventral striatum is coactive with the cortical transitory clusters (transitory-coactive areas), and a few ventro-medial voxels are coactive with the cortical nodes of DMN (Y=9,15). Consistent with the cortex and most other subcortical regions, at the sign-switching timepoints, activity expands from the DMN- or transitory-coactive to the FPN/VAN-coactive areas, along both rostro-caudal and medial-lateral axes. The propagation axis is again along the striatal FCG, from the most rostral to the most caudal areas. *During the activation regimen of FPN/VAN, striatum lead with a median of only 3 timepoints (2.1s)*, less than the lead times of the thalamus and brain stem nuclei.

3.3.3 QPP3

Within QPP3, the **cortical** areas that belong to the unimodal SMN and VN are anticorrelated with one another. The cortical nodes of the VAN and DMN are correlated with the cortical areas of SMN, and the cortical nodes of DAN and FPN are correlated with the cortical nodes of VN.

QPP3 matches the cortical FCG2 and mainly involves a simple cycle of activation and deactivation of the cortical areas of SMN, in an anti-correlated fashion with the cortical areas of VN. However, as activation levels are switching in the areas of SMN and VN and for a short time afterwards, focal propagations occur from the areas of SMN/DMN via the nodes of VAN, to the nodes of DAN, later the nodes of FPN, and finally towards the nodes of DMN.

Note the flow of activity across the following nodes. From SMN eye area via 55b to PEF/FEF and later to DLPFC/superior-preM, from FPC via ifs to DLPFC (Figure 24d) and finally towards ifg, from FPC directly to lateral orbitofrontal cortex (lOFC) (Figure 24d) and last towards ifg, via mI to aI, via temporo-parieto-occipital junction (TPOJ) to MT (timepoint 14) later temporo-occipital junction (TOJ) and finally towards mTL, via area PF to inferior parietal lobe (IPL) later smg and finally towards Ag, from SMN foot area via mid cingulate cortex (MCC) to dACC, importantly, from PCC directly to RSC and POS (timepoint 13). *Note,* the RSC and POS are coactive with a band in the medial VN, near and along its border with the PCC, and activation expands from this band towards the medial VN.

While the nuanced dynamics of the focal propagations are not reflected in the summary maps in Figure 24a, some gross noteworthy features are, which are worth highlighting here.

First, nodes of the salience network [47], dACC and aI, are coactive with the VN.

Second, when activation is switching from the SMN to the VN, earlier activity occurs in the well-known motion-vision areas of FEF, MT, even RSC [56], and interestingly, the superior colliculus (SC) (X=-4,5).

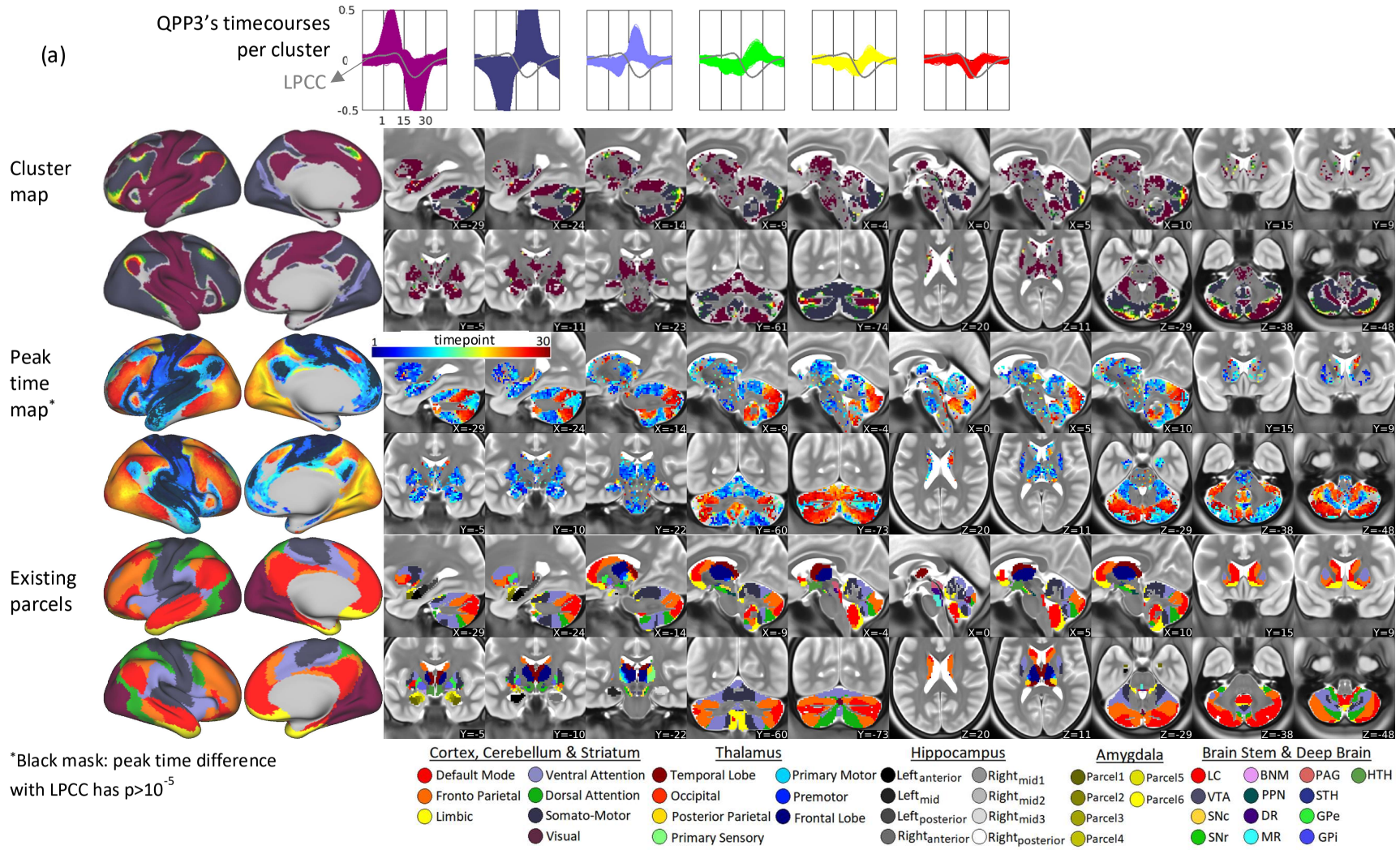

Figure 24 (a) QPP3's summary of activity. (b) Examples of timecourses per existing parcels. (c) #Voxels /peak time and /cluster. (d) Peak time map frontal and dorsal views. (f) Closeness of flow of peak activation is not captured by the current clustering.

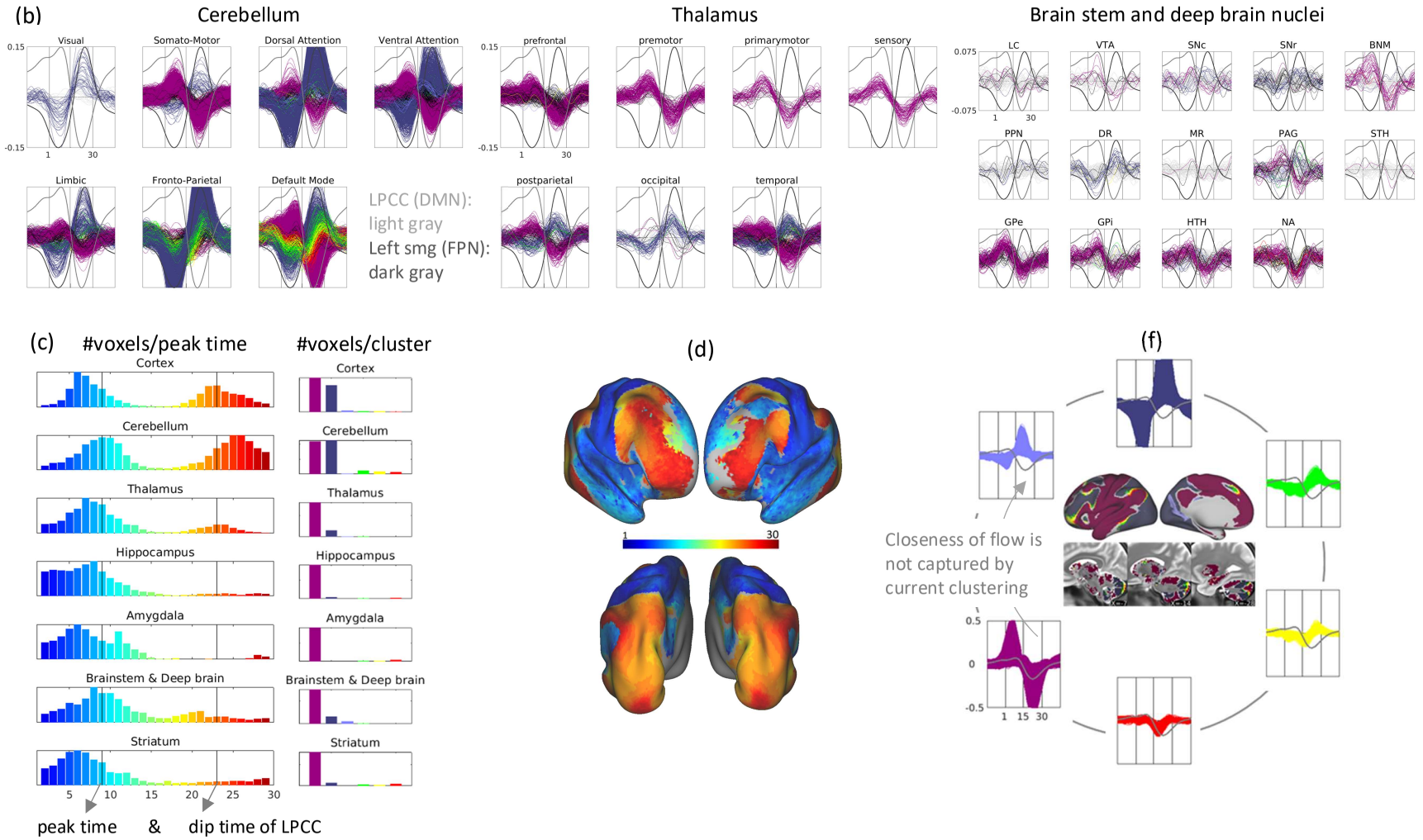

Figure 24 continued

Third, timings of peak activation in different regions again form a closed flow, which is evident based on the histogram of peak times (Figure 24c) – clustering parameters can be tuned to readily reflect this point (Figure 24f).

Fourth, in a QPP3 with reversed phase, where the VN is activated first, the direction of the focal propagations exactly reverses, i.e., from FPN to DAN and via VAN to SMN/DMN, or from POS/RSC/VN-band to PCC.

Finally, about laterality, the first cluster, which includes nodes of DMN, is wider at left ifg, Ag, even PCC and includes left 55b.

Cerebellar coactivity still matches Buckner's parcellation, with propagation from FPN to DMN after the switching timepoints, a *slight lag relative to the cortex*, and a wider first cluster in the right hemisphere. *Interestingly*, now the primary SMN map in lobules I-V exhibits strong amplitude. *Also,* the pons, or possibly the pontine nucleus, is pronouncedly coactive with the SMN/DMN.

Postero-lateral and notably medial areas of the **thalamus** are coactive with the SMN/DMN (X=0 to -14), while a small area, located even more postero-laterally, is coactive with the VN (X=-14, Z=11).

Hippocampus, **amygdala** and **posterior putamen** are mostly coactive with the SMN/DMN, however *similar to SMN, with overall earlier peak times compared to the DMN* (also note scattered red voxels in with earlier dip times). A Few voxels in the **anterior caudate** are coactive with the cortical areas mediating the late focal propagations.

3.3.4 QPPG

Within QPPG, activity propagates along the **cortical** FCG1, from the areas of SMN to the nodes of DMN, particularly obvious in the high anti-correlator subgroup (Figure 25, note the shift in the average peak time of timecourses in the first cluster, the transitory green and yellow clusters and the second cluster, also note the gradient of peak times).

Propagation along FCG1 occurs within QPP1 and QPPG. As shown in the previous chapter, the contributing segments to these two patterns are statistically interleaved. Moreover, within QPP1, the respiration variation (RV) peaks around the switching time of areas belonging to the SMN and DMN, while within QPPG, the RV peaks around the same time with all areas but the nodes of DMN, i.e., the RV peaks at the same time of the global signal (GS). Also, laterality, as a neurocognitive feature, is less pronounced in QPPG (not shown). *Together,* these statements can imply *two different neurophysiological patterns give rise to the cortical FCG1, one being more neuronal (QPP1), the other being more physiological, or in other words, both non-neuronal and neuronal (QPPG).*

Cerebellar coactivity still matches Buckner's parcellation, specifically around crus I/II (the primary and secondary maps of the DMN) and lobule IX/X (the tertiary map of the DMN), with a *slight lag relative to the cortex*, which is particularly obvious in the high anti-correlator subgroups.

The MD nucleus of the **thalamus**, particularly the medial part, and other arousal promoting nuclei in the **brain stem and deep brain**, particularly the BNM, SN, and NA are anticorrelated with the global activity or the GS, *an indicator of low arousal* [28,57]. This anticorrelation is in line with a recent report [28] which only involved MD and BNM.

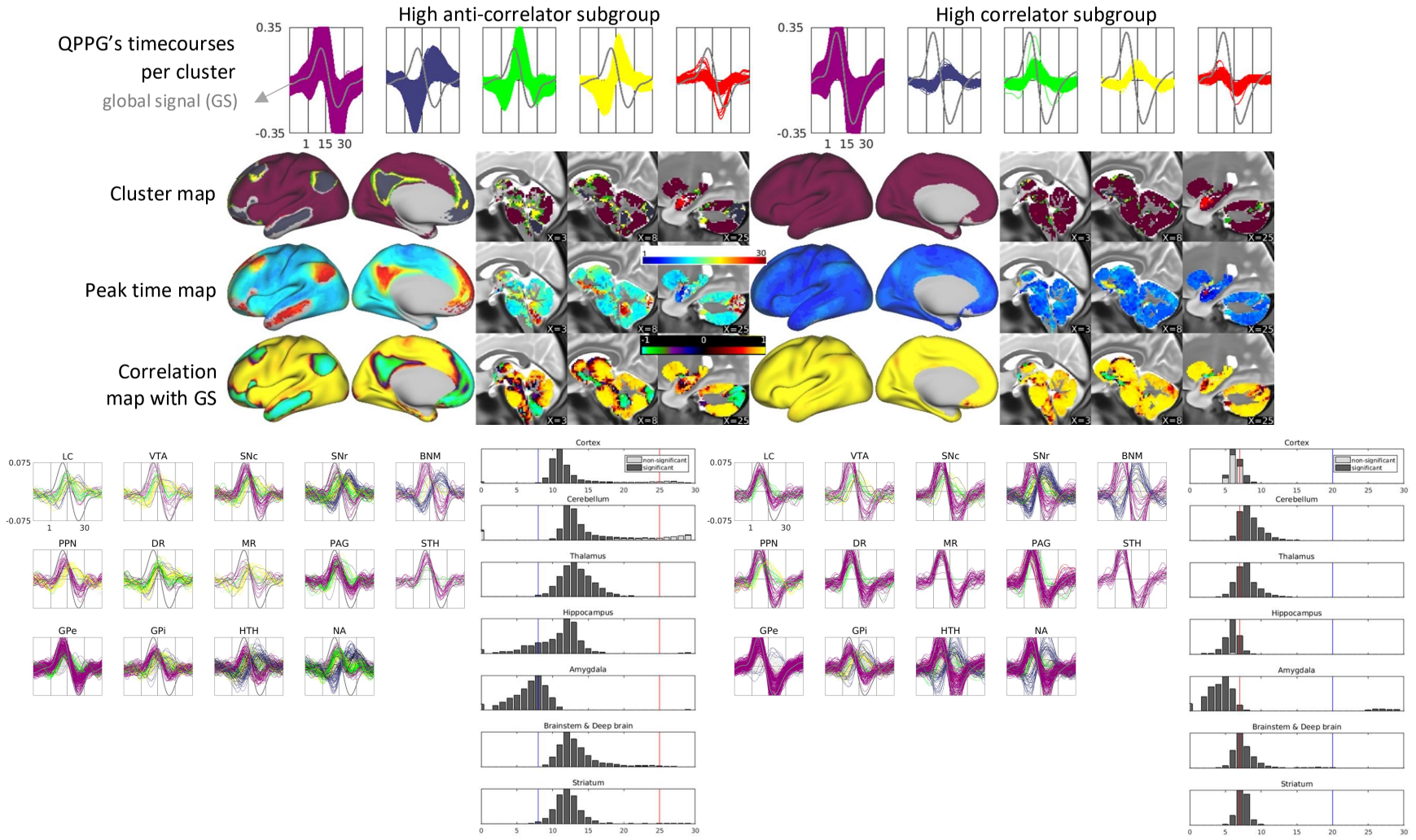

Figure 255 QPPG's summary of activity, number of voxels per peak time and timecourses per brain stem and deep brain nuclei.

Importantly, this trend is more spread and obvious in the high anti-correlator subgroup, where earlier activity in other nuclei such as LC, DR, and VTA compared to BNM, SN and NA are also evident. *It is worth emphasizing,* BNM, SN, and NA are strongly correlated with the DMN. *Interestingly, the thalamus, the brain stem and deep brain nuclei, and the striatum, all slightly lag the cortex*. This could be in line with the reported cortical lead during sleep [58].

Anterior hippocampus and amygdala, *interestingly, are no more coactive with the DMN* but with all other areas including the SMN, i.e., *they are coactive with the GS*. *Importantly*, anterior hippocampus and amygdala exhibit a *relatively earlier peak/dip time compared to the GS* (red cluster), i.e., they initiate the cycle. This can be in line with the reports on the global activity locked with the hippocampal sharp-wave ripples (SWR) [4,59]. Additionally, the posterior part of the hippocampus exhibits the same peak/dip time as the GS. The last two points together indicate *an anterior to posterior flow of activity along the hippocampus. This can be again contrasted with QPP1, with a similar cortical flow but reversed hippocampal flow.*

As a final note, based on our description of QPPG, *activity initiates in the anterior hippocampus and amygdala propagates along FCG1 across the cortex, but terminates in the DMN*. Therefore, the *flow of activity is not closed within QPPG*, which can be viewed as another difference with QPP1.

3.3.5 Supporting analyses

Patterns obtained based on the timeseries with no filtering or nuisance regression (not shown), qualitatively have all the main characteristics reported here for QPPs 1-3, such as coordinated propagations in all regions along FCGs, proving our results are not

artifacts of preprocessing. Patterns with a reverse phase (not shown) exhibit all the main characteristics, such as coordinated propagations in all regions along FCGs, nuanced driving relation between regions and closed flow of activity, proving our results do not depend on a particular phase of the cycle.

3.4 Discussion

Summary and significance. QPPs involve coordinated propagating activity along the functional gradients at the cerebral cortex and most subcortical regions, matching the consensus on tract-based connectivity. Nuanced timing differences between regions and the closed flow of activity throughout the brain suggest drivers and origins for these patterns. The characteristics of these patterns are not artifacts of filtering, nuisance regression, or a particular phase.

Our thorough characterization of the activity within QPPs, as recurring patterns that dominate the intrinsic functional connectivity, has revealed a handful of novel aspects about the brain's self-organization, and we will discuss the more important and more specific aspects in the next chapter. In what follows, method related aspects of the results of this chapter are discussed.

QPPs reflect neuronal activity. QPPs 1-3 reflect neuronal activity for the following reasons. *First,* these patterns qualitatively give rise to the cortical RSNs, each of which is shown to have a domain-general functionality in a wide range of tasks (see appendix D) or behavioral-level correlates, paradigms that are attributed to the functionality of the brain [3,12-13]. Moreover, evidence for the RSNs exists based on more direct neuroimaging modalities, such as electroencephalography (EEG) [60-63], electrocorticography (ECoG) [64-66] or magnetoencephalography (MEG) [67], even

based on *microanatomical constraints, such as categories of gene expression* [68] and *cyto-/myelo-architecture* [69-71], or baseline metabolism rates [72-74].

Second, QPPs 1-3 involve a handful of nuanced neuronal features, *the most pronounced being* the laterality, e.g., within these patterns, the cluster of areas belonging to DMN are wider in the left cortical hemisphere, while those belonging to TPN are wider in the right, both being functionally relevant. Laterality exist elsewhere as well, such as left areas of 55b, IFJ, and SFL that are involved in language, or the area in the mid ventral visual stream that possibly has a microanatomical correspondence [75]. *Another exemplary neuronal feature* is the focal cortical gradients, with functional or microanatomical correlates, such as along V1, across TL [76], or in the PPL (note the axes of division from 7 to 17 RSNs as speculated by Yeo and colleagues).

Third and equally important, coactivity between the subcortical and cortical areas mostly matches the consensus about their tract-based connectivity. Laterality in the cerebellum matches its contralateral polysynaptic connections with the cerebrum. The postero-lateral areas of the thalamus are coactive with the cortical areas of SMN and VN, or the most medial areas in the MD nucleus are coactive with the medial PFC. Propagation along rostral-caudal and medial-lateral axes in the striatum matches its topographical tract connections with the cerebrum. Laterality in the brain stem matches its ipsilateral connections with the cerebrum. Additionally, propagation along the hippocampus matches the axis of its functional and microanatomical differentiation.

Finally, QPPs 1-3 are not affected by nuisance regression including the gray matter signal, and their contributing segments are interleaved with those of QPPG, which might be more physiological than neuronal.

The following points about non-neuronal confounds are noteworthy. First, although the CSF signal is regressed, the residuals seems to have remained in the borders between the ventricles and almost all the subcortical regions. In Figure 21 and Figure 25, note the caudate bordering the lateral ventricles, the medial thalamus and the hypothalamus surrounding the third ventricle, the brain stem nuclei or the cerebellar lobule X neighboring the fourth ventricle, and the hippocampus and amygdala along the temporal horns of the lateral ventricles which not easily observable.

Since the CSF signal is negatively correlated with the global signal (GS), as mentioned in the previous chapter, and the GS is negligible within QPPs 1-3, likely the CSF signal should be small within these patterns, which can easily be inspected in future. *Regardless*, it is unlikely that the CSF residuals, in the borders with the ventricles, affects the trends of activity across all areas in the subcortical regions within QPPs 1-3, because these trends can be neuronally supported as mentioned above. Within QPPG, CSF residuals are larger, and the subcortical trends should be viewed with more caution.

Second, the hemodynamic response function (HRF) is variable across brain areas, and our results is centered around timing differences between areas, mostly between time of peak activations but also based on times of sign switching or dip of deactivation. Therefore, as will be recommended for further research, it is necessary to examine datasets without HRF confound, which are based on more direct neuroimaging modalities, such as ECoG or MEG in humans (limited to cortical areas), or invasive recordings in non-humans (can include subcortical areas).

Finally, although QPPs reflect neuronal activity, as just discussed, likely they have neurophysiological basis, as argued in the previous chapter. Therefore, certain aspects

of systemic physiological fluctuations that include non-neuronal sources, might be inherent part of these patterns. As recommended for further research, all parts of our results, including possible neurophysiological basis of QPPs, need stronger characterizations, e.g., invasive recordings in non-humans in controlled settings.

Conquering the dominance of QPPs in the cerebral cortex. Brain is a complex system and exhibits varied dynamics regimes of coherent activity. In the rsfMRI timeseries, along QPPs, very likely, fast focal spatiotemporal patterns exist, linearly superimposed or non-linearly interactive. Systematically addressing the dominance of QPPs, which might have neurophysiological basis, by temporarily regressing them, can possibly enhance the detectability of the minor patterns, which might have more neuronal basis.

Explained variability in subcortical regions. As pointed earlier, if the input for the QPP analysis includes timeseries of the cortical and subcortical regions, the output would be dictated by the cortical events and the subcortical activity would basically be coactivity locked with those cortical events. The variability explained in each subcortical region by such coactivity can easily be inspected in future. As recommended for further research, existence of independent recurring patterns in each subcortical region can be explored, by considering the timeseries of only that region for the QPP analysis.

Medulla. Since the medulla contains nuclei for respiration control [77-78] and all QPPs have a principled relation with the respiration variation, the medulla's activity, which is observed in all QPPs, can be easily included in our future reports.

Propagation speed. Speed of propagation can be calculated *for the cortex based on the geodesic distances* (i.e., distance across the 2D surface of the cortical sheet) and for

the subcortical regions based on the Euclidean distances (i.e., distance in 3D space). A unit of distance might be taken to obtain a speed map, since qualitatively propagation speed does not seem constant. Quantifying the propagation speed is the first step for speculating (even examining) the possible mechanisms for propagation of activity.

Significance of timings in QPPs. For all QPPs, we have only tested significance of difference for the peak times between all areas and LPCC, between pairs of clusters or pairs of RSNs, with all qualitative differences being quantitatively significant. *Comprehensive significance testing* can be easily performed in future. For each QPP, timecourses per cluster per subregion can be calculated and significance of differences in the times of peak, dip and switching between any pair can be tested. By subregion, we are referring to the anatomically separated areas per each of the seven regions, e.g., in the cortex, having subregions of the lateral PFC, or aI/dACC, or in the cerebellum having subregions of the crus I/II or lobules IX/X.

Furthermore, significance testing can easily be done for the patterns obtained without filtering and nuisance regression or the patterns with a reverse phase.

Significance of amplitudes in QPPs. To visualize QPPs in grayordinates, no threshold for amplitude was considered, unlike the report by Majeed and colleagues. Our approach can reveal the continuous trends more clearly, i.e., weak amplitudes that get stronger within the duration of the patterns. What amplitude is significant was examined based on two approaches. *First,* randomly selected segments, equal to the number of the contributing segments of each QPP, were averaged, repeated multiple times. In all cases, the 30-timepoint timecourses of all areas, had almost zero peak-to-dip amplitudes ($<10^{-4}$). *Second,* the distribution of the peak-to-dip amplitude of all timecourses for each

QPP was examined. All distributions were bimodal with the lower mode being ~0.05 and mostly corresponding to the subcortical areas. For clustering and finding peak times, we considered only those timecourses with peak-to-dip amplitude above 0.05 for the subcortical areas but above 0.1 for the cortical areas. The latter threshold was more a qualitative choice and does not influence any piece of the results.

QPP4 and above. Although out of the scope of this thesis, qualitative inspection of QPPs 4 to 7 based on a random subset of individuals revealed these patterns still involve propagation. However, constellation of correlation between nodes of RSNs or the axes of macroscale and focal propagations are unique to each pattern.

Minimum group size. Main characteristics of QPPs, including propagations across the cortex and subcortical regions, are easily observable based on ~20 individuals of the HCP dataset with 1hr resting-state scan per individual and an exemplary quality. We did not easily observed propagation at the individual-level, based on a few individuals we randomly inspected. However, this needs to be quantitatively examined as a future work.

CHAPTER 4: DISCUSSION

4.1 Introduction

To better understand QPPs, as recurring patterns of brain's intrinsic activity that might serve self-organization, we have improved the detection method of QPPs, showed the extent of their contribution to the functional connectivity (FC), and thoroughly characterized them.

QPPs involve coordinated propagating activity along the functional gradients at the cerebral cortex and most subcortical regions, mainly matching the consensus about the tract-based connectivity. Nuanced timing differences between regions and the closed flow of activity throughout the brain suggest drivers and origins for these patterns. QPPs dominantly contribute to the FC between brain areas, within and particularly between the resting-state networks (RSNs). These patterns reflect neuronal activity and are not artifacts of preprocessing such as global signal regression or filtering. Due to a principled timing relation with the slow variations in respiration and heart rate, QPPs might have a neurophysiological basis. Overall, our results suggest *a few recurring spatiotemporal patterns of intrinsic activity might be dominantly coordinating the whole-brain functional connections, serving the purpose of self-organization*.

Furthermore, QPPs reveal novel specific aspects about RSNs and FC gradients (FCGs), and also about the driving relations between regions and the origins of QPP cycles. We start this chapter by discussing such aspects. Since our results are mainly based on contribution to FC and propagation of activity, we further discuss how QPPs relate to the already known contributing factors to FC and existing reports of propagation of activity.

4.2 Functional networks and gradients

The first novel specific aspect revealed by QPPs is related to the RSNs and FCGs. The discussion ahead is separated for the cerebral cortex and the subcortical regions, since QPPs are dictated by the cortical events, as pointed in the previous chapter.

Cerebral cortex. QPPs give rise to the FC between cortical areas, the FC between areas is the basis to obtain the macroscale cortical RSNs, and these RSNs are observable within QPPs. Therefore, *QPPs very likely give rise to the macroscale cortical RSNs*, which can be quantitatively shown by analyzing the residuals after regressing these patterns and using the same clustering algorithm. *Importantly, the borders of the major cortical RSNs*, e.g., between FPN and DMN or between SMN and DAN, *are attainable based on the summary of at least two QPPs*, e.g., QPPs 1 and 2 or 1 and 3.

This point significantly enriches our insight about the macroscale cortical RSNs, suggesting they are overlaid snapshots of a few dominant coordinated propagating patterns across the whole brain, with each pattern representing a certain set of segments and entailing a handful of nuanced information. Furthermore, this point implicates in the macroscale parcellations of the subcortical regions with regards to the macroscale cortical RSNs, as discussed next. It can also inform the hypotheses about functionality served by QPPs, their task interactions or behavioral correlates, as will be recommended for further research.

It is worth rewording, the same cortical areas that exhibit gradual change in one QPP (e.g., gradual shift in peak times), can exhibit a very sharp change in another QPP. Constrained by the same macroscale anatomical architecture, different macroscale functionalities can be expressed by the differential activity of the same areas.

QPPs give rise to FC, FC is used to obtain the macroscale cortical FC gradients (FCGs), and these cortical FCGs are swept within QPPs. Therefore, *QPPs very likely give rise to the macroscale cortical FCGs* as well, which can be shown quantitatively. This point is also significantly insightful, suggesting each macroscale cortical FCG is a snapshot of a coordinated propagating pattern across the whole brain that represents a certain set of segments and entails nuanced information. *Recall,* macroscale FCGs and RSNs match one another, one entailing gradual or sharp changing values and the other parcels and borders. Note, similar to QPPs, at least two FCGs are required to obtain the borders of the major RSNs (FCGs 1 and 2 or 2 and 3).

Subcortical regions. Our discussion in the subcortical regions first starts by the thalamus and later the argument is generalized to other subcortical regions.

In QPPs 1-2, activity propagates along the cortical, cerebellar, hippocampal and striatal FCGs, and these four FCGs have already been reported. The propagation of activity in the thalamus, from the posterolateral unimodal to the remaining transmodal areas in QPP1, and from the medial mediodorsal nucleus (MD) to the lateral MD and later to the anterolateral transmodal areas in QPP2 are novel suggestions for two thalamic FCGs.

Existing studies on the thalamic FC alone are either inconsistent, particularly with regards to the *FC with the cortical RSNs (RSN-based parcellation)*, or do not readily match the tractography-based connectivity [79-81]. Since QPPs likely give rise to the cortical RSNs, they can offer insight about RSN-based parcellation of the thalamus - Regarding what follows, have in mind, each QPP is an average of certain segments of rsfMRI timeseries, and borders of all cortical RSNs are not attainable within one QPP.

Although the unimodal thalamic areas are coactive with the unimodal cortical areas within all QPPs, a given transmodal thalamic voxel is not necessarily coactive with a given cortical vertex, when considering all QPPs. In other words, *RSN-based parcels in the transmodal thalamus change between QPPs.* Thankfully, consistent rules exist. For example, a large portion of the transmodal thalamus is coactive with the transitory areas extending across the borders of the trasnsmodal cortical RSNs in QPPs 1-2. Another example is the most medial MD that is coactive with the DMN within all QPPs, perhaps due to its known tract connection to the medial prefrontal cortex.

Taken together, to obtain clear RSN-based parcellation in the thalamus, it might be essential to (i) consider only certain segments of rsfMRI timeseries at a time, even further averaging them, as opposed to the common practice of including the whole timeseries, (ii) expect a few parcellation schemes for the transmodal thalamus not just one, and (iii) credit the borders of RSNs as much as the RSNs themselves.

Similar to the thalamus, for other subcortical regions, QPPs offer insight about the RSN-based parcellation (i.e., coactivity map), given the inconsistent related literature.

Brainstem and deep brain nuclei are coactive with the FPN/DMN in QPP1 and the FPN/ventral attention network (VAN) in QPP2, with some voxels coactive with the transitory areas in both QPPs. See [82-84] for examples of inconsistent related reports.

Amygdala is coactive with the superior temporal sulcus (STS) and anterior hippocampus in QPP1 and the DMN, superior temporal lobe (sTL) and hippocampus in QPPs 2-3. See [85-86] for examples of inconsistent reports.

Coactivity of the lobules I-V and VIII-X of the *cerebellum* and the *striatum* with the cortical RSNs *changes between QPPs*, respectively see [30] and [42,87] for the discussion on inconsistencies. Qualitatively, all QPPs are required to obtain the borders suggested by Bucker's and Choi's schemes for these regions.

In sum, in most subcortical regions, for a clear RSN-based parcellation, considering certain segments of rsfMRI timeseries at a time, expecting a few parcellations schemes and not just one, and equally crediting the cortical RSN borders might be essential.

It is worth emphasizing, similar to the cortical FCGs, *QPPs likely give rise to the cerebellar, striatal and hippocampal FCGs*, which can be examined quantitatively.

4.3 Drivers and origins

Other novel specific aspects revealed by QPPs are about the driving relations between brain regions and that peak activities form closed flows indicating the origins of infraslow rhythms. *These suggestions are perhaps the main benefit of a propagating pattern*.

Driving relation between brain regions. *As the starting clarification,* in healthy humans and with non-invasive functional imaging, *any claim about the driving relation between brain regions is unavoidably based on temporal precedence with a weak basis* [90]. A strong claim requires invasive and comprehensive characterizations of causal relationships, mostly in non-humans, based on extensive and non-trivial procedures. *Moreover,* we have used the term "propagation" for temporal precedence within each brain region and the term "drive" for between regions (see appendix C for another clarification about these two terms).

As the summary of results, in all QPPs, *the cerebellum* lags the cerebral cortex, in other words, the cerebellum is driven by the cortex. *The transmodal thalamus and the brain stem and deep brain nuclei* take lead as activity propagates to the cortical nodes of FPN/DMN in QPP1 and FPN/VAN in QPP2, in other words and in brief, the thalamus and brain stem drive the cortex in the switching phase of the TPN and DMN in QPPs 1 and 2 (medians: 4.3s and 4.3s for the thalamus, 2.9s and 3.6s for the brain stem, in QPPs 1 and 2, respectively). *The striatum* is in synch with the cortical FPN/DMN in QPP1 but take a slight lead (median: 2.1s) relative to the cortical FPN/VAN in QPP.

That the *cerebellum* is driven by the cortex in all QPPs, and that QPPs organize the brain, together, can imply the cerebellar organization is influenced by that of the cortex. Through intrinsic recurrence over time, such cortical influence can form and refine the functional connections that underlie the known cerebellar role in skilled motor and cognitive executions [29-30,48-49] *(see appendix D for a summary of functionality of brain regions and cortical RSNs)*.

That the *thalamus and brain stem* drive the cortex when the TPN and DMN are switching, first, reveals a specific key role for the thalamus in switching the focus of attention between externally oriented and internally oriented, in line with its general role in attention control [50-51,88]. Second, the brain stem, that can promote arousal and reinforce attentiveness [84,89], has a secondary role relative to the thalamus in such attentional switching, due to a shorter lead time, even in QPP2.

Two points are noteworthy. Intrinsic activation of the DMN is not always associated with a subjective report of internally oriented attention or other cognitive processes attributed to the DMN [91]. However, intrinsic activation, specifically as part of a well-coordinated

pattern, can always be viewed as serving the brain's self-organization, e.g., by activating the functional connections that underlie meaningful processes for the future tasks, based on the aggregate of the previous experiences with similar tasks.

Furthermore, switching phase of TPN-DMN is a simplified and common statement, and the dynamics of switching are still not well studied (see the latest citations of [47]). Based on QPPs 1and 2, we are referring to the timepoints when the activation is expanding from the VAN to FPN/DMN in QPP1 and from the DMN to FPN/VAN in QPP2. Qualitatively, the cortical nodes of *FPN, or the executive control network* [44], are the commonality between these two QPPs. This point is worth inspecting in future. For instance, examining whether the common cortical areas belong to one of the two subnetworks of FPN (one involved in the initiation of new strategies and the other in task-maintenance). *Moreover,* such inspection informs the interpretation of the activity and timings in the *striatum* as well, because of similar qualitative commonality between QPPs 1 and 2 regarding the executive control network, and given the known involvement of the striatum (or basal ganglia in general) in the motor and cognitive executions [41-42,87].

As the closing highlight, despite a weak basis for our claim about the driving relations, *there is higher confidence* in our results, compared to similar non-invasive reports in humans (elaborated with citation in the last section), because of inclusion of all regions in the brain. For example, the driving relation between two regions is not attributable to a third region which was not included because of the imaging limitations. *It is worth emphasizing,* our claim about driving relation is at the macroscale and infraslow band (<0.1Hz), indicates average of similar segments, and does not include possible indirect influences between regions that can result in similar outcomes. As will be recommended

for further research, it is easily possible that activities outside of QPPs, e.g., which are focal fast, play a role as drivers within the cycles of these patterns.

Origins. Having all regions of the brain with peak activities that form closed flows within the ~20s-long cycles of QPPs 1-3 indicates infraslow rhythms of ~0.05Hz comprised of back-to-back cycles can exist.

As the essential starting clarifications, note the following. Although the phase of the QPP cycles are adjustable, we have described the activity as being initiated or terminated in certain regions/areas. Terms “initiation” and “termination” are adopted from the reports on the propagating activity. They are meaningless for a rhythm which is ongoing and is absolutely robust to the external perturbations. If a cycle is totally suppressed due to external perturbations, *there is a need for an initiation mechanism to resume the rhythm*. If a region/area is a *cardinal oscillator*, e.g., based on its cell properties in certain conditions like the thalamocortical units, it can be recognized as the *initiator of the cycle* and *the phase of the cycle can be set accordingly*. For brevity in what follows, we have considered regions/areas of initiation and termination as the initiators, even if the termination region/area might just contribute to the conditions required for the oscillation of the initiation region/area.

As the final clarification, ~0.05Hz is the mid frequency of 0.01-0.1Hz, the widely used range for filtering the *inherently slow* BOLD-based fMRI timeseries. Such range (0.01-0.1Hz) belongs to the infraslow band, the *most liberally taken as the frequency band less than 1Hz*, in studies which are based on more direct neuro-imaging modalities than BOLD-based fMRI. The closest neighbors of infraslow band (<1Hz) are the delta band (~1-4Hz) and the well-known slow waves (~1Hz).

Neuronal activity in the infraslow band, as recorded by more direct neuroimaging modalities, is *widely known to be arrhythmic*, because of no apparent “bump” in the power spectrum but 1/f distribution [5] – the *neuronal basis* of this band is supported by various evidences such as attenuation by the onset of a task as recorded by ECoG [5,64] or attenuation by neuro-blockers as recorded by EEG [92]. *Moreover*, the infraslow activity is *widely thought to only arise from the collective interaction of faster rhythms*, with a body of evidence solely showing the amplitude of the faster rhythms fluctuates infraslowly [5,9,60-63] – even slower rhythms with a spectral “bump” (~1-10Hz) are also known to arise from faster rhythms, even further modulating those faster rhythms, giving rise to the complexities in the generation of all neuronal rhythms regardless of the frequency [5]. *Despite of the prevailing perspective about the origin of the infraslow activity,* Hughes and colleagues [52] have shown, ex-vivo, that the thalamic relay cells can generate an infraslow rhythm (<0.1Hz), specifically, spike bursts which are a-few-tens-of-seconds apart, given the right excitability, with an astrocytic-dependent mechanism – it is known that the thalamic cells can also generate slower rhythms (~1-10Hz) in the low arousal states and, in-vivo, the thalamus closely interacts with the cortex in this regard, to the extent that the thalamocortical units are viewed as cardinal oscillators [54-55]. *Taken together, just like all other slower bands, the neural activity in the infraslow band arises from the interaction of the faster bands but also can possibly be generated by the thalamocortical units.*

As the summary of results, in QPPs 1-3, the unimodal thalamus, anterior hippocampus and amygdala are the *subcortical initiators* of the cycle. This is because each QPP begins by the activation of the cortical areas of SMN. In QPP1, the most postero-lateral part of the unimodal thalamus along two other abovementioned regions are slightly earlier than the SMN. In QPPs 2-3, all three regions are roughly in synch with the SMN.

Moreover, the prominent *cortical initiators* of the cycle in QPP1 are areas of foot and genitalia, STS, inferior frontal junction (IFJ), left superior frontal language area (SFL), even left 55, and in QPP2 are the DAN borders with the unimodal networks (SMN/VN), and notably left areas of 55b, IFJ, even SFL, and mid ventral visual stream.

Finally, by considering the subcortical and cortical initiators together and keeping minimal details for our discussion ahead, *the closed flows* can be summarized as follows. In QPP1, activity propagates from the initiators to the SMN, and from the SMN to the DMN, and via the posterior hippocampus back to the initiators, with the flow not trackable between the subcortical initiators (the amygdala and thalamus) but along the narrow-spread cortical initiators. In QPP2, activity propagates from the initiators to the SMN/VN and DMN (including the posterior hippocampus), and from the DMN back to the initiators, with the flow clearly trackable across the wide-spread cortical initiators. In QPP3, activity focally propagates from the initiators that include the SMN to the VN and trends back towards the initiators, with the trackability of the flow needing further work.

That the unimodal thalamus is a subcortical initiator in QPPs 1-3 (particularly QPP1), in synch with the cortical SMN (likely topographically), can ensure resuming a cycle of each QPP, if perturbed. One known condition to us is the right excitability of the thalamocortical units to initiate a cycle. Excitability can possibly be set by the amygdala, another subcortical initiator, via modulating the autonomous nervous system (ANS) [85-86,93-94], or it can be set by any other region, such as the anterior insula, a cortical modulator of ANS [47], the neuromodulatory brain stem nuclei [84,89], or possibly the synchronous activity of a few critical regions. We sum by sculpted questions that require extensive invasive approaches in non-humans to address. Is the synchrony between the unimodal thalamus and a few other areas critical for a cycle to be initiated? Once a cycle

is initiated, to what extent it is robust to the perturbations so that the flow of activity can close and lead to the next cycle? Since the contributing segments of QPPs 1-3 are interleaved, should we even expect a back-to-back occurrence?

4.4 Known contributors to functional connectivity and QPPs in comparison

The *most known contributor* to the intrinsic FC between areas is perhaps connectedness via myelinated tracts that collectively form the white matter 3,6-7,95-101]. For instance, homologous areas between the two cortical hemispheres, particularly in the unimodal networks, tend to exhibit positive FC, because of the direct commissural tract between them. On the other hand, the complex combination of the *local mesoscale oscillations and macroscale connectomics can* result in two areas exhibiting negative FC.

Another contributor to FC, which has recently been established, is the geodesic distance between area (distance across the 2D surface of the cortical sheet, and not the Euclidean distance in 3D space). For instance, the cortical areas maximally distant from the unimodal networks exhibit positive FC and form the default mode network [13].

Other known contributors to the FC between areas are common subcortical inputs [7,95,101] or similar responses to the physiological fluctuations [3,6,9,15,21-22,101-102]. *Note*, fast focal regimes of activity, which are not necessarily bilateral, or generally speaking, not necessarily as constraint by the *macroscale* anatomical architecture, likely exist (examples can be propagating activities in various contexts, mentioned in the next section, or the varied dynamic regimes of coherent activity, mentioned in the introduction). If often and strong enough they can contribute to FC.

Finally, and perhaps the least established contributor to FC is recurring propagating patterns of activity that results in systematic timing difference between areas [16,103-

105], also see [9,15]. For instance, according to our QPPs, two areas exhibit positive/negative FC if their locations correspond to the same/opposite phase of a propagating pattern, or two areas may exhibit no FC while they have a systematic lag.

It is *crucial to note all of these contributing factors are undoubtedly interrelated*. For example, with the evolution being accountable, during the embryonic phase in humans, tract-connections forms between the cortical areas which have maximal geodesic distance from the unimodal areas [7]. As another example, homologous areas in the unimodal networks, which are connected via commissural tracts, more often receive common subcortical inputs or have similar response to the physiological fluctuations.

QPPs, as the propagating pattern that contribute to FC, match the consensus on tract-based connectivity both between cortical areas, e.g., the coarse symmetry between hemispheres, and between cortical and subcortical areas, as elaborated previously. QPPs are about propagation of activity along the cortical sheet, such that areas at varied geodesic distances experience varied phases of the same cycle of these recurring patterns. Within QPPs, the driving influence of the subcortical areas are coarsely symmetric between hemispheres, so is the lagged activity in the corresponding cortical areas. *Taken together,* QPPs as contributors to the intrinsic FC between areas, are in interrelated with other known contributors (i.e., QPPs match other contributors and might reinforce them).

4.5 Existing reports on propagation, mechanisms and our report in comparison

Propagation of activity has been reported in a *range of species* (e.g., humans, monkeys or mice) (see [106] unless otherwise noted), and *arousal states* (awake intrinsic/task-evoked/epileptic, sleep or anesthetized) based on *varied modalities* (e.g., EEG and

ECoG, fMRI [16-17,103-105,107], voltage sensitive dyes [108-109] or genetically encoded calcium imaging [110-113] mostly simultaneous with local field potential recordings or hemoglobin imaging, even modelling [114]) at *multiple spatial scales* (e.g., between cortical lobes, within cortical unimodal areas, or along hippocampus), *frequency bands* (e.g., alpha (~10Hz), theta (~4-10Hz), delta (~1-4Hz), slow (~1Hz) and infraslow (<~0.1Hz)) *and speeds* (~1-10m/s (myelinated tracts of white matter) or ~0.1-1m/s (unmyelinated horizontal collaterals of cortical layers)).

Note, the term “propagation” unanimously refers to the systematic phase shifts or timing difference between the activity of different areas which collectively form either a simple travelling wave (planar/radial/spiral) or any spatiotemporal pattern [106]. By the term “activity”, we broadly refer to the rhythmic synchronies within a population of neurons which induce signal fluctuations in common frequency bands and modalities [106,114].

For the *mechanisms of propagation*, limited candidates have been proposed which include myelinated tracts for speeds ~1-10m/s, unmyelinated collaterals for speeds 0.1-1m/s, subcortical-mediators particularly thalamo-cortical interactions [104,106,113], and additionally for the infraslow band, astrocytic-mediators [116] (also see [17,113]) and hemodynamic waves [117].

The most relevant reports of propagation to our work are those based on rsfMRI in humans. *Majeed and colleagues* 2011 report [16] of QPP1, the foundation of our work, matches our results regarding the focal propagations specifically in the medial PFC, from the mid cingulate cortex to ACC.

Hindriks and colleagues 2019 report [105] of propagation from the task positive network (TPN) to the default mode network (DMN) and from the anterior primary visual (V1) to

the posterior V1 is another match to part of our results. Their argument that RSNs possibly arise from propagating patterns is quantitatively illustrated by us.

Mitra and colleagues reports of the lag threads since 2014 in varied settings [103-104,113], although *far most inspirational and seminal for us*, do not closely match our results primarily due to the following reasons – note, lag threads are principle components of a delay matrix, in which each entry is the interpolated maximum of cross-covariance between timeseries of a pair of voxels. RSNs are shown to arise from one-directional motifs which are common among a few reproducible lag threads, no RSN leads or lags the other, and the range of lags in the threads are ~±1 second, however, with multiple neighboring maxima and minima across the cortex.

Compared to Mitra and colleagues, RSNs are readily observable within QPPs and they clearly exhibit lead/lag relationships. *Compared to all other reports on propagation,* the extent of coordination across the whole brain, accordance with the consensus on tract-based connectivity, and novel nuanced information within QPPs constitute the uniqueness of our report. *Additionally,* the quantitative demonstration of contribution of QPPs to functional connectivity between area and examination of these pattern versus the global signal and particularly the physiological signals are other unique aspects of our report.

CHAPTER 5: CONCLUDING REMARKS

This thesis aimed a better understanding of QPPs in humans, as recurring spatiotemporal patterns of brain's intrinsic activity that might serve self-organization. As the first step, several method improvements were implemented to robustly detect the QPPs. The next step was to demonstrate the contribution of these patterns to the functional connectivity between brain areas, as the most widely used metric of intrinsic organization. As a necessary step, the activity within QPPs were thoroughly characterized, and the novel aspects they reveal about the brain's self-organization, were identified and discussed.

QPPs involve coordinated propagating activity along the functional gradients at the cerebral cortex and most subcortical regions, mainly matching the consensus about the tract-based connectivity. Nuanced timing differences between regions and the closed flow of activity throughout the brain suggest drivers and origins for these patterns. QPPs dominantly contribute to the functional connectivity between brain areas. These patterns are not artifacts of preprocessing such as filtering or global signal regression. QPPs reflect neuronal activity, however, due to a principled timing relation with the slow variations in the respiration and heart rate, these patterns might have a neurophysiological basis. Together, our results suggest a few recurring spatiotemporal patterns of intrinsic activity can dominantly coordinate the functional connections across the whole brain and serve self-organization.

The following paths are recommended for further research.

Optimal detection method. The current method to detect QPPs requires selecting an initial segment with a preset duration and choosing a correlation threshold. This method was developed near a decade ago, as the first attempt to identify similar recurring segments. To this date, we know of two recent and very different methods (unpublished), with minimal requisites, that can detect patterns which are qualitatively very similar to QPPs 1-3 and QPPG. An optimal method to detect QPPs and the extent of our results that can be replicated are worth investigating.

Conquering the dominance of QPPs in the cerebral cortex. Brain is a complex system and exhibits varied dynamics regimes of coherent activity. In the rsfMRI timeseries, along QPPs, very likely, fast focal spatiotemporal patterns exist, linearly superimposed or non-linearly interactive. Examples of such spatiotemporal patterns can be fast focal propagating activity in varied contexts, reviewed in the last section of the discussion chapter. Systematically addressing the dominance of QPPs, which might be neurophysiological patterns, by temporarily regressing them, has the potential to enhance the detectability of the minor patterns, which might be more neuronal, or even might play a role as drivers within the cycles of QPPs or as initiators of the cycles.

Independent subcortical patterns. When the input for the QPP analysis includes timeseries of the cortical and subcortical regions, the output would be dictated by the cortical events and the subcortical activity would basically be coactivity locked with those cortical events. Existence of independent recurring patterns in each subcortical region can be explored, by considering the timeseries of only that region for the QPP analysis, as also reported by Majeed and colleagues [16]. Optimal order for such exploration might be thalamus, hippocampus/amygdala, and basal ganglia. Furthermore, if a neuronally meaningful independent pattern is detected for a subcortical region, coactivity

of other regions, including the cerebral cortex, can be easily explored. The transition matrix between independent patterns of different regions can also be easily examined.

Invasive examinations of propagation and possible mechanisms, drivers, origins and neurophysiological basis. Our report is solely based on a non-invasive indirect and inherently slow imaging modality. Our characterizations, although very likely reflective of neuronal activity to our best of knowledge, are still only based on relative timings and have a weak basis. Strengthening the basis requires invasive and comprehensive examination of causal relationships between brain areas in rodents or primates, based on more direct and faster neuroimaging modalities, perhaps combined with fMRI for whole brain coverage, in controlled settings, even by using various interventions (e.g., electrical stimulation or pharmaceutical agents), e.g., to test driving relations. However, such examinations are inherently extensive and can become non-trivial. Additionally, since the ultimate goal is to understand our own brain, in health and disease, lessons learned from stronger characterizations in non-humans can inform our further investigations in humans. These two avenues complement each other and should be paved in parallel.

Served purpose and task interaction. What purposes are served by QPPs? This question has the ultimate importance, in my view. QPPs should be functionally organizing the brain, at a domain-general level, i.e., with a wide range of behavioral-level manifestations. What purposes are served by the brain itself at a general level to our best of knowledge? What are the primary functionalities of each brain region at a general level to our best of knowledge? *How might the specific activity within each QPP between the brain regions serve the purposes the that are to be served by the brain as a whole, given the primary functionality of each region?* Our best of speculations about these

questions can *form hypotheses to be tested* about possible purposes served by QPPs. Regarding testing such hypotheses, interaction of these intrinsic patterns with task-evoked activations should be very insightful, primarily because of the reduced variability across individuals and the quantifiable behavioral-level manifestation of the brain activity. How might the activity within QPPs change as a task starts, continues and ends? What features of QPPs can predict task performance, at different stages of a task? To what extent these questions can offer insight into purposes served by QPPs?

Clinical alteration and behavioral correlates. Intrinsic functional connectivity (FC) is widely used as a biomarker in psychiatric disorders and neurological diseases or as a predictor of cognitive and psychological traits and states in healthy populations. As dominant contributors to FC, QPPs entail nuanced information, e.g., relative timings between important areas and multiple patterns, which could be more sensitive metrics and cannot be extracted from the FC alone. How various features of QPPs alter in the common clinical conditions or correlate with the behavioral measures are promising avenues to pursue.

APPENDIX A: RV AND HV TIMESERIES

Preprocessing the physiological traces (Figure 10). Both physiological traces were despiked using Matlab medfilt1 and amplitude clipped to -2.5 to +3.5 standard deviation from mean to remove outliers not fixed by despiking. Further, traces were band pass filtered, using fourth order Butterworth with 1dB cutoff frequencies of 0.01 and 1 Hz for respiratory and 0.6 and 3 Hz for cardiac, along with Matlab fdesign and filtfilt functions and zeros pads, inserted at both ends before filtering and removed afterwards to minimize transient effects. Amplitudes of the traces were rescaled to 0–100. Traces per scan per individual were visually inspected based on histograms of amplitudes in time and spectrums in frequency domain (Figure 10b) and only the good quality scans were selected for further processing.

RV timeseries. RV was calculated as the standard deviation of the respiratory trace within a sliding window of 7.2s (10 timepoints), ~ two respiratory cycles, centered around each timepoint of the fMRI scan. Respiratory traces might have short belt detachments or other problems that cause large changes in RV. To identify unacceptable scans, the standard deviation of RV (std RV) for all scans and all individuals were calculated. Only individuals whose std RV for all four scans were within three standard deviations above the median were included.

HV timeseries. HV was calculated as the average of time between successive peaks of the cardiac trace within a sliding window of 7.2s centered around each timepoint of the fMRI scan. For peak detection, Matlab findpeaks function was used with the minimum peak distance set to the temporal value that corresponded to the two-thirds of the largest peak in the frequency domain (Figure 10a showcases the effectiveness of this simple

method). Based on the histogram of the standard deviation of HV (std HV), only individuals whose std HV for all four scans were within three standard deviations above the median were included.

APPENDIX B: AMYGDALA PARCELS

Amygdala parcels by Tyszka and Pauli 2016 [36] include *deep or basolateral group* (lateral (La), basolateral (BL), accessory basal (BM), paralaminar (BLV)), *superficial or corticomedial group* (corticomedial nucleus (CMN), periamygdaloid cortex (ATA)), *remaining nuclei* (central nucleus (CEN), anterior amygdaloid area (AAA), intercalated nuclei (AMY)), and transition areas (amygdalostriatal transition area (ASTA)).

To simplify the qualitative comparison between amygdala parcels and summary of activity within QPPs in Figures 22 to 24, we named La as parcel1, LB as parcel2, BM as parcel3, BLV as parcel4, but grouped CMN and CEN as parcel5, and ATA, AAA, AMY and ASTA as parcel6.

APPENDIX C: NOTIONS OF DRIVE AND PROPAGATION

Regarding usage of terms “drive” and “propagation”, both of which based on temporal precedence, the following provides a further clarification.

Particularly applicable to the cortex and thalamus but generalizable to *any two or more* regions, assume regions C and T each have only three areas with two pairs of areas bidirectionally connected with different latencies, meaning C1<=>C2<->C3 and T1<··>T2<·>T3. Further assume C1 and T1 are directly connected with negligible latency. However, C2 and T2 have complicated connections with any possible latency, likewise C3 and T3.

We see C1 precedes C2, and C2 precedes C3, or C1→C2→C3. We also see T1→T2→T3. Further, we find C1 and T1 are synchronous, likewise C2 and T2, however T3 precedes C3. Based on all the connections between areas and regions, we can say *“C1 and T1 together drive C2 and T2” and “C2 and T2 together drive C3 and T3 with T3 also driving C3”*. We have chosen to say *“activity propagates along C, activity propagates along T consistent and time-locked with C, and as activity propagates to C3, T3 takes a lead”*.

APPENDIX D: GENERAL FUNCTIONALITY OF NETWORKS AND REGIONS

The following provides my personal summary of the domain-general functionality of each transmodal cortical RSN and an overall functionality of each subcortical region.

The DMN is involved in a range of tasks that require internally oriented attention or rely on the internal integrated representations, e.g., thinking about self, social inferences, semantic processing and language [3,7,12-13,45,91,118]. The *TPN* is involved in a range of tasks that require externally oriented attention, and is comprised of the DAN, VAN and FPN [44,47]. The *DAN* is involved in top-down attention, *VAN* in bottom-up attention, and *FPN*, or the executive control network, is involved in the initiation of new strategies and task-maintenance [44]. The FPN includes lateral prefrontal areas involved in the working memory [119] and is known to be human-specific [7,120]. The limbic network (LN) is involved in motivations and regulation of emotions [47,87].

About laterality, as a neurocognitive feature, the DMN nodes are wider on the left cortical hemisphere, while TPN nodes, particularly FPN and VAN, are wider on the right [44].

The *cerebellum* is involved in skilled executions, motor and cognitive [29-30,48].

The *striatum*, as part of basal ganglia (BG), is involved in motivated, goal-directed executions, motor and cognitive [42,87,119,121].

Both the cerebellum and striatum (via other parts of BG) project to the thalamus, not directly to the cortex – and both are known to play role in the procedural non-declarative memories [122].

The *thalamus* relays the sensory inputs to the primary unimodal cortex and is involved in both fast and sustained control of attention in almost all cognitive processes 50-51,88]. Close interaction of the thalamus and cortex can *generate rhythms* of low arousal (~1-10Hz) [54-55] even infraslow (<0.1Hz) [52-53] - thalamocortical units are cardinal oscillators.

The *hippocampus* is involved in encoding and retrieval of the navigational, episodic (self/internally oriented), and declarative memories, interacts with the LN and amygdala, and can *generate unique rhythms* such as sharp-wave ripples [4,122-125].

The *amygdala* is involved in emotions, particularly the fast fear responses, by modulating the autonomous nervous system (ANS), and is also involved in the memory consolidation [85,123,126-127].

The *Brain stem and deep brain nuclei* are involved in tonic and phasic modulation of arousal and attentiveness, modulation of ANS and a host of homeostatic regulations [84,89,128].

REFERENCES

1 Friston, K. (2013). Life as we know it. Journal of the Royal Society Interface, 10(86).

2 Friston, K. (2010). The free-energy principle: A unified brain theory? Nature Reviews Neuroscience, 11(2), 127–138.

3 Raichle, M. E. (2015). The restless brain: How intrinsic activity organizes brain function. Philosophical Transactions of the Royal Society B: Biological Sciences, 370(1668).

4 Logothetis, N. K. (2015). Neural-Event-Triggered fMRI of large-scale neural networks. Current Opinion in Neurobiology, Vol. 31, pp. 214–222.

5 Buzsáki, G., Logothetis, N., & Singer, W. (2013). Scaling brain size, keeping timing: Evolutionary preservation of brain rhythms. Neuron, 80, 751–764.

6 Fox, M. D., & Raichle, M. E. (2007). Spontaneous fluctuations in brain activity observed with functional magnetic resonance imaging. Nature Reviews Neuroscience, 8(9), 700–711.

7 Buckner, R. L., & Krienen, F. M. (2013). The evolution of distributed association networks in the human brain. Trends in Cognitive Sciences, 17(12), 648–665.

8 Logothetis, N. K. (2008). What we can do and what we cannot do with fMRI. Nature, 453(7197), 869–878.

9 Keilholz, S. D. (2014). The neural basis of time-varying resting-state functional connectivity. Brain Connectivity, 4(10), 769–779.

10 Thompson, G. J. (2018). Neural and metabolic basis of dynamic resting state fMRI. NeuroImage, 180, 448–462.

11 Smith, S. M., Nichols, T. E., Vidaurre, D., Winkler, A. M., Behrens, T. E. J., Glasser, M. F., … Miller, K. L. (2015). A positive-negative mode of population covariation links brain connectivity, demographics and behavior. Nature Neuroscience, 18(11), 1565–1567.

12 Yeo, B. T.T., Krienen, F. M., Sepulcre, J., Sabuncu, M. R., Lashkari, D., Hollinshead, M., … Buckner, R. L. (2011). The organization of the human cerebral cortex

estimated by intrinsic functional connectivity. Journal of Neurophysiology, 106(3), 1125–1165.

13 Margulies, D. S., Ghosh, S. S., Goulas, A., Falkiewicz, M., Huntenburg, J. M., Langs, G., … Smallwood, J. (2016). Situating the default-mode network along a principal gradient of macroscale cortical organization. Proceedings of the National Academy of Sciences of the United States of America, 113(44), 12574–12579.

14 Lurie, D. J., Kessler, D., Bassett, D. S., Betzel, R. F., Breakspear, M., & Keilholz, S. (2018). On the nature of time-varying functional connectivity in resting fMRI. PsyArXiv, 1–34.

15 Keilholz, S. D., Pan, W. J., Billings, J., Nezafati, M., & Shakil, S. (2017). Noise and non-neuronal contributions to the BOLD signal: applications to and insights from animal studies. NeuroImage, 154, 267–281.

16 Majeed, W., Magnuson, M., Hasenkamp, W., Schwarb, H., Schumacher, E. H., Barsalou, L., & Keilholz, S. D. (2011). Spatiotemporal dynamics of low frequency BOLD fluctuations in rats and humans. NeuroImage, 54(2), 1140–1150.

17 Thompson, G. J., Pan, W. J., Magnuson, M. E., Jaeger, D., & Keilholz, S. D. (2014). Quasi-periodic patterns (QPP): Large-scale dynamics in resting state fMRI that correlate with local infraslow electrical activity. NeuroImage, 84, 1018–1031.

18 Yousefi, B., Shin, J., Schumacher, E. H., & Keilholz, S. D. (2018). Quasi-periodic patterns of intrinsic brain activity in individuals and their relationship to global signal. NeuroImage, 167, 297–308.

19 Van Essen, D. C., Smith, S. M., Barch, D. M., Behrens, T. E. J., Yacoub, E., & Ugurbil, K. (2013). The WU-Minn Human Connectome Project: An overview. NeuroImage, 80, 62–79.

20 Power, J. D., Plitt, M., Laumann, T. O., & Martin, A. (2017). Sources and implications of whole-brain fMRI signals in humans. NeuroImage, 146, 609–625.

21 Chang, C., Cunningham, J. P., & Glover, G. H. (2009). Influence of heart rate on the BOLD signal: The cardiac response function. NeuroImage, 44(3), 857–869.

22 Birn, R. M., Diamond, J. B., Smith, M. A., & Bandettini, P. A. (2006). Separating respiratory-variation-related fluctuations from neuronal-activity-related fluctuations in fMRI. NeuroImage, 31(4), 1536–1548.

23 Caballero-Gaudes, C., & Reynolds, R. C. (2017). Methods for cleaning the BOLD fMRI signal. NeuroImage, 154, 128–149.

24 Glasser, M. F., Sotiropoulos, S. N., Wilson, J. A., Coalson, T. S., Fischl, B., Andersson, J. L., … Jenkinson, M. (2013). The minimal preprocessing pipelines for the Human Connectome Project. NeuroImage, 80, 105–124.

25 Glasser, M. F., Smith, S. M., Marcus, D. S., Andersson, J. L. R., Auerbach, E. J., Behrens, T. E. J., … Van Essen, D. C. (2016). The Human Connectome Project's neuroimaging approach. Nature Neuroscience, 19(9), 1175–1187.

26 Glasser, M. F., Coalson, T. S., Robinson, E. C., Hacker, C. D., Harwell, J., Yacoub, E., … Van Essen, D. C. (2016). A multi-modal parcellation of human cerebral cortex. Nature, 536(7615), 171–178.

27 Preti, M. G., Bolton, T. A., & Van De Ville, D. (2017). The dynamic functional connectome: State-of-the-art and perspectives. NeuroImage, 160(December), 41–54.

28 Liu, X., Zhang, N., Chang, C., & Duyn, J. H. (2018). Co-activation patterns in resting-state fMRI signals. NeuroImage, 180, 485–494.

29 Buckner, R.L., Krienen, F.M., Castellanos, A., Diaz, J.C., Yeo, B.T.T. (2011). The organization of the human cerebellum estimated by intrinsic functional connectivity. Journal of Neurophysiology. 106, 2322–2345.

30 Guell, X., Schmahmann, J. D., Gabrieli, J. DE, & Ghosh, S. S. (2018). Functional gradients of the cerebellum. ELife, 7, 1–22.

31 Behrens, T. E., Johansen-Berg, H., Woolrich, M. W., Smith, S. M., Wheeler-Kingshott, C. A., Boulby, P. A., … Matthews, P. M. (2003). Non-invasive mapping of connections between human thalamus and cortex using diffusion imaging. Nature Neuroscience, 6(7), 750—7.

32 Krauth, A., Blanc, R., Poveda, A., Jeanmonod, D., Morel, A., & Székely, G. (2010). A mean three-dimensional atlas of the human thalamus: Generation from multiple histological data. NeuroImage, 49(3), 2053–2062.

33 Robinson, J. L., Barron, D. S., Kirby, L. A. J., Bottenhorn, K. L., Hill, A. C., Murphy, J. E., … Fox, P. T. (2015). Neurofunctional topography of the human hippocampus. Human Brain Mapping, 36(12), 5018–5037.

34 Eickhoff, S.B., Stephan, K.E., Mohlberg, H., Grefkes, C., Fink, G.R., Amunts, K., & Zilles, K. (2005) A new SPM toolbox for combining probabilistic cytoarchitectonic maps and functional imaging data. Neuroimage, 25, 1325–1335.

35 Vos De Wael, R., Larivière, S., Caldairou, B., Hong, S. J., Margulies, D. S., Jefferies, E., … Bernhardt, B. C. (2018). Anatomical and microstructural determinants of hippocampal subfield functional connectome embedding. Proceedings of the National Academy of Sciences of the United States of America, 115(40), 10154–10159.

36 Tyszka, J. M., & Pauli, W. M. (2016). In vivo delineation of subdivisions of the human amygdaloid complex in a high-resolution group template. Human Brain Mapping, 37(11), 3979–3998.

37 Keren, N. I., Lozar, C. T., Harris, K. C., Morgan, P. S., & Eckert, M. A. (2009). In vivo mapping of the human locus coeruleus. NeuroImage, 47(4), 1261–1267.

38 Pauli, W. M., Nili, A. N., & Michael Tyszka, J. (2018). Data Descriptor: A high-resolution probabilistic in vivo atlas of human subcortical brain nuclei. Scientific Data, 5, 1–13.

39 Li, C. shan R., Ide, J. S., Zhang, S., Hu, S., Chao, H. H., & Zaborszky, L. (2014). Resting state functional connectivity of the basal nucleus of Meynert in humans: In comparison to the ventral striatum and the effects of age. NeuroImage, 97, 321–332.

40 Edlow, B. L., Takahashi, E., Wu, O., Benner, T., Dai, G., Lihong Bu, M., … Folkerth, R. D. (2012). Neuroanatomic Connectivity of the Human Ascending Arousal System Critical to Consciousness and Its Disorders. Journal of Neuropathology and Experimental Neurology, 71(6), 601.

41 Choi, E. Y., Yeo, B. T. T., & Buckner, R. L. (2012). The organization of the human striatum estimated by intrinsic functional connectivity. Journal of Neurophysiology, 108(8), 2242–2263.

42 Marquand, A. F., Haak, K. V., & Beckmann, C. F. (2017). Functional corticostriatal connection topographies predict goal-directed behaviour in humans. Nature Human Behaviour, 1(8), 1–11.

43 Haak, K. V., Marquand, A. F., & Beckmann, C. F. (2018). Connectopic mapping with resting-state fMRI. NeuroImage, 170, 83–94.

44 Petersen, S. E., & Posner, M. I. (2012). The Attention System of the Human Brain: 20 Years After. Annual Review of Neuroscience, 35(1), 73–89.

45 Binder, J. R., & Desai, R. H. (2011). The neurobiology of semantic memory. Trends in Cognitive Sciences, 15(11), 527–536.

46 Rilling, J.K., Stout, D. (2014). Evolution of the neural bases of higher cognitive function in humans. Gazzaniga, M.S., Mangun, G.R., The Cognitive Neurosciences, MIT Press, Cambridge, MA, pp. 41-49

47 Menon, V., & Uddin, L. Q. (2010). Saliency, switching, attention and control: a network model of insula function. Brain Structure & Function, 214(5–6), 655–667.

48 Buckner, R. L. (2013). The cerebellum and cognitive function: 25 years of insight from anatomy and neuroimaging. Neuron, 80(3), 807–815.

49 Marek, S., Siegel, J. S., Gordon, E. M., Raut, R. V., Gratton, C., Newbold, D. J., … Dosenbach, N. U. F. (2018). Spatial and Temporal Organization of the Individual Human Cerebellum. Neuron, 100(4), 977-993.e7.

50 Sherman, S.M., Guillery, R.W. (2013). Functional Connection Of Cortical Areas: A New View From The Thalamus. Cambridge, MA: MIT Press

51 Halassa, M. M., & Kastner, S. (2017). Thalamic functions in distributed cognitive control. Nature Neuroscience, 20(12), 1669–1679.

52 Hughes, S. W., Lorincz, M. L., Parri, H. R., & Crunelli, V. (2011). Infraslow (<0.1Hz) oscillations in thalamic relay nuclei. basic mechanisms and significance to health and disease states. Progress in Brain Research, 193, 145–162.

53 Watson, B. O. (2018). Cognitive and physiologic impacts of the infraslow oscillation. Frontiers in Systems Neuroscience, 12.

54 Crunelli, V., David, F., Lorincz, M. L., & Hughes, S. W. (2015). The thalamocortical network as a single slow wave-generating unit. Current Opinion in Neurobiology, 31, 72–80.

55 Crunelli, V., Larincz, M. L., Connelly, W. M., David, F., Hughes, S. W., Lambert, R. C., … Errington, A. C. (2018). Dual function of thalamic low-vigilance state oscillations: Rhythm-regulation and plasticity. Nature Reviews Neuroscience, 19(2), 107–118.

56 Vann, S. D., Aggleton, J. P., & Maguire, E. A. (2009). What does the retrosplenial cortex do? Nature Reviews Neuroscience, 10(11), 792–802.

57 Wong, C. W., Olafsson, V., Tal, O., & Liu, T. T. (2013). The amplitude of the resting-state fMRI global signal is related to EEG vigilance measures. NeuroImage, 83, 983–990.

58 Mitra, A., Snyder, A. Z., Tagliazucchi, E., Laufs, H., & Raichle, M. E. (2015). Propagated infra-slow intrinsic brain activity reorganizes across wake and slow wave sleep. ELife, 4, 1–19.

59 Ramirez-Villegas, J. F., Logothetis, N. K., & Besserve, M. (2015). Diversity of sharp-wave-ripple LFP signatures reveals differentiated brain-wide dynamical events. Proceedings of the National Academy of Sciences of the United States of America, 112(46), E6379–E6387.

60 Laufs, H., Krakow, K., Sterzer, P., Eger, E., Beyerle, A., Salek-Haddadi, A., & Kleinschmidt, A. (2003). Electroencephalographic signatures of attentional and cognitive default modes in spontaneous brain activity fluctuations at rest. Proceedings of the National Academy of Sciences of the United States of America, 100(19), 11053–11058.

61 Mantini, D., Perrucci, M. G., Gratta, C. Del, Romani, G. L., & Corbetta, M. (2007). Electrophysiological signatures of resting state networks in the human brain. Proceedings of the National Academy of Sciences of the United States of America, 104(32), 13170–13175.

62 Palva, J. M., & Palva, S. (2012). Infra-slow fluctuations in electrophysiological recordings, blood-oxygenation-level-dependent signals, and psychophysical time series. NeuroImage, 62(4), 2201–2211.

63 Hiltunen, T., Kantola, J., Elseoud, A. A., Lepola, P., Suominen, K., Starck, T., … Matias Palva, J. (2014). Infra-slow EEG fluctuations are correlated with resting-state network dynamics in fMRI. Journal of Neuroscience, 34(2), 356–362.

64 He, B. J., Snyder, A. Z., Zempel, J. M., Smyth, M. D., & Raichle, M. E. (2008). Electrophysiological correlates of the brain's intrinsic large-scale functional architecture. Proceedings of the National Academy of Sciences of the United States of America, 105(41), 16039–16044.

65 Kucyi, A., Schrouff, J., Bickel, S., Foster, B. L., Shine, J. M., & Parvizi, J. (2018). Intracranial electrophysiology reveals reproducible intrinsic functional connectivity within human brain networks. Journal of Neuroscience, 38(17), 4230–4242.

66 Fox, K. C. R., Foster, B. L., Kucyi, A., Daitch, A. L., & Parvizi, J. (2018). Intracranial Electrophysiology of the Human Default Network. Trends in Cognitive Sciences, 22(4), 307–324.

67 Brookes, M. J., Woolrich, M., Luckhoo, H., Price, D., Hale, J. R., Stephenson, M. C., … Morris, P. G. (2011). Investigating the electrophysiological basis of resting state networks using magnetoencephalography. Proceedings of the National Academy of Sciences of the United States of America, 108(40), 16783–16788.

68 Burt, J. B., Demirtaş, M., Eckner, W. J., Navejar, N. M., Ji, J. L., Martin, W. J., … Murray, J. D. (2018). Hierarchy of transcriptomic specialization across human cortex captured by structural neuroimaging topography. Nature Neuroscience, 21(9), 1251–1259.

69 Fornito, A., Arnatkevičiūtė, A., & Fulcher, B. D. (2019). Bridging the Gap between Connectome and Transcriptome. Trends in Cognitive Sciences, 23(1), 34–50.

70 Goulas, A., Zilles, K., & Hilgetag, C. C. (2018). Cortical Gradients and Laminar Projections in Mammals. Trends in Neurosciences, 41(11), 775–788.

71 Glasser, M. F., Goyal, M. S., Preuss, T. M., Raichle, M. E., & Essen, D. C. Van. (2014). NeuroImage Trends and properties of human cerebral cortex: Correlations with cortical myelin content. NeuroImage, 93, 165–175.

72 Vaishnavi, S. N., Vlassenko, A. G., Rundle, M. M., Snyder, A. Z., Mintun, M. A., & Raichle, M. E. (2010). Regional aerobic glycolysis in the human brain. Proceedings of the National Academy of Sciences, 107(41), 17757–17762.

73 Blazey, T., Snyder, A. Z., Su, Y., Goyal, M. S., Lee, J. J., Vlassenko, A. G., … Raichle, M. E. (2018). Quantitative positron emission tomography reveals regional differences in aerobic glycolysis within the human brain. Journal of Cerebral Blood Flow and Metabolism.

74 Hyder, F., Herman, P., Bailey, C. J., Møller, A., Globinsky, R., Fulbright, R. K., … Gjedde, A. (2015). Uniform distributions of glucose oxidation and oxygen extraction in gray matter of normal human brain: No evidence of regional differences of aerobic glycolysis. Journal of Cerebral Blood Flow and Metabolism, 36(5), 903–916.

75 Gomez, J., Zhen, Z., & Weiner, K. S. (2019). Human visual cortex is organized along two genetically opposed hierarchical gradients with unique developmental and evolutionary origins. PLOS Biology, 17(7), e3000362.

76 Faber, M., Przezdzik, I., Fernandez, G., Beckmann, C., & Haak, K. (2019). Overlapping connectivity gradients underlie functional multiplicity in the anterior temporal lobe. 25th Annual Meeting of the Organization for Human Brain Mapping, Rome, Italy, T266.

77 Kleinfeld, D., Deschênes, M., Wang, F., & Moore, J. D. (2014). More than a rhythm of life: Breathing as a binder of orofacial sensation. Nature Neuroscience, 17(5), 647–651.

78 Kurnikova, A., Moore, J. D., Liao, S. M., Deschênes, M., & Kleinfeld, D. (2017). Coordination of Orofacial Motor Actions into Exploratory Behavior by Rat. Current Biology, 27(5), 688–696.

79 Kumar, V. J., van Oort, E., Scheffler, K., Beckmann, C. F., & Grodd, W. (2017). Functional anatomy of the human thalamus at rest. NeuroImage, 147, 678–691.

80 O'muircheartaigh, J., Keller, S. S., Barker, G. J., & Richardson, M. P. (2015). White matter connectivity of the thalamus delineates the functional architecture of competing thalamocortical systems. Cerebral Cortex, 25(11), 4477–4489.

81 Zhang, D., Snyder, A. Z., Shimony, J. S., Fox, M. D., & Raichle, M. E. (2010). Noninvasive functional and structural connectivity mapping of the human thalamocortical system. Cerebral Cortex, 20(5), 1187–1194.

82 Bär, K. J., De la Cruz, F., Schumann, A., Koehler, S., Sauer, H., Critchley, H., & Wagner, G. (2016). Functional connectivity and network analysis of midbrain and brainstem nuclei. NeuroImage, 134, 53–63.

83 Zhang, S., Hu, S., Chao, H. H., & Li, C. S. R. (2016). Resting-State Functional Connectivity of the Locus Coeruleus in Humans: In Comparison with the Ventral Tegmental Area/Substantia Nigra Pars Compacta and the Effects of Age. Cerebral Cortex, 26(8), 3413–3427.

84 Shine, J. M. (2019). Neuromodulatory Influences on Integration and Segregation in the Brain. Trends in Cognitive Sciences, 23(7), 572–583.

85 Bzdok, D., Laird, A. R., Zilles, K., Fox, P. T., & Eickhoff, S. B. (2013). An investigation of the structural, connectional, and functional subspecialization in the human amygdala. Human Brain Mapping, 34(12), 3247–3266.

86 Bickart, K. C., Hollenbeck, M. C., Barrett, L. F., & Dickerson, B. C. (2012). Intrinsic amygdala-cortical functional connectivity predicts social network size in humans. Journal of Neuroscience, 32(42), 14729–14741.

87 Pauli, W. M., O'Reilly, R. C., Yarkoni, T., & Wager, T. D. (2016). Regional specialization within the human striatum for diverse psychological functions. Proceedings of the National Academy of Sciences, 113(7), 1907–1912.

88 Crosson, B. (2013). Thalamic mechanisms in language: a reconsideration based on recent findings and concepts. Brain and Language, 126(1), 73–88.

89 Avery, M. C., & Krichmar, J. L. (2017). Neuromodulatory Systems and Their Interactions: A Review of Models, Theories, and Experiments. Frontiers in Neural Circuits, 11, 1–18.

90 Valdes-Sosa, P. A., Roebroeck, A., Daunizeau, J., & Friston, K. (2011). Effective connectivity: Influence, causality and biophysical modeling. NeuroImage, 58(2), 339–361.

91 Kucyi, A. (2018). Just a thought: How mind-wandering is represented in dynamic brain connectivity. NeuroImage, 180, 505–514.

92 Chan, A. W., Mohajerani, M. H., LeDue, J. M., Wang, Y. T., & Murphy, T. H. (2015). Mesoscale infraslow spontaneous membrane potential fluctuations recapitulate high-frequency activity cortical motifs. Nature Communications, 6, 1–12.

93 Pape, H. C., & Pare, D. (2010). Plastic synaptic networks of the amygdala for the acquisition, expression, and extinction of conditioned fear. Physiological Reviews, 90(2), 419–463.

94 Pessoa, L., & Adolphs, R. (2010). Emotion processing and the amygdala: From a “low road” to “many roads” of evaluating biological significance. Nature Reviews Neuroscience, 11(11), 773–782.

95 Drew, P. J., Duyn, J. H., Golanov, E., & Kleinfeld, D. (2008). Finding coherence in spontaneous oscillations. Nature Neuroscience, 11(9), 991–993.

96 Honey, C. J., Sporns, O., Cammoun, L., Gigandet, X., Thiran, J. P., Meuli, R., & Hagmann, P. (2009). Predicting human resting-state functional connectivity from structural connectivity. Proceedings of the National Academy of Sciences of the United States of America, 106(6), 2035–2040.

97 Deco, G., Jirsa, V. K., & McIntosh, A. R. (2013). Resting brains never rest: Computational insights into potential cognitive architectures. Trends in Neurosciences, 36(5), 268–274.

98 Breakspear, M. (2017). Dynamic models of large-scale brain activity. Nature Neuroscience, 20(3), 340–352.

99 Bassett, D. S., & Sporns, O. (2017). Network Neuroscience. Nature Neuroscience, 20(3), 353–364.

100 Kashyap, A., & Keilholz, S. D. (2018). Dynamic properties of simulated brain network models and empirical resting-state data. Network Neuroscience, 3(2), 405–426.

101 Mateo, C., Knutsen, P. M., Tsai, P. S., Shih, A. Y., & Kleinfeld, D. (2017). Entrainment of Arteriole Vasomotor Fluctuations by Neural Activity Is a Basis of Blood-Oxygenation-Level-Dependent "Resting-State" Connectivity. Neuron, 96(4), 936-948.e3.

102 Keilholz, S. D., Pan, W. J., Billings, J., Nezafati, M., & Shakil, S. (2017). Noise and non-neuronal contributions to the BOLD signal: applications to and insights from animal studies. NeuroImage, 154, 267–281.

103 Mitra, A., Snyder, A. Z., Blazey, T., & Raichle, M. E. (2015). Lag threads organize the brain's intrinsic activity. Proceedings of the National Academy of Sciences of the United States of America, 112(52), E7307.

104 Mitra, A., & Raichle, M. E. (2016). How networks communicate: Propagation patterns in spontaneous brain activity. Philosophical Transactions of the Royal Society B: Biological Sciences, 371(1705).

105 Hindriks, R., Mantini, R., Gravel, N., & Deco, G. (2019). Latency analysis of resting-state BOLD-fMRI reveals traveling waves in visual cortex linking task-positive and task-negative networks. NeuroImage, 200, 259–274.

106 Muller, L., Chavane, F., Reynolds, J., & Sejnowski, T. J. (2018). Cortical travelling waves: Mechanisms and computational principles. Nature Reviews Neuroscience, 19(5), 255–268.

107 Magnuson, M. E., Thompson, G. J., Pan, W. J., & Keilholz, S. D. (2014). Effects of severing the corpus callosum on electrical and bold functional connectivity and spontaneous dynamic activity in the rat brain. Brain Connectivity, 4(1), 15–29.

108 Mohajerani, M. H., Chan, A. W., Mohsenvand, M., Ledue, J., Liu, R., McVea, D. A., … Murphy, T. H. (2013). Spontaneous cortical activity alternates between motifs defined by regional axonal projections. Nature Neuroscience, 16(10), 1426–1435.

109 Greenberg, A., Abadchi, J. K., Dickson, C. T., & Mohajerani, M. H. (2018). New waves: Rhythmic electrical field stimulation systematically alters spontaneous slow dynamics across mouse neocortex. NeuroImage, 174, 328–339.

110 Matsui, T., Murakami, T., & Ohki, K. (2016). Transient neuronal coactivations embedded in globally propagating waves underlie resting-state functional

connectivity. Proceedings of the National Academy of Sciences of the United States of America, 113(23), 6556–6561.

111 Ma, Y., Shaik, M. A., Kozberg, M. G., Kim, S. H., Portes, J. P., Timerman, D., & Hillman, E. M. C. (2016). Resting-state hemodynamics are spatiotemporally coupled to synchronized and symmetric neural activity in excitatory neurons. Proceedings of the National Academy of Sciences of the United States of America, 113(52), E8463–E8471.

112 Vanni, M. P., Chan, A. W., Balbi, M., Silasi, G., & Murphy, T. H. (2017). Mesoscale mapping of mouse cortex reveals frequency-dependent cycling between distinct macroscale functional modules. Journal of Neuroscience, 37(31), 7513–7533.

113 Mitra, A., Kraft, A., Wright, P., Acland, B., Snyder, A. Z., Rosenthal, Z., … Raichle, M. E. (2018). Spontaneous Infra-slow Brain Activity Has Unique Spatiotemporal Dynamics and Laminar Structure. Neuron, 98(2), 297-305.e6.

114 Roberts, J. A., Gollo, L. L., Abeysuriya, R. G., Roberts, G., Mitchell, P. B., Woolrich, M. W., & Breakspear, M. (2019). Metastable brain waves. Nature Communications, 10(1), 1–17.

115 Buzsáki, G., & Watson, B. O. (2012). Brain rhythms and neural syntax: Implications for efficient coding of cognitive content and neuropsychiatric disease. Dialogues in Clinical Neuroscience, 14(4), 345–367.

116 Poskanzer, K. E., & Yuste, R. (2011). Astrocytic regulation of cortical UP states. Proceedings of the National Academy of Sciences of the United States of America, 108(45), 18453–18458.

117 Aquino, K. M., Schira, M. M., Robinson, P. A., Drysdale, P. M., & Breakspear, M. (2012). Hemodynamic traveling waves in human visual cortex. PLoS Computational Biology, 8(3).

118 Huth, A. G., De Heer, W. A., Griffiths, T. L., Theunissen, F. E., & Gallant, J. L. (2016). Natural speech reveals the semantic maps that tile human cerebral cortex. Nature, 532(7600), 453–458.

119 Badre, D., & Nee, D. E. (2018). Frontal Cortex and the Hierarchical Control of Behavior. Trends in Cognitive Sciences, 22(2), 170–188.

120 Xu, T., Sturgeon, D., Ramirez, J. S. B., Froudist-Walsh, S., Margulies, D. S., Schroeder, C. E., … Milham, M. P. (2019). Interindividual Variability of Functional

Connectivity in Awake and Anesthetized Rhesus Macaque Monkeys. Biological Psychiatry: Cognitive Neuroscience and Neuroimaging, 4(6), 543–553.

121 Galvan, A., Devergnas, A., & Wichmann, T. (2015). Alterations in neuronal activity in basal ganglia-thalamocortical circuits in the parkinsonian state. Frontiers in Neuroanatomy, 9, 1–21.

122 Squire, L. R. (2004). Memory systems of the brain: A brief history and current perspective. Neurobiology of Learning and Memory, 82(3), 171–177.

123 Manns, J. R., & Bass, D. I. (2016). The Amygdala and Prioritization of Declarative Memories. Current Directions in Psychological Science, 25(4), 261–265.

124 Singer, A. C., Carr, M. F., Karlsson, M. P., & Frank, L. M. (2013). Hippocampal SWR Activity Predicts Correct Decisions during the Initial Learning of an Alternation Task. Neuron, 77(6), 1163–1173.

125 Mitra, A., Snyder, A. Z., Hacker, C. D., Pahwa, M., Tagliazucchi, E., Laufs, H., … Raichle, M. E. (2016). Human cortical-hippocampal dialogue in wake and slow-wave sleep. Proceedings of the National Academy of Sciences of the United States of America, 113(44), E6868–E6876.

126 Hamann, S. (2012). Mapping discrete and dimensional emotions onto the brain: Controversies and consensus. Trends in Cognitive Sciences, 16(9), 458–466.

127 Inman, C. S., Manns, J. R., Bijanki, K. R., Bass, D. I., Hamann, S., Drane, D. L., … Willie, J. T. (2018). Direct electrical stimulation of the amygdala enhances declarative memory in humans. Proceedings of the National Academy of Sciences of the United States of America, 115(1), 98–103.

128 Kandel, E.R., Schwartz, J.H., Jessell, T.M., Siegelbaum, S.A. & Hudspeth, A.J. (2013). Principles of Neural Science. New York, NY: McGraw-Hill Education.